



Phosphoprotein-based biomarkers as predictors for cancer therapy

Angela M. Carter^a, Chunfeng Tan^b, Karine Pozo^{c,d}, Rahul Telange^a, Roberto Molinaro^{e,f}, Ailan Guo^g, Enrica De Rosa^{e,h}, Jonathan O. Martinez^e, Shanrong Zhangⁱ, Nilesh Kumarⁱ, Masaya Takahashiⁱ, Thorsten Wiederhold^k, Hans K. Ghayee^l, Sarah C. Oltmann^{d,m}, Karel Pacakⁿ, Eugene A. Woltering^o, Kimmo J. Hatanpaa^p, Fiemu E. Nwariaku^{d,m}, Elizabeth G. Grubbs^q, Anthony J. Gill^r, Bruce Robinson^s, Frank Gillardon^t, Sushanth Reddy^{a,u}, Renata Jaskula-Sztul^{a,u}, James A. Mobley^v, M. Shahid Mukhtar^{a,j}, Ennio Tasciotti^{e,w}, Herbert Chen^{a,u}, and James A. Bibb^{a,u,1}

^aDepartment of Surgery, University of Alabama at Birmingham, Birmingham, AL 35233; ^bDepartment of Psychiatry, University of Texas Southwestern Medical Center, Dallas, TX 75390; ^cDepartment of Neuroscience, University of Texas Southwestern Medical Center, Dallas, TX 75390; ^dDepartment of Surgery, University of Texas Southwestern Medical Center, Dallas, TX 75390; ^eRegenerative Medicine Program, Houston Methodist Research Institute, Houston, TX 77030; ^fDepartment of Biomolecular Sciences, University of Urbino Carlo Bo, 61029, Urbino, Italy; ^gBluefin Biomedicine, Beverly, MA 01915; ^hDepartment of Nanomedicine, Houston Methodist Research Institute, Houston, TX 77030; ⁱAdvanced Imaging Research Center, University of Texas Southwestern Medical Center, Dallas, TX 75390; ^jDepartment of Biology, University of Alabama at Birmingham, Birmingham, AL 35233; ^kCell Signaling Technology, Danvers, MA 01923; ^lDepartment of Internal Medicine, Division of Endocrinology, University of Florida College of Medicine and Malcom Randall VA Medical Center, Gainesville, FL 32608; ^mHarrold B. Simmons Comprehensive Cancer Center, University of Texas Southwestern Medical Center, Dallas, TX 75390; ⁿSection on Medical Neuroendocrinology, Eunice Kennedy Shriver National Institute of Child Health and Human Development, National Institutes of Health, Bethesda, MD 20892; ^oDepartment of Surgery, Louisiana State University Health Sciences Center, New Orleans, LA 70112; ^pDepartment of Pathology, University of Texas Southwestern Medical Center, Dallas, TX 75390; ^qDepartment of Surgical Oncology, University of Texas MD Anderson Medical Center, Houston, TX 77030; ^rCancer Diagnosis and Pathology Group, Kolling Institute of Medical Research, University of Sydney, 2065 St Leonards, Australia; ^sKolling Institute and Department of Endocrinology, Royal North Shore Hospital, University of Sydney, 2065 St Leonards, Australia; ^tCentral Nervous System (CNS) Diseases Research, Boehringer Ingelheim Pharma GmbH & Co. KG, 88397 Biberach an der Riss, Germany; ^uO'Neal Comprehensive Cancer Center, University of Alabama at Birmingham, Birmingham, AL 35233; ^vDepartment of Anesthesiology and Perioperative Medicine, University of Alabama at Birmingham, Birmingham, AL 35233; and ^wHouston Methodist Orthopedic and Sports Medicine, Houston Methodist Hospital, Houston, TX 77030

Edited by Tony Hunter, Salk Institute for Biological Studies, La Jolla, CA, and approved June 16, 2020 (received for review June 2, 2020)

Disparities in cancer patient responses have prompted widespread searches to identify differences in sensitive vs. nonsensitive populations and form the basis of personalized medicine. This customized approach is dependent upon the development of pathway-specific therapeutics in conjunction with biomarkers that predict patient responses. Here, we show that Cdk5 drives growth in subgroups of patients with multiple types of neuroendocrine neoplasms. Phosphoproteomics and high throughput screening identified phosphorylation sites downstream of Cdk5. These phosphorylation events serve as biomarkers and effectively pinpoint Cdk5-driven tumors. Toward achieving targeted therapy, we demonstrate that mouse models of neuroendocrine cancer are responsive to selective Cdk5 inhibitors and biomimetic nanoparticles are effective vehicles for enhanced tumor targeting and reduction of drug toxicity. Finally, we show that biomarkers of Cdk5-dependent tumors effectively predict response to anti-Cdk5 therapy in patient-derived xenografts. Thus, a phosphoprotein-based diagnostic assay combined with Cdk5-targeted therapy is a rational treatment approach for neuroendocrine malignancies.

predictive biomarkers | neuroendocrine tumors | cyclin-dependent kinase 5

Cyclin-dependent kinases (Cdks) are a family of proline-directed serine/threonine kinases that are required for progression of normal cell division. Typical Cdks are regulated through binding to cyclins, proteins which are expressed at varying levels at distinct stages of the cell cycle (1). As master regulators of cell division, Cdk1/2/4/6 currently serve as popular targets for cancer therapy development (2–4). Although Cdk5 shares ~60% sequence identity with founding family members Cdk1 and Cdk2 (5), it possesses noncanonical features. Specifically, Cdk5 is not required for normal cell cycle progression and is not activated by cyclins. Cdk5 is regulated instead through interactions with cofactors p35 and p39 (6). Although Cdk5 is expressed in a broad number of tissues (5), its activators are mostly restricted to neuronal cells (7) where Cdk5 activity is important for central nervous system (CNS) development and cognitive processes such as learning and memory (8). Cleavage of p35 and p39 by calpain produces truncated activators, p25 and

p29, respectively (9). These cleavage products have increased protein stability and mislocalize in cells due to removal of an N-terminal myristoylation site (10). In neurons, p25 aberrantly activates Cdk5 and has been linked to neurotoxicity, neuronal injury, and neurodegeneration (6).

Recent research suggests the aberrant activation of Cdk5 in nonneuronal cells can usurp signaling components involved in the cell cycle to drive proliferation (11). Expression of Cdk5 as well as p35 and/or p25 (p35/p25) has been shown for three types of neoplasms originating from neuroendocrine (NE) cells:

Significance

This study validates a path toward personalized medicine that utilizes a survey of the effective signaling state of tumors via posttranslational modification analysis as a diagnostic alternative to direct examination of genetic mutations. Here, this approach is utilized to identify biomarkers for Cdk5-driven tumors. The same approach could be adapted to identify markers of other tumor drivers. As the number of cancer types in which Cdk5 is implicated is rising and as drugs with the potential to selectively target Cdk5 are moved toward the clinic, the translational potential of this diagnostic–therapeutic coupled system will be broad.

Author contributions: A.M.C., R.M., S.C.O., F.E.N., S.R., E.T., and J.A.B. designed research; A.M.C., C.T., K. Pozo, R.T., R.M., A.G., E.D.R., J.O.M., S.Z., M.T., T.W., R.J.-S., and J.A.M. performed research; H.K.G., K. Pacak, E.A.W., K.J.H., E.G.G., A.J.G., B.R., F.G., and H.C. contributed new reagents/analytic tools; A.M.C., E.D.R., N.K., J.A.M., and M.S.M. analyzed data; A.M.C. and J.A.B. wrote the paper; and E.T., H.C., and J.A.B. supervised the study.

The authors declare no competing interest.

This article is a PNAS Direct Submission.

Published under the PNAS license.

Data deposition: Phosphoproteomic data can be accessed on PhosphositePlus using the following link: https://www.phosphosite.org/Supplemental_Files.action.

¹To whom correspondence may be addressed. Email: jbibb@uab.edu.

This article contains supporting information online at <https://www.pnas.org/lookup/suppl/doi:10.1073/pnas.2010103117/-DCSupplemental>.

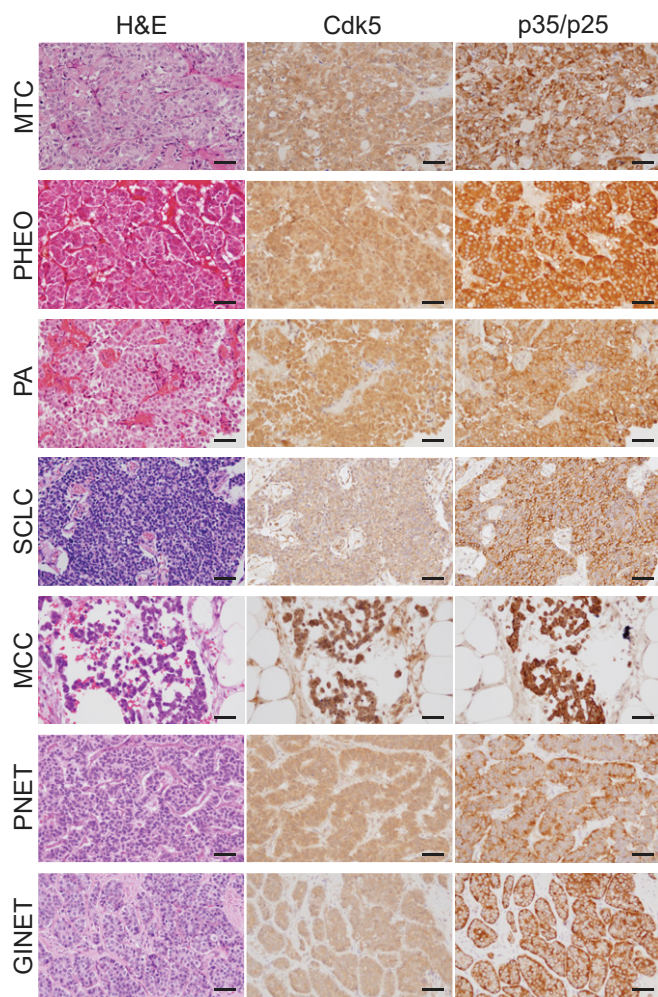


Fig. 1. Cdk5 pathway components are present in human NE tumors. H&E stain, immunohistochemistry (IHC) for Cdk5, and IHC for p35/p25 in human NE tumors (Scale bars, 50 μm .)

medullary thyroid carcinoma (MTC) (12), small cell lung cancer (SCLC) (13), and pituitary adenomas (PAs) (14). In MTC, inhibition of Cdk5 activity decreases rates of cell growth (12, 15); in SCLC and PA, it decreases migration and invasion (16, 17). Expression of p25 in thyroid C cells produces MTC in mice (12), in part through alteration of traditional cell cycle regulatory components (18). Here we show that Cdk5 and p35/p25 expression may be an important driver of many types of NE cancer and that aberrant Cdk5 activity allows for a diagnostic-coupled treatment strategy that targets this protein kinase.

Results

Cdk5 in NE Neoplasms. To better understand the potential role of Cdk5 across multiple forms of NE malignancies, we assessed expression of the kinase and its activating cofactors in as many different NE tumor and cancer types as we could obtain samples. Histological analysis demonstrated that Cdk5 and p35/p25 are present throughout various human NE neoplasms including MTC, pheochromocytoma (Pheo), PA, SCLC, Merkel cell carcinoma (MCC), pancreatic NE tumors (PNETs), and gastrointestinal NE tumors (GINETs) (Fig. 1). Furthermore, these proteins are present in cell lines derived from multiple types of NE neoplasms, including three human MTCs (TT, MTC-SK, and SIN-J), a human progenitor PHEO (hPheo1) (19), a human

pancreatic carcinoid (BON), a rat insulinoma (INS), and two human SCLCs (H146 and H1184) (Fig. 2A and *SI Appendix, Fig. S1A*). Selective Cdk5 inhibition by Indolinone A (IndoA) blocked all human NE cancer cell growth more potently than it affected normal human fibroblasts or rat INS cells (Fig. 2B and *SI Appendix, Fig. S2 A–H*). NE cell lines treated with Cdk5 inhibitors typically showed flattening and smoothing of cell body consistent with a less malignant phenotype, except the rat INS line (Fig. 2C and *SI Appendix, Fig. S1B*). Interestingly, the aberrant Cdk5 activator, p25, was present in all human cell lines derived from naturally occurring tumors but not the rat INS line generated using irradiation (20) (Fig. 2A), indicating that the presence of p25 was responsible for driving aberrant proliferation downstream of Cdk5.

IndoA inhibits Cdk5 activity with high affinity, but also targets Cdk4. Therefore, this compound potentially acts in cells as a Cdk4/5 inhibitor (4/5i) (21). Importantly, the structurally related Cdk4-specific inhibitor (4i), IndoB, was 6.4- to 15.4-fold less potent at preventing human NE cell proliferation (Fig. 2B and *SI Appendix, Fig. S2 A–H*). Growth of multiple NE cancer cell lines

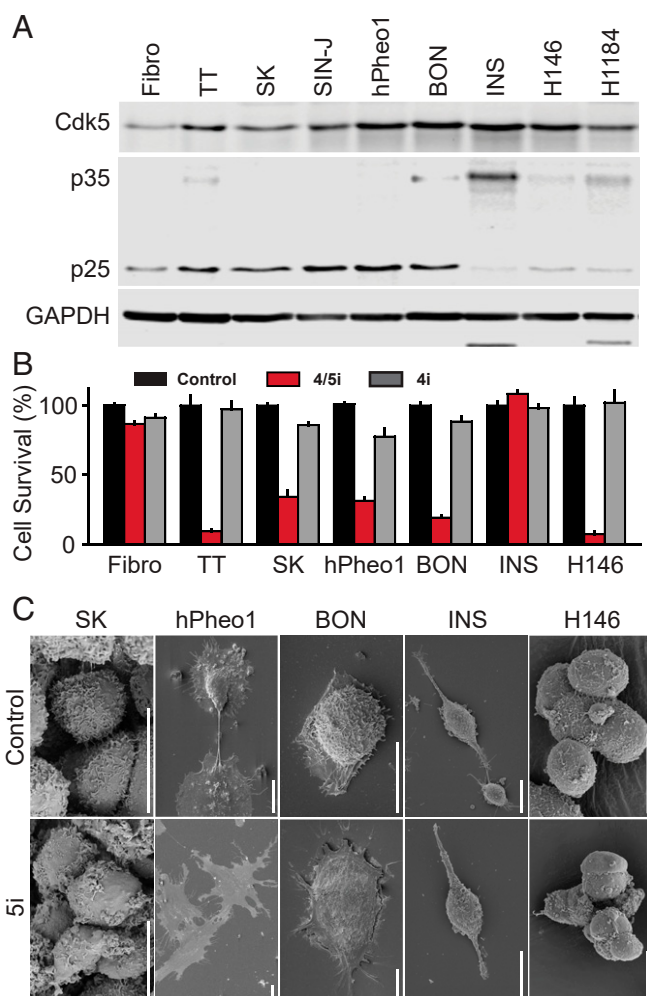


Fig. 2. Cdk5 promotes growth in human NE cells. (A) Immunoblot of Cdk5 pathway components in fibroblasts and NE cells. (B) Fibroblasts and NE cell lines were treated with 0.02% DMSO (control), 0.3 μM IndoA (4/5i), or 0.3 μM IndoB (4i) and monitored for effects on cell growth. Error bars represent SEM. (Full curves and IC_{50} values are reported in *SI Appendix, Fig. S1*.) (C) Scanning electron microscopy of NE cells treated with control (0.02% DMSO) or 5i (hPheo1 and BON, 2 μM IndoA; SK and H146, 5 μM CP6813101) for 4 h. (Scale bars, 10 μm .)

was likewise blocked by the broad spectrum Cdk inhibitors roscovitine and dinaciclib. CP681301, a selective inhibitor of both Cdk2 and Cdk5, also blocked growth of NE cancer cells, whereas the Cdk2-specific inhibitor CVT313 had a greatly reduced effect (*SI Appendix, Fig. S2 I–L*). Thus, Cdk5 inhibition was necessary to robustly inhibit proliferation of cells derived from multiple forms of NE neoplasms. Previous work demonstrated cell growth inhibition of MTC cells using kinase dead mutants of Cdk5 as well as siRNA targeting the Cdk5 activator p35 (12). Together, these data indicate that Cdk5 and p35/25 expression characterize at least a portion of all NE neoplasms and aberrant Cdk5 activity is a major contributor to the growth of NE cancer cells.

Downstream Targets of Cdk5. To determine which pathways Cdk5 may target to drive NE cell proliferation, we used a unique bitransgenic mouse model of MTC (NSE-p25OE mice), developed in our laboratory, in which tumors arise at the natural organ site in the presence of an intact immune system. These mice express an activator of Cdk5, p25-GFP, in C cells of the thyroid under the control of a doxycycline (dox) regulatable promoter (Fig. 3A) (12). This system can be used to generate actively growing MTC tumors through expression of p25-GFP as well as growth-arrested MTC tumors through initial expression and subsequent suppression of p25-GFP via readministration of dox (Fig. 3A–C). As C cells only comprise 3% of a normal thyroid, this system allows generation of sufficient quantities of C cells for direct comparison of the signaling states between dividing and nondividing populations.

Phosphoproteomic analysis of growing vs. arrested MTC tumors was performed using PhosphoScan technology that included trypsin digest and peptide immunoprecipitation utilizing antibodies that recognize proline-directed phosphorylation of serine or threonine in the context of a MAPK or CDK consensus sequence (22). This analysis revealed global differences in the proline-directed S/T phosphosignaling network including over 250 peptides with elevated phosphorylation levels in growing tumors (Fig. 3D and *SI Appendix, Table S1*). From this set of phosphorylation sites, those not conserved in humans or conforming to a stringent Cdk5 phosphorylation sequence (S/T-P-x-K/H/R) were eliminated. From the remaining proteins, 50 of the most highly up-regulated phosphorylation sites, with preference for those with established or suggested roles in cancer, were selected for investigation as potential tumorigenic regulators (*SI Appendix, Table S2*). Short interfering peptides (SIPs) containing the phosphorylation site flanked by eight amino acids on both the N- and C-terminal sides were designed to selectively interfere with phosphorylation or function of the 50 targets. A cell-penetrating sequence (RQIKIWFQNRRMKWKK) from penetratin (PEN) was added to the N terminus of peptides to facilitate entry into cells. A high-throughput proliferation-based assay identified 15 SIPs that inhibited growth of NE cancer cells but not normal primary fibroblasts (Fig. 3E and F and *SI Appendix, Table S2*), suggesting that these sites may be important for NE cancer cell growth.

We performed ingenuity pathway analysis (IPA) to ascertain major signaling cascades and pathways that are associated with these 15 proteins. Among the predicted 25 statistically enriched canonical pathways, cell cycle regulation, DNA repair, and diverse cancer signaling pathways are a predominant feature (Fig. 3F and *SI Appendix, Table S3*). Thus, the downstream targets identified here are associated with common cancer mechanisms.

Biomarkers of Cdk5 Activity. Phosphorylation state-specific antibodies were successfully generated for detection of six sites: Ser608 Additional Sex Combs Like 2 (ASXL2), Thr143 Family with Sequence Similarity 53 Member C (FAM53C), Thr709

Filamin B (FLNB), Thr202 La Ribonucleoprotein Domain Family Member 6 (LARP6), Ser110 Kinetochore-Associated Protein Homolog (KNL-2), and Ser988 Retinoblastoma-Like Protein 1 (RBL1). Phosphorylation state-specific antibodies were also generated to two sites previously identified as targets of Cdk2: Ser17 Histone 1.5 (H1.5) (23, 24) and Ser391 Suppressor of Variegation 3-9 Homolog 1 (SUV39H1) (25) (*SI Appendix, Fig. S3*). Phosphorylation of these eight sites, as well as the thoroughly established Ser807/Ser811 sites on retinoblastoma-associated protein (RB) (26, 27), was confirmed in mouse MTC tumors, in which growth was driven by expression of p25-GFP, and reduced in arrested tumors (Fig. 4A). In agreement, phosphorylation levels of six of these sites were dose-dependently decreased by the 4/5i, IndoA, in hPheo1 cells (Fig. 4B). Similar decreases in these phosphorylation sites were observed in human MTC-SK, TT, and BON cells (Fig. 4C and *SI Appendix, Fig. S4*). This effect appeared Cdk5 specific as addition of the 4i, IndoB, to multiple NE cell lines had significantly less effect on the phosphorylation states of Thr143 FAM53C, Thr709 FLNB, Ser17 H1.5, and Thr202 LARP6 compared to IndoA. In contrast, phosphorylation of Ser807/Ser811 RB, a known target of multiple Cdks, was decreased upon treatment with both inhibitors. Interestingly, the phosphorylation of the RB family member, RBL1, was more responsive to IndoA than IndoB in TT cells, whereas phosphorylation of Ser391 SUV39H1 was more responsive to IndoA than IndoB in BON cells (Fig. 4C and *SI Appendix, Fig. S4*). Overall, these data demonstrate that phosphorylation of these six proteins is dependent upon Cdk5 activity and suggests that these phosphorylation sites could serve as biomarkers for many types of Cdk5-driven NE tumors. Attempts to produce antibodies for the remaining seven sites identified by SIP inhibition of cell growth were unsuccessful and therefore the capacity of these sites to serve as biomarkers could not be evaluated.

To determine if these Cdk5-dependent biomarkers occurred in human NE tumors, cohorts of MTC patient tumors and normal human thyroid tissues were compared. Immunoblot analysis revealed that three of the phosphorylation sites, Ser17 H1.5, Thr202 LARP6, and Ser988 RBL1, were significantly elevated in the total tumor population and exhibited a positive correlation with overall Cdk5 expression levels (Fig. 5A and B). The phosphorylation state of Ser391 SUV39H1 was only increased in a small portion of tumor samples but retained a positive correlation with Cdk5 expression. Distribution of all four phosphosites varied across patients with phospho-LARP6 being the most commonly detected followed by phosphorylation of H1.5 and RBL1, respectively (Fig. 5C). Although 73% of patient tumors exhibited elevated Cdk5 levels, only 21% presented with elevation of all four biomarkers of Cdk5 pathway activity, emphasizing the fact that presence of a protein does not correlate 100% with function of that protein and highlighting the need for direct readouts of pathway activity such as phosphorylation of downstream substrates. Thus, Cdk5-dependent tumorigenic signaling may be considered patient specific. Furthermore, detection of all four biomarkers in a patient could predict positive response to a Cdk5-targeted therapeutic approach.

Cdk5 Inhibitors as Effective Therapeutics in NE Models. To evaluate the efficacy of anti-Cdk5 therapy when administered systemically, IndoA was utilized in multiple animal models of NE cancer. IndoA was chosen for these studies as this compound is more selective for Cdk5 than dinaciclib and more potent than roscovitine and CP681301 (*SI Appendix, Fig. S2*) (12, 28, 29). First, the transgenic model of MTC driven directly by activation of Cdk5, NSE-p25OE, was treated with vehicle or IndoA (10 to 30 mg/kg body weight [BW]) once every 3 d for 2 wk. Tumor growth was significantly reduced by 20 and 30 mg/kg of IndoA compared to control animals (Fig. 6A and B). Plasma levels of

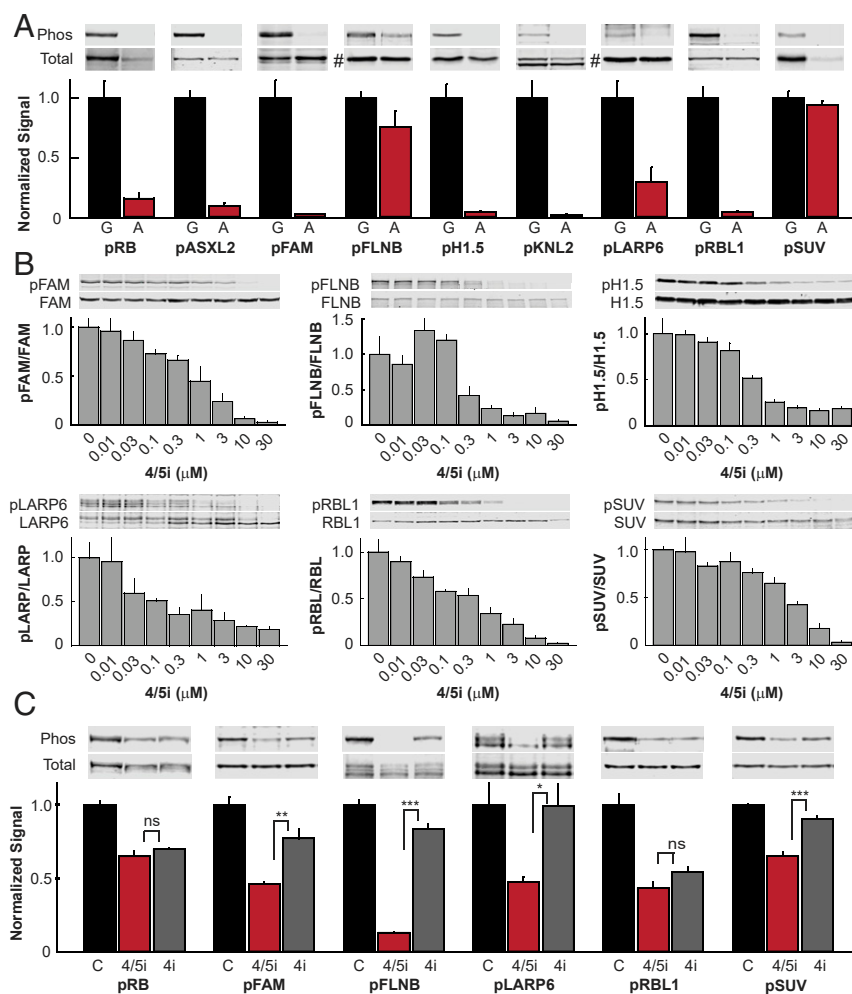


Fig. 4. Phosphoproteins are biomarkers of Cdk5 activity. (A) Immunoblot analysis of phosphoproteins in growing (G) and arrested (A) mouse MTC tumors. For pFLNB and pLARP6, total blot is actin (#); all others are normalized to each specific protein ($n = 3$ to 4). (B) Immunoblot analysis of phosphoproteins in human hPheo1 cells treated with increasing concentrations of IndoA (4/5i) for 4 h ($n = 3$ to 4 for all except 0.01, 1, and 30 μM points of pLARP6 where $n = 2$). (C) Immunoblot analysis of phosphoproteins in BON cells treated with 0.3% DMSO (control), 2 μM IndoA (4/5i), or 2 μM IndoB (4i) for 4 h. All error bars represent SEM. Simple comparisons between two groups of normally distributed data were performed using two-tailed Student's t test. * $P < 0.05$, ** $P < 0.01$, *** $P < 0.001$; ns, not significant.

upon passive targeting through enhanced permeability and retention (EPR) of unhealthy tumor vasculature (39). Although still benefitting from EPR, LKs actively target activated endothelium via chemotactic mechanisms analogous to those utilized by white blood cells (40). Importantly, LKs are successfully camouflaged by leukocyte membrane proteins, leading to lower total opsonization and avoidance of the rapid immune clearance observed with purely synthetic nanoparticle platforms (41–43).

As tumors are generally highly inflamed and attract multiple types of immune cells (44, 45), we tested the ability of LKs to traffic to MTC tumors of NSE-p25OE mice and to stabilize lower doses of IndoA. Using intravital microscopy, LKs were verified to exhibit increased tumor localization compared to control liposomes (LPs) and to time-dependently spread from the vasculature into surrounding tumor tissue (Fig. 7A and B). Maximum encapsulation of IndoA into LKs had no deleterious effects on particle size or homogeneity (SI Appendix, Fig. S7) and allowed a dosage of 5 mg/kg BW IndoA per retroorbital injection. High performance liquid chromatography/mass spectrometry (HPLC/MS) analysis of blood plasma demonstrated a sixfold stabilization of encapsulated drug compared to free drug at these lower dosage levels (Fig. 7C).

IndoA delivered at 10 mg/kg BW in the free form had no effect on tumor growth in transgenic MTC animals (Fig. 6B). In contrast, delivering only 5 mg/kg BW IndoA encapsulated in LKs had the same effect as delivering 20 mg/kg BW free drug (Figs. 6B and 7D). Thus, the LK delivery system generated an equivalent effect utilizing a 75% lower dosage. LKs also protected animals against hepatic and renal toxicity (Fig. 7E and F). While complete tumor arrest or shrinkage was not observed at 5 mg/kg BW, further modifications to allow higher encapsulation of drug could provide additional benefit for this unique delivery approach.

Discussion

The development of advanced sequencing techniques has led to an explosion of information pertaining to the genomic landscape of cancer. In some cases, this information successfully progressed to the development of personalized medicine. For example, mutations at Val600 in the serine/threonine kinase B-Raf are predictive of response to B-Raf inhibitors in patients with metastatic melanoma (46, 47). However, the majority of B-Raf mutant papillary thyroid cancer and colon cancer patients do not respond to B-Raf-targeted inhibitors (48), emphasizing the

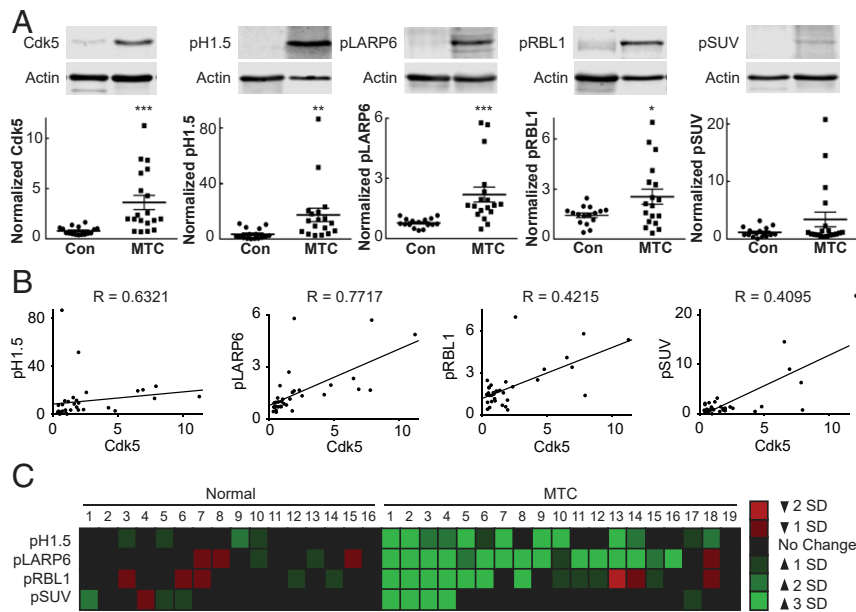


Fig. 5. Phosphoprotein biomarkers are present in subgroups of human MTC patients. (A) Immunoblot analysis of Cdk5 and phosphoproteins in normal human thyroid tissue and human MTC tumors. Due to sample size, samples were processed on three separate gels, each containing a reference for normalization. Error bars represent SEM. (B) Phosphoprotein level vs. Cdk5 expression in samples represented in A, analyzed by Spearman rank-order analysis; rho (R). (C) Heat map representation of immunoblot analysis of phosphoproteins from A, relative to the average and SD of the total normal thyroid population, grouped by individual patient sample. Simple comparisons between two groups of normally distributed data were performed using two-tailed Student's *t* test. **P* < 0.05, ***P* < 0.01, ****P* < 0.001.

difficulty designing treatment options based on single gene mutations.

For NE neoplasms, mutations are prominent in genes encoding the scaffolding protein menin and the receptor tyrosine kinase RET. Menin mutations were initially identified over 20 y ago in patients with multiple endocrine neoplasia (MEN) type 1 syndrome (49, 50). Menin is a broadly expressed tumor suppressor in which mutations typically cause protein truncation (51, 52). Currently there are no therapeutics with the potential to circumvent these mutations.

Mutations in the protooncogene RET were discovered over 20 y ago in patients with MEN2 syndrome (53–55). The development of vandetanib and carbazantinib, tyrosine kinase inhibitors that target RET, generated hope that patients possessing RET mutations could be successfully treated. Unfortunately, human trials revealed no correlation between the presence of a RET mutation and patient response to therapy (56–58).

As with all cancers, many mutations, in addition to RET, are present within each MTC cancer cell. These additional mutations can alter the diverse input nodes of the signaling network that drive cancer cell growth and survival. For these reasons, looking at the signaling network with a broader lens that includes posttranslational modifications could be beneficial and aid in the elimination of “false positive” nonresponders, that would be predicted responders, from genomic or proteomic information alone. The current study reveals that Cdk5 is likely a contributor to at least a portion of all NE tumor types. This study also identifies a set of phosphorylation-based biomarkers which indicate that not only are Cdk5 pathway components present, but Cdk5 is actively modulating the signaling network and regulating cancer physiology. It is important to note that additional experiments will be necessary to determine if each of these proteins are direct targets of Cdk5. Regardless, the dependence of these phosphorylation sites on Cdk5 activity validates them as biomarkers of Cdk5 pathway activation.

In addition to being biomarkers of Cdk5 pathway activity, the phosphoproteins identified here are potentially directly involved

in promotion of cell growth and/or survival. For example, RBL1 is a member of the retinoblastoma (RB) family of proteins that includes the tumor suppressor RB and RBL2. The RB family plays a major role in cell cycle regulation and is also involved in modulating senescence, apoptosis, and chromosomal stability (27). Although functional compensation has been observed among the family members, some differences exist. Unlike RB, RBL1 and RBL2 do not bind to activating transcription factors E2F1–3. They interact instead with transcriptional repressors E2F4 and E2F5 (59–61). Remarkably, both RBL1 and RBL2, but not RB, are members of the DREAM complex, a regulatory unit that mediates cell entry into quiescence (62, 63).

Emerging information suggests Cdk5 may play a role in non-NE cancers as well (11). High Cdk5 expression in neuroblastoma, a rare but deadly childhood cancer (64–66), is correlated with worse overall survival, and inhibition of Cdk5 amplifies the potency of Cdk2 inhibitors in neuroblastoma cell lines (67). The Cdk5 gene is amplified in pancreatic ductal adenocarcinoma (PDAC) and blockage of Cdk5 activity inhibits migration and invasion in PDAC cell lines. Involvement of Cdk5 is also implicated in colorectal cancer (68), breast cancer (69), glioblastoma (70), and prostate cancer (71). These findings suggest that Cdk5 is a vulnerable node that can be targeted in most tissues to facilitate cancer development and/or progression and that Cdk5 likely plays a role in subgroups of many cancer types. As the heterogeneity between tumors of the same cancer type is becoming more apparent, the likelihood that treatment approaches will evolve based on individual tumor signaling states instead of general tumor type classification is increasing. The biomarkers identified in this study are not limited to use for NE cancer patients. Indeed, the ovarian and PDAC PDX models analyzed here (Fig. 6G), both non-NE by diagnosis, exhibit high levels of NE features as well as biomarkers of Cdk5 pathway activation.

To be useful clinically, antibodies to detect these biomarkers will need to be developed into an easy-to-use assay that allows reliable quantitation of biomarker levels in patient tumors, preferably in relatively small samples such as core biopsies.

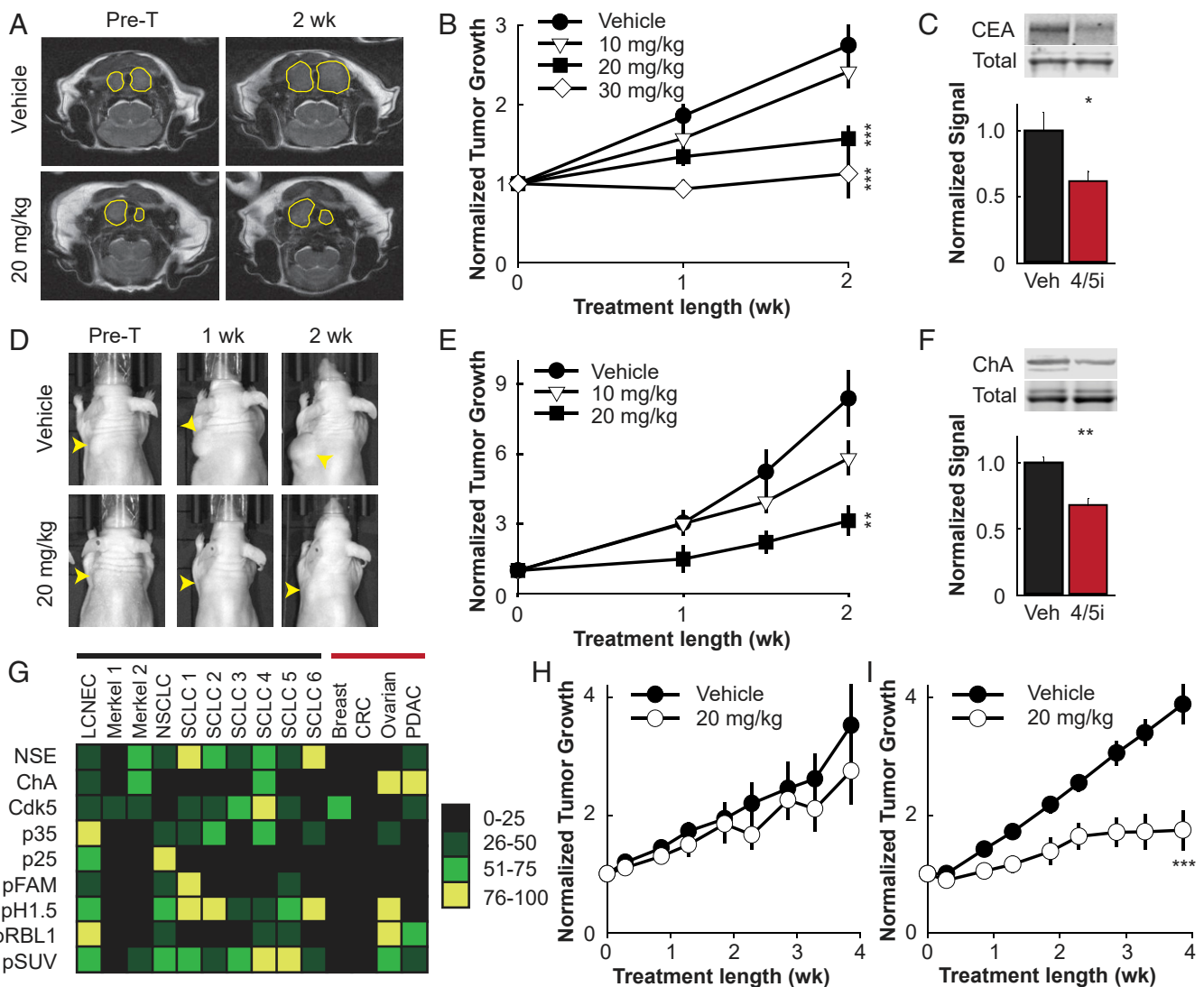


Fig. 6. Cdk5-targeted therapy is effective in biomarker (+) tumors. (A) Representative MRIs of NSE-p25OE MTC model mice prior to treatment (Pre-T) or treated for 2 wk with vehicle or 20 mg/kg BW IndoA. Tumors are outlined in yellow. (B) Quantitation of tumor growth over time from MRI of NSE-p25OE MTC mice treated with vehicle ($n = 6$) or 10 mg/kg ($n = 4$), 20 mg/kg ($n = 6$), or 30 mg/kg ($n = 3$ to 4) BW IndoA. (C) Immunoblot analysis of blood plasma for CEACAM1 (CEA) in vehicle and 20 or 30 mg/kg BW IndoA (4/5i) animals from B. (D) Representative images of TT cell xenograft MTC model mice treated for 2 wk with vehicle or 20 mg/kg BW IndoA. Tumors are marked by yellow arrowheads. (E) Quantitation of tumor growth over time from caliper measurements of TT cell xenograft MTC model mice treated with vehicle or 10 mg/kg or 20 mg/kg BW IndoA ($n = 5$ to 7). (F) Immunoblot analysis of blood plasma in vehicle and 20 mg/kg BW IndoA (4/5i) animals from E. (G) Heat map of protein and phosphoprotein population percentile ranking from immunoblot analysis of NE tumors (black bar) and non-NE tumors (red bar) from PDX model mice. (H and I) Quantitation of tumor growth over time from biomarker-negative Merkel 1 (H; $n = 8$) and biomarker-positive NSCLC (I; $n = 8$) PDX model mice treated with vehicle or 20 mg/kg BW IndoA (20 mg/kg). All error bars represent SEM. Simple comparisons between two groups of normally distributed data were performed using two-tailed Student's t test. * $P < 0.05$, ** $P < 0.01$, *** $P < 0.001$.

Current progress in multiplexed assay systems make these platforms especially attractive for clinical analysis of groups of biomarkers from relatively small biological sources. For example, bead-based multianalyte profiling has been employed for the evaluation of 22 cytokines in a single serum sample from cancer patients (72). This technology has the capacity to distinguish up to 100 different analytes per sample and is compatible with several forms of biological samples, including solid tissue lysates. Once a clinically applicable assay platform is generated, additional preclinical surveys for these biomarkers in multiple PDX models, coupled with Cdk5 inhibitor testing, could aid delineation of finite cutoffs for classification of multiple forms of cancer as predicted responders for Cdk5-targeted therapy and validate progression of such an assay, coupled with novel Cdk5 inhibitors, into clinical trials. At this stage, establishment of standard

operating procedures for collection, handling, storage, and processing of human tumor samples will be critical for ensuring protein- and phosphoprotein-based biomarker integrity and will facilitate ease of implementation in the clinic. Using a multi-analyte platform, analysis of biomarkers for additional oncogenic pathways could be combined with analysis for biomarkers of Cdk5-driven tumors to yield a network readout of the broader signaling state of the tissue. Assessing signaling states across a network of pathways might allow more accurate, stage-dependent, therapeutic decisions to be made for individual patients.

Materials and Methods

Animal Research. All animal work was performed in accordance with the guidelines of the Animal Welfare Act and the Guide for the Care and Use of Laboratory Animals under approved protocols by University of Texas

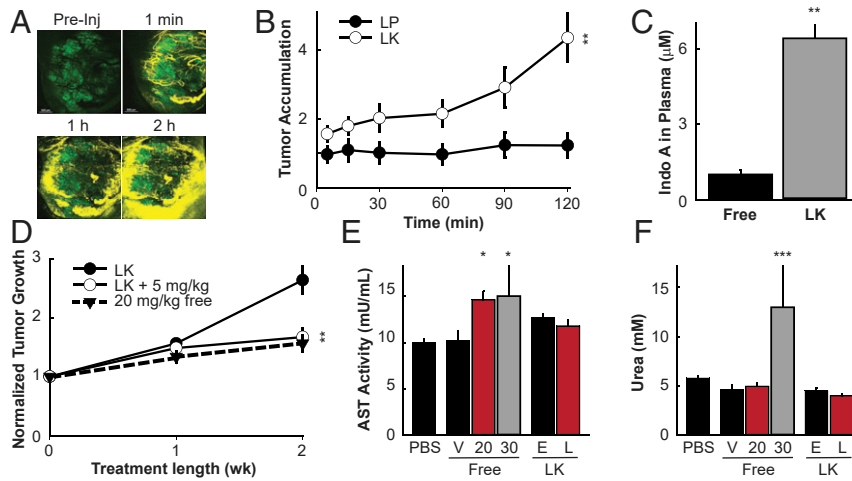


Fig. 7. Targeted delivery of Cdk5 inhibitors via leukosomes. (A) Representative images of MTC tumors from NSE-p25OE mice injected with Cy5.5-labeled LKs and imaged in vivo over 2 h using IVM. Green, tumor cells; yellow, LKs. (B) Quantitation of accumulation of Cy5.5-labeled LPs and LKs in MTC tumors of NSE-p25OE mice over time normalized by total tumor size ($n = 7$ to 8). (C) HPLC-MS analysis of IndoA in blood plasma from NSE-p25OE MTC mice treated with 5 mg/kg BW IndoA (free) or 5 mg/kg BW IndoA encapsulated in LKs (LK) ($n = 3$). (D) Quantitation of tumor growth over time from MRI of NSE-p25 MTC mice treated with empty LKs or 5 mg/kg BW IndoA encapsulated in LKs (LK + 5 mg/kg) compared to 20 mg/kg BW free IndoA from Fig. 6B ($n = 5$ to 6). (E and F) Analysis of blood plasma for AST activity (E) and urea level (F) in animals treated with PBS, unencapsulated IndoA (free) (V, vehicle alone, 20 mg/kg BW, or 30 mg/kg BW), or IndoA encapsulated in LKs (E, empty LK, L, drug loaded LK). All error bars represent SEM. Simple comparisons between two groups of normally distributed data were performed using two-tailed Student's t test. * $P < 0.05$, ** $P < 0.01$, *** $P < 0.001$.

Southwestern (UTSW), University of Alabama at Birmingham (UAB), and Houston Methodist Research Institute (HMRI) Institutional Animal Care and Use Committees.

Antibody Production and Purification. Phosphopeptides (SIT*SPNRTGC-ASXL2, CAPSKLW*TPIKH-FAM53C, CSY*TPVKAIK-FLNB, CAPVEK*SPAK-H1.5, CAN-YE*SPGKI-KNL2, CALA*TPQKNG-LARP6, CSYI*SPHKN-RBL1, CAGLPG*SPKK-SUV39H1; *indicates a phosphorylated residue) were conjugated to *Limulus polyphemus* hemocyanin (Sigma H1757), emulsified with Freund's adjuvant (Sigma F5881 or F5506), and injected s.c. into New Zealand white rabbits (Charles River Laboratories). Rabbits were boosted once and blood was collected twice over a 5-wk period for 12 mo. Blood was allowed to clot at 4 °C for 24 h, centrifuged at 1,000 $\times g$, and plasma was isolated and stored at -20 °C. Phosphorylation state-specific antibodies were purified from plasma using phosphopeptide affinity columns by elution with 100 mM glycine pH 2.5 into 1 M Tris pH 8.6 (11:1 volume ratio, final 80 mM Tris pH ~ 7.5). Antibodies were dialyzed into 50 mM Tris pH 7.6 plus 150 mM NaCl and stored at -20 °C.

Cell Culture and Assays. All cells were tested and verified to be free of mycoplasma contamination. Cell lines were probed for NE markers to verify identity. Cells were cultured at 37 °C and 5% CO₂ in a humidified incubator. Fibroblasts were cultured in Dulbecco's modified Eagle medium (DMEM) with 10% fetal bovine serum (FBS). TT, MTC-SK, and SIN-J cells were cultured in Ham's F-12:medium 199 (1:1) with 10% FBS. hPheo1, H146, and H1184 cells were cultured in RPMI with 10% FBS, 1 mM Na-pyruvate, and 10 mM Hepes. BON cells were cultured in DMEM:Ham's F-12 (1:1) with 10% FBS. INS cells were cultured in RPMI with 10% FBS, 1 mM Na-pyruvate, 10 mM Hepes, 4.5 g/L glucose, and 50 μ M β -ME. TT-RLuc cells were cultured in RPMI with 20% FBS, 100 μ g/mL penicillin, and 100 μ g/mL streptomycin.

Growth assays. Cells were seeded onto a black 96-well plate with a clear optical bottom and allowed to recover overnight. Growth of hPheo1 cells was measured 2 d after inhibitor treatment; and growth of Fibro, TT, MTC-SK, BON, INS, and H146 cells was measured 6 d after inhibitor treatment using Cyquant direct proliferation assay (Invitrogen) and an Optima Fluostar plate reader (BMG LabTech). For SIP experiments, cells received two SIP treatments per experiment. Growth of BON and hPheo1 cells was measured 2 d after initial SIP treatment and growth of Fibro and MTC-SK cells was measured 6 d after initial SIP treatment using procedures described above.

Immunoblot analysis. Cells were seeded onto 6-well dishes and allowed to recover overnight. Cells were treated for 4 h with inhibitors and then lysed in 50 mM NaF and 1% sodium dodecyl sulfate (SDS) with brief sonication. Samples were diluted to equivalent total protein concentrations in 1 \times

Laemmli buffer and separated by SDS/polyacrylamide gel electrophoresis (PAGE). Proteins were transferred onto nitrocellulose for immunoblotting utilizing in-house phosphorylation state-specific antibodies, anti-Cdk5 (sc-173), anti-p35 (sc-820), anti-GAPDH (Sigma G8795), anti-actin (Abcam ab6276), anti-ASXL2 (Abcam ab106540, Sigma sab1407639), anti-Fam53C (Abcam 105679), anti-FLNB (Abnova PAB30702), anti-H1.5 (sc-247158), anti-KNL2 (sc-162587), anti-RBL (sc-318-G), anti-LARP6 (Sigma sab1407657), and anti-SUV39H1 (Sigma S8316). Anti-goat, -rabbit, and -mouse secondary antibodies conjugated to either IRdye 680RD or IRdye 800CW (LiCor) were used for detection on a LiCor Odyssey CLx. Actin and GAPDH were used as sample processing controls. Other total proteins were probed on the same membrane as phosphoproteins unless antibody conditions did not allow.

Human Tissue Analysis.

Collection. Human tissues were collected with patient consent and in accordance with institutional review board (IRB) regulations. Samples were collected under University of Wisconsin-Madison IRB 2011-0145, MD Anderson IRB PA11-0744, University of Texas Southwestern Medical Center IRB STU102010-042 and STU102010-051, National Institute of Child Health and Human Development IRB 00-CH-0093, Louisiana State University IRB 5774, and University of Sydney LNR/13/HAWKE/424-1312-417M. All samples were deidentified prior to use.

Histology. Formalin-fixed, paraffin-embedded samples were cut into 5- μ m sections, deparaffinized, and subjected to microwave antigen retrieval (citrate buffer, pH 6.0). Sections were then stained using standard protocols for H&E or immunostained with antibodies recognizing p35/p25 (sc-820, Santa Cruz Biotechnology) or Cdk5 (308-Cdk5, PhosphoSolutions). For immunostaining, sections were permeabilized with 0.3% Triton X-100, quenched free of endogenous peroxidases, and blocked with 2.5% normal goat serum prior to overnight incubation with primary antibodies at 4 °C. Bound primaries were detected by sequential incubation with biotinylated-secondary antisera, streptavidin-peroxidase (Vector Laboratories), and diaminobenzidine chromogen (DAKO) following the manufacturer's directions.

Immunoblot analysis. Tissues were crushed while frozen then lysed in 50 mM NaF and 1% SDS with brief sonication. Samples were diluted to equivalent total protein concentrations in 1 \times Laemmli buffer and separated by SDS/PAGE. Proteins were transferred onto nitrocellulose for immunoblotting as described above.

Intravital Microscopy. Intravital microscopy (IVM) was performed using an upright Nikon A1R laser scanning confocal microscope with a resonance scanner, motorized and heated stage, and Nikon long-working distance 4 \times and 20 \times dry plan-apochromat objectives housed within the IVM Core at the

MRI. For imaging, NSE-p25OE mice were anesthetized with isoflurane and the ventral surface of the neck was opened to expose the trachea, salivary glands, and MTC tumors. Tumors were positioned in direct contact with the coverslip, visualized using the GFP signal, and positions were selected for imaging. After selection of positions, Cy5.5-labeled LKs and LPs were administered via retroorbital injection and mice were imaged continuously for 2 h using the 4× objective. Images were quantified using Nikon Elements. The tumor accumulation reported was normalized by dividing the area occupied by LKs or LPs by the area occupied by the tumor within each image.

LCMS2 Analysis of IndoA.

Extraction. Sera (25 μ L) were reconstituted in 25 μ L of extraction solution (25% acetonitrile [ACN]/75% H₂O), vortexed for 1 min, diluted with 25 μ L of 100% ACN, followed by two cycles of vortexing for 1 min and incubating at room temperature (RT) for 10 min. Samples were then diluted with 200 μ L of 100% ACN, vortexed for 1 min, then stored at -20° C overnight. Samples were thawed at RT for \sim 10 min, centrifuged at 14,000 \times g for 10 min at 4 $^{\circ}$ C to remove cell debris, then supernatants were transferred to 2-mL tinted glass vials and dried down to \sim 5 to 10 μ L under argon gas at 25 $^{\circ}$ C for 25 min. Samples were immediately reconstituted (adjusted to 210 μ L) in 25% ACN/1% trifluoroacetic acid (TFA)/74% H₂O and centrifuged at 14,000 \times g for 10 min at 4 $^{\circ}$ C to remove any residual debris. The supernatants were then transferred to tinted vials prior to analysis.

LC/MS. Analysis was performed on a Dionex Ultimate 3000 UHPLC+ Focused Stack & Auto Sampler (Thermo Fisher Scientific/Dionex) using a RP C18 Hypersil Gold (100 mm inner diameter [I.D.] \times 4.6 mm, 5 mm 175- \AA pore size; Thermo Fisher Scientific) in-line with an LTQXL mass spectrometer equipped with a heated electrospray ionization source (Thermo Fisher Scientific), and all data were collected in selective reaction monitoring (SRM) mode. The HPLC was configured with binary mobile phases that include solvent A (0.1% TFA/99.9% H₂O), and solvent B (0.1% TFA/15% H₂O/5% ACN). The gradient program steps were run in linear mode as follows; 0 to 6 min at 75 to 50% B (200 μ L/min), 6 to 7 min at 50 to 80% B (200 μ L/min), 7 to 11 min at 80 to 90% B (200 μ L/min), 11 to 12 min at 90 to 25% B (500 μ L/min), and finally 12 to 16 min at 25% B (200 μ L/min). SRM mode was optimized using a parent ion window of 453.2 ± 1.0 *m/z*, 20% normalized collision energy, activation energy at 0.240, activation time of 30 ms, with a daughter ion window of 306.5 ± 1.5 *m/z*. The resultant Xcalibur RAW files were collected in profile mode and the SRM base peak values processed and extracted using Xcalibur version 2.2 sp1.48.

Leukosome Synthesis and Characterization. LKs were developed as previously reported (38). Briefly, 1,2-dipalmitoyl-*sn*-glycero-3-phosphocholine (DPPC) and 1,2-dioleoyl-*sn*-glycero-3-phosphocholine (DOPC) and cholesterol (Avanti Polar Lipids) (4:3:3 molar ratio) were dissolved in ethanol at a final lipid concentration of 9 mM and mixed with membrane proteins, previously resuspended in aqueous buffer at 1:50 protein to-lipid concentrations, using the NanoAssemblr Benchtop platform (Precision NanoSystems, Inc.). Passive loading of IndoA within LKs was obtained by dissolving the drug in the ethanol mixture containing the lipids. Size and polydispersity index were determined through dynamic light scattering analysis using a Nanosizer ZS (Malvern Instruments). Surface charge (zeta potential) was measured using a ZetaSizer Nano ZS (Malvern Instruments).

Magnetic Resonance Imaging. MRI conducted at University of Texas Southwestern Medical Center was performed using a 7-Tesla small animal MRI system (Agilent Inc.) with a 40 mm (I.D.) radio frequency (RF) coil and a 400 mT/m gradient coil set. Animals were anesthetized with isoflurane and imaged in a supine position, head first with the thyroid centered with respect to the center of a RF coil. Two-dimensional (2D) fast spin-echo (FSE) images on three orthogonal planes (transverse, coronal, and sagittal) were first acquired to ensure the position and the orientation of the thyroid tumors. For volume measurements of the thyroid tumors, the high-resolution T₂-weighted FSE axial images was acquired. Major imaging parameters were: repetition time/echo time = 2,500/40 ms, field-of-view = 25.6 \times 25.6 mm, matrix size = 256 \times 256, slice thickness = 1 mm, no gap, eight averages, affording 100- μ m in-plane resolution.

Phosphoproteomics.

Peptide preparation. Mouse tumors were homogenized in 8 M urea lysis buffer (20 mM Hepes pH 8.0, 9 M urea, 1 mM sodium vanadate, 2.5 mM sodium pyrophosphate, 1 mM β -glycerol-phosphate), sonicated, then centrifuged for 15 min at 4 $^{\circ}$ C at 20,000 \times g. Supernatants were reduced with 4.5 mM dithiothreitol for 30 min at 55 $^{\circ}$ C followed by alkylation with 10 mM iodoacetamide. The samples were then digested with trypsin overnight at

room temperature. Digests were acidified with 1% TFA and peptides desalted and purified over Sep-Pak C18 columns (Waters, WAT051910) using 40% acetonitrile in 0.1% TFA for elution. Elutes were lyophilized and stored at -80° C.

Immunoaffinity purification of peptides. Lyophilized peptides were dissolved in immunoaffinity purification (IAP) buffer (50 mM Mops pH 7.2, 10 mM sodium phosphate, 50 mM NaCl), sonicated, and insoluble matter was removed by centrifugation. CDK substrate motif antibody (Cell Signaling Technology, 2324) and MAPK substrate motif antibody (Cell Signaling Technology, 2325) was coupled to protein A beads (Roche). Immobilized antibody was incubated with peptide mixtures, immunoprecipitation was carried out at 4 $^{\circ}$ C overnight, then washed with IAP buffer, and eluted with 0.15% TFA. Eluates were further purified using C18 microtips (StageTips or Eppendorf C18 PerfectPure tips) with elution in 60% MeCN, 0.1% TFA, and then lyophilized. **Analysis by LC-MS/MS.** Purified peptide mixtures were loaded onto a 10 cm \times 75 μ m PicoFrit capillary column (New Objective) packed with Magic C18 AQ reversed-phase resin (Michrom Bioresources) using a Famos autosampler with an inert sample injection valve (Dionex). The column was developed with a 45-min gradient of acetonitrile in 0.125% formic acid (Ultimate pump, Dionex), and tandem mass spectra were collected in a data-dependent manner with a Thermo Fisher Scientific LTQ ion trap mass spectrometer equipped with electron transfer dissociation (ETD) module or with an Orbitrap mass spectrometer.

Assigning peptide sequences using Sequest. MS/MS spectra were evaluated using TurboSequest in the Sequest Browser package supplied as part of BioWorks 3.3 (Thermo Fisher Scientific). Searches were performed against the National Center for Biotechnology Information (NCBI) human protein database. Cysteine carboxamidomethylation was specified as a static modification and phosphorylation was allowed as a variable modification on serine and threonine.

Preclinical Drug Testing. A bitransgenic mouse model of MTC was generated as previously described by crossing NSE-rTA and TetOp-p25GFP parental lines (12). Bitransgenic litters were monitored by MRI. Beginning at 10 to 40 mm³ bilateral tumor volume, animals were treated once every 3 d by immunoprecipitation (IP) with vehicle (0.7% dimethyl sulfoxide [DMSO], 3.4% EtOH, 7.4% PEG400, 3.4% propylene glycol, 3.4% Kolliphor EL, 1.1% Tween 80 in 1 \times phosphate buffered saline), 10 mg/kg, 20 mg/kg, or 30 mg/kg BW IndoA. Animals were monitored by MRI for 2 wk then killed 24 h postfinal injection by CO₂ euthanasia and cardiac perfusion with 0.1 mM ammonium molybdate, 5 mM ethylene glycol-bis(β -aminoethyl ether)-*N,N,N',N'*-tetraacetic acid, 50 mM NaF, 2 mM Na orthovanadate, 10 mM Na pyrophosphate, and protease inhibitors (Sigma S8820) in PBS. Tissues were frozen or fixed in 4% paraformaldehyde for 24 h and submitted for paraffin embedding. Human BON and TT cell xenograft mouse models were generated by implanting 5e⁶ BON or TT-Luc cells s.c. in the NU/NU nude mouse (Cri:NU-Foxn1^{nu}) strain from Jackson Laboratories. Beginning at tumor volumes of 100 to 450 mm³ (average starting sizes between groups varied less than 40 mm³), animals were treated as described above and monitored by caliper measurement for 2 wk. Animals were killed and tissue was processed as described above. All animals were randomly assigned to treatment groups but blinding was not possible.

Scanning Electron Microscopy. Cells were fixed on coverslips with 2.5% (vol/vol) glutaraldehyde in 0.1 M sodium cacodylate buffer overnight at 4 $^{\circ}$ C. After three rinses in 0.1 M sodium cacodylate buffer, they were postfixed with 1% osmium tetroxide in 0.1 M sodium cacodylate buffer for 45 min. Cells were rinsed with water and dehydrated with increasing concentration of ethanol, followed by increasing concentrations of hexamethyldisilazane in ethanol. Cells were air dried under the hood, mounted on SEM stubs and sputter coated with gold palladium in a Cressington 108 auto sputter coater. Images were acquired on a field-emission scanning electron microscope (Zeiss Sigma) at 3.00-kV accelerating voltage.

Statistical Analysis. Shapiro–Wilk tests were performed to determine normality of data. Preclinical drug testing in animal models and accumulation of nanoparticles were analyzed by two-way ANOVA with repeated measures. The Holm–Sidak method was used for all ANOVA tests and all indications of significance are for the treatment group over the entire time period, not individual time points. Immunoblots containing more than two conditions, AST assays, and urea assays were analyzed by one-way ANOVA. Immunoblots of human tumors generated data that were not distributed normally. For this reason, comparisons between distributions of groups were performed using the Kolmogorov–Smirnov test and correlations between data were performed by Spearman rank-order analysis. Simple comparisons

between two groups of normally distributed data were performed using two-tailed Student's *t* test. Sample sizes are provided within figure legends or in results (**P* < 0.05, ***P* < 0.01, ****P* < 0.001).

Toxicity Assays. Prior to cardiac perfusion, blood was collected from animal subjects via retroorbital bleeding. Blood was immediately mixed with (ethylenedinitrilo)tetraacetic acid (10 mM final) then centrifuged at 1,000 × *g* for 10 min at 4 °C to allow isolation of plasma. AST assays (Sigma MAK055) and urea assays (Sigma MAK006) were performed on plasma per the manufacturer's instructions.

Data Availability. Phosphoproteomic data are deposited in PhosphoSitePlus (https://www.phosphosite.org/Supplemental_Files.action). Reprints and permissions information is available at www.pnas.org. Readers are welcome to comment on the online version of the paper. Correspondence and requests for materials should be addressed to J.A.B. (jbibb@uab.edu).

ACKNOWLEDGMENTS. We thank Melanie Cobb, Joseph Goldstein, John Minna, Roswitha Pfragner, and Courtney Townsend for cell lines and Eric Knudsen for primary fibroblast cultures. We thank Haydn Ball and the University of Texas Southwestern Medical Center (UTSW) Protein Technology Core for peptide synthesis, the UTSW Animal Resource Center for antigen injection and blood collection, Robyn Leidel and Kate Luby-Phelps

for help with SEM, Kelly Hartman for assistance with leukosome preparation, John Totenhagen and Samuria Thomas and the University of Alabama at Birmingham (UAB) Small Animal Imaging Facility for additional MRI, and HMRI Intravital Microscopy Core for IVM. We thank Champions Oncology for PDX tissue and preclinical testing in PDX models, and Pfizer for CP681301. We thank Peter Kipp for collegial advice and support. We thank Eckard Wimmer for his contribution to this work. This work was supported by an American Cancer Society Postdoctoral Fellowship (A.M.C.) and the Sackler Foundation (A.M.C. and J.A.B.); a North American Neuroendocrine Tumor Society fellowship (K. Pozo); NIH award S10OD023552-01 (M.T.); an American Thyroid Association Research Grant and the Dedman Family Scholar in Clinical Care Award (S.C.O.); an American Cancer Society Institutional Research Grant Junior Faculty Development Award (S.R.) and the SDHB Pheo/Para Coalition (S.R. and J.A.B.); a North American Neuroendocrine Tumor Society/Neuroendocrine Tumor Research Foundation Basic/Translational Science Investigator Award (R.J.-S.); the William Randolph Heart Foundation, the Robert J. Kleberg, Jr. and Helen C. Kleberg Foundation, Cancer Prevention & Research Institute of Texas Award ID RP170466, and National Cancer Institute (NCI) and the Office of Research on Women's Health Grant 1R56CA213859 (E.T.); an American Cancer Society Research Scholars Award, and NIH awards DA033485-01, MH083711-01, NS073855-01, and R56MH116896 (J.A.B.); and NCI awards 5P30CA142543 (UTSW Simmons Comprehensive Cancer Center) and P30CA013148 (UAB O'Neal Comprehensive Cancer Center).

1. M. Malumbres, M. Barbacid, Mammalian cyclin-dependent kinases. *Trends Biochem. Sci.* **30**, 630–641 (2005).
2. S. Vijayaraghavan, S. Moulder, K. Keyomarsi, R. M. Layman, Inhibiting CDK in cancer therapy: Current evidence and future directions. *Target. Oncol.* **13**, 21–38 (2018).
3. G. I. Shapiro, Cyclin-dependent kinase pathways as targets for cancer treatment. *J. Clin. Oncol.* **24**, 1770–1783 (2006).
4. U. Asghar, A. K. Witkiewicz, N. C. Turner, E. S. Knudsen, The history and future of targeting cyclin-dependent kinases in cancer therapy. *Nat. Rev. Drug Discov.* **14**, 130–146 (2015).
5. R. Dhavan, L. H. Tsai, A decade of CDK5. *Nat. Rev. Mol. Cell Biol.* **2**, 749–759 (2001).
6. F. A. Dhariwala, M. S. Rajadhyaksha, An unusual member of the Cdk family: Cdk5. *Cell. Mol. Neurobiol.* **28**, 351–369 (2008).
7. L. H. Tsai, I. Delalle, V. S. Caviness Jr., T. Chae, E. Harlow, p35 is a neural-specific regulatory subunit of cyclin-dependent kinase 5. *Nature* **371**, 419–423 (1994).
8. M. Angelo, F. Plattner, K. P. Giese, Cyclin-dependent kinase 5 in synaptic plasticity, learning and memory. *J. Neurochem.* **99**, 353–370 (2006).
9. M. S. Lee et al., Neurotoxicity induces cleavage of p35 to p25 by calpain. *Nature* **405**, 360–364 (2000).
10. G. N. Patrick et al., Conversion of p35 to p25 deregulates Cdk5 activity and promotes neurodegeneration. *Nature* **402**, 615–622 (1999).
11. K. Pozo, J. A. Bibb, The emerging role of Cdk5 in cancer. *Trends Cancer* **2**, 606–618 (2016).
12. K. Pozo et al., The role of Cdk5 in neuroendocrine thyroid cancer. *Cancer Cell* **24**, 499–511 (2013).
13. K. Wei et al., An immunohistochemical study of cyclin-dependent kinase 5 (CDK5) expression in non-small cell lung cancer (NSCLC) and small cell lung cancer (SCLC): A possible prognostic biomarker. *World J. Surg. Oncol.* **14**, 34 (2016).
14. W. Xie et al., CDK5 and its activator P35 in normal pituitary and in pituitary adenomas: Relationship to VEGF expression. *Int. J. Biol. Sci.* **10**, 192–199 (2014).
15. H. Lin, M. C. Chen, C. Y. Chiu, Y. M. Song, S. Y. Lin, Cdk5 regulates STAT3 activation and cell proliferation in medullary thyroid carcinoma cells. *J. Biol. Chem.* **282**, 2776–2784 (2007).
16. A. Demelash et al., Achaete-scute homologue-1 (ASH1) stimulates migration of lung cancer cells through Cdk5/p35 pathway. *Mol. Biol. Cell* **23**, 2856–2866 (2012).
17. W. Xie et al., Phosphorylation of kinase insert domain receptor by cyclin-dependent kinase 5 at serine 229 is associated with invasive behavior and poor prognosis in prolactin pituitary adenomas. *Oncotarget* **7**, 50883–50894 (2016).
18. K. Pozo et al., Differential expression of cell cycle regulators in CDK5-dependent medullary thyroid carcinoma tumorigenesis. *Oncotarget* **6**, 12080–12093 (2015).
19. H. K. Ghayee et al., Progenitor cell line (hPheo1) derived from a human pheochromocytoma tumor. *PLoS One* **8**, e65624 (2013).
20. M. Asfari et al., Establishment of 2-mercaptoethanol-dependent differentiated insulin-secreting cell lines. *Endocrinology* **130**, 167–178 (1992).
21. J. H. Weishaupt et al., Inhibition of CDK5 is protective in necrotic and apoptotic paradigms of neuronal cell death and prevents mitochondrial dysfunction. *Mol. Cell. Neurosci.* **24**, 489–502 (2003).
22. K. Rikova et al., Global survey of phosphotyrosine signaling identifies oncogenic kinases in lung cancer. *Cell* **131**, 1190–1203 (2007).
23. B. Sarg, W. Helliger, H. Talasz, B. Förg, H. H. Lindner, Histone H1 phosphorylation occurs site-specifically during interphase and mitosis: Identification of a novel phosphorylation site on histone H1. *J. Biol. Chem.* **281**, 6573–6580 (2006).
24. H. Talasz, B. Sarg, H. H. Lindner, Site-specifically phosphorylated forms of H1.5 and H1.2 localized at distinct regions of the nucleus are related to different processes during the cell cycle. *Chromosoma* **118**, 693–709 (2009).
25. S. H. Park, S. E. Yu, Y. G. Chai, Y. K. Jang, CDK2-dependent phosphorylation of Suv39H1 is involved in control of heterochromatin replication during cell cycle progression. *Nucleic Acids Res.* **42**, 6196–6207 (2014).
26. S. M. Rubin, Deciphering the retinoblastoma protein phosphorylation code. *Trends Biochem. Sci.* **38**, 12–19 (2013).
27. F. A. Dick, S. M. Rubin, Molecular mechanisms underlying RB protein function. *Nat. Rev. Mol. Cell Biol.* **14**, 297–306 (2013).
28. W. F. De Azevedo et al., Inhibition of cyclin-dependent kinases by purine analogues: Crystal structure of human cdk2 complexed with roscovitine. *Eur. J. Biochem.* **243**, 518–526 (1997).
29. D. Parry et al., Dinaciclib (SCH 727965), a novel and potent cyclin-dependent kinase inhibitor. *Mol. Cancer Ther.* **9**, 2344–2353 (2010).
30. S. Turkdogan et al., Carcinoembryonic antigen levels correlated with advanced disease in medullary thyroid cancer. *J. Otolaryngol. Head Neck Surg.* **47**, 55 (2018).
31. F. R. Nobels et al., Chromogranin A as serum marker for neuroendocrine neoplasia: Comparison with neuron-specific enolase and the alpha-subunit of glycoprotein hormones. *J. Clin. Endocrinol. Metab.* **82**, 2622–2628 (1997).
32. K. Hirabayashi et al., Histopathology of gastrointestinal neuroendocrine neoplasms. *Front. Oncol.* **3**, 2 (2013).
33. E. G. Giannini, R. Testa, V. Savarino, Liver enzyme alteration: A guide for clinicians. *CMAJ* **172**, 367–379 (2005).
34. A. Grigorian, C. B. O'Brien, Hepatotoxicity secondary to chemotherapy. *J. Clin. Transl. Hepatol.* **2**, 95–102 (2014).
35. S. Gowda et al., Markers of renal function tests. *N. Am. J. Med. Sci.* **2**, 170–173 (2010).
36. A. Ruggiero, P. Ferrara, G. Attinà, D. Rizzo, R. Riccardi, Renal toxicity and chemotherapy in children with cancer. *Br. J. Clin. Pharmacol.* **83**, 2605–2614 (2017).
37. R. Molinaro et al., Biomimetic proteolipid vesicles for targeting inflamed tissues. *Nat. Mater.* **15**, 1037–1046 (2016).
38. R. Molinaro et al., Design and development of biomimetic nanovesicles using a microfluidic approach. *Adv. Mater.* **30**, e1702749 (2018).
39. H. Kobayashi, R. Watanabe, P. L. Choyke, Improving conventional enhanced permeability and retention (EPR) effects; what is the appropriate target? *Theranostics* **4**, 81–89 (2013).
40. J. O. Martinez et al., Biomimetic nanoparticles with enhanced affinity towards activated endothelium as versatile tools for theranostic drug delivery. *Theranostics* **8**, 1131–1145 (2018).
41. C. Corbo et al., Effects of the protein corona on liposome-liposome and liposome-cell interactions. *Int. J. Nanomedicine* **11**, 3049–3063 (2016).
42. C. Corbo et al., Unveiling the in vivo protein corona of circulating leukocyte-like carriers. *ACS Nano* **11**, 3262–3273 (2017).
43. C. Corbo et al., The impact of nanoparticle protein corona on cytotoxicity, immunotoxicity and target drug delivery. *Nanomedicine (Lond.)* **11**, 81–100 (2016).
44. L. M. Coussens, Z. Werb, Inflammation and cancer. *Nature* **420**, 860–867 (2002).
45. H. Gonzalez, C. Hagerling, Z. Werb, Roles of the immune system in cancer: From tumor initiation to metastatic progression. *Genes Dev.* **32**, 1267–1284 (2018).
46. G. Bollag et al., Clinical efficacy of a RAF inhibitor needs broad target blockade in BRAF-mutant melanoma. *Nature* **467**, 596–599 (2010).
47. K. T. Flaherty et al., Inhibition of mutated, activated BRAF in metastatic melanoma. *N. Engl. J. Med.* **363**, 809–819 (2010).
48. W. Fiskus, N. Mitsiades, B-Raf inhibition in the clinic: Present and future. *Annu. Rev. Med.* **67**, 29–43 (2016).
49. S. C. Chandrasekharappa et al., Positional cloning of the gene for multiple endocrine neoplasia-type 1. *Science* **276**, 404–407 (1997).
50. I. Lemmens et al., Identification of the multiple endocrine neoplasia type 1 (MEN1) gene. The European Consortium on MEN1. *Hum. Mol. Genet.* **6**, 1177–1183 (1997).
51. M. C. Lemos, R. V. Thakker, Multiple endocrine neoplasia type 1 (MEN1): Analysis of 1336 mutations reported in the first decade following identification of the gene. *Hum. Mutat.* **29**, 22–32 (2008).
52. S. K. Agarwal et al., Menin molecular interactions: Insights into normal functions and tumorigenesis. *Horm. Metab. Res.* **37**, 369–374 (2005).

53. L. M. Mulligan *et al.*, Germ-line mutations of the RET proto-oncogene in multiple endocrine neoplasia type 2A. *Nature* **363**, 458–460 (1993).
54. H. Donis-Keller *et al.*, Mutations in the RET proto-oncogene are associated with MEN 2A and FMTC. *Hum. Mol. Genet.* **2**, 851–856 (1993).
55. R. M. Hofstra *et al.*, A mutation in the RET proto-oncogene associated with multiple endocrine neoplasia type 2B and sporadic medullary thyroid carcinoma. *Nature* **367**, 375–376 (1994).
56. S. A. Wells Jr. *et al.*, Vandetanib in patients with locally advanced or metastatic medullary thyroid cancer: A randomized, double-blind phase III trial. *J. Clin. Oncol.* **30**, 134–141 (2012).
57. R. Kurzrock *et al.*, Activity of XL184 (Cabozantinib), an oral tyrosine kinase inhibitor, in patients with medullary thyroid cancer. *J. Clin. Oncol.* **29**, 2660–2666 (2011).
58. S. I. Sherman, Lessons learned and questions unanswered from use of multitargeted kinase inhibitors in medullary thyroid cancer. *Oral Oncol.* **49**, 707–710 (2013).
59. R. L. Beijersbergen *et al.*, E2F-4, a new member of the E2F gene family, has oncogenic activity and associates with p107 in vivo. *Genes Dev.* **8**, 2680–2690 (1994).
60. E. M. Hijmans, P. M. Voorhoeve, R. L. Beijersbergen, L. J. van 't Veer, R. Bernards, E2F-5, a new E2F family member that interacts with p130 in vivo. *Mol. Cell. Biol.* **15**, 3082–3089 (1995).
61. J. M. Trimarchi, J. A. Lees, Sibling rivalry in the E2F family. *Nat. Rev. Mol. Cell Biol.* **3**, 11–20 (2002).
62. L. Litovchick *et al.*, Evolutionarily conserved multisubunit RBL2/p130 and E2F4 protein complex represses human cell cycle-dependent genes in quiescence. *Mol. Cell* **26**, 539–551 (2007).
63. S. Sadasivam, J. A. DeCaprio, The DREAM complex: Master coordinator of cell cycle-dependent gene expression. *Nat. Rev. Cancer* **13**, 585–595 (2013).
64. J. L. Weinstein, H. M. Katzenstein, S. L. Cohn, Advances in the diagnosis and treatment of neuroblastoma. *Oncologist* **8**, 278–292 (2003).
65. E. A. Newman, J. G. Nuchtern, Recent biologic and genetic advances in neuroblastoma: Implications for diagnostic, risk stratification, and treatment strategies. *Semin. Pediatr. Surg.* **25**, 257–264 (2016).
66. H. Toyoda, J. Yin, S. Mueller, E. Wimmer, J. Cello, Oncolytic treatment and cure of neuroblastoma by a novel attenuated poliovirus in a novel poliovirus-susceptible animal model. *Cancer Res.* **67**, 2857–2864 (2007).
67. Z. Chen *et al.*, Multiple CDK inhibitor dinaciclib suppresses neuroblastoma growth via inhibiting CDK2 and CDK9 activity. *Sci. Rep.* **6**, 29090 (2016).
68. K. Zhuang *et al.*, CDK5 functions as a tumor promoter in human colorectal cancer via modulating the ERK5-AP-1 axis. *Cell Death Dis.* **7**, e2415 (2016).
69. S. Goodyear, M. C. Sharma, Roscovitine regulates invasive breast cancer cell (MDA-MB231) proliferation and survival through cell cycle regulatory protein cdk5. *Exp. Mol. Pathol.* **82**, 25–32 (2007).
70. R. Liu *et al.*, Cdk5-mediated regulation of the PIKE-A-Akt pathway and glioblastoma cell invasion. *Proc. Natl. Acad. Sci. U.S.A.* **105**, 7570–7575 (2008).
71. C. J. Strock *et al.*, Cyclin-dependent kinase 5 activity controls cell motility and metastatic potential of prostate cancer cells. *Cancer Res.* **66**, 7509–7515 (2006).
72. Z. A. Dehqanzada *et al.*, Assessing serum cytokine profiles in breast cancer patients receiving a HER2/neu vaccine using Luminex technology. *Oncol. Rep.* **17**, 687–694 (2007).
73. A. Carter *et al.*, Supplementary Files For Selected High Throughput Protein Modification Publications from Cell Signaling Technology. PhosphositePlus. https://www.phosphosite.org/Supplemental_Files.action. Deposited 20 March 2020.

Preclinical characterization of tyrosine kinase inhibitor-based targeted therapies for neuroendocrine thyroid cancer

Karine Pozo^{1,2}, Stefan Zahler³, Keisuke Ishimatsu⁴, Angela M. Carter⁵, Rahul Telange⁵, Chunfeng Tan⁶, Shuaijun Wang³, Roswitha Pfragner⁷, Junya Fujimoto⁸, Elizabeth Gardner Grubbs⁹, Masaya Takahashi⁴, Sarah C. Oltmann² and James A. Bibb^{5,10}

¹Department of Neuroscience, The University of Texas Southwestern Medical Center, Dallas TX, USA

²Department of Surgery, The University of Texas Southwestern Medical Center, Dallas TX, USA

³Center for Drug Research, Ludwig-Maximilians-Universität, Munich, Germany

⁴Advanced Imaging Research Center, The University of Texas Southwestern Medical Center, Dallas TX, USA

⁵Department of Surgery, The University of Alabama, Birmingham AL, USA

⁶Department of Psychiatry, The University of Texas Southwestern Medical Center, Dallas TX, USA

⁷Institute of Pathophysiology and Immunology, Medical University of Graz, Graz, Austria

⁸Department of Translational Molecular Pathology, The University of Texas MD Anderson Cancer Center, Houston TX, USA

⁹Department of Surgical Oncology, The University of Texas MD Anderson Cancer Center, Houston TX, USA

¹⁰Comprehensive Cancer Center, The University of Alabama at Birmingham Medical Center, Birmingham AL, USA

Correspondence to: James A. Bibb, **email:** jbibb@uab.edu

Keywords: medullary thyroid carcinoma; tyrosine kinase inhibitors; vandetanib; targeted therapy; animal model

Received: September 17, 2018

Accepted: December 05, 2018

Published:

Copyright: Pozo et al. This is an open-access article distributed under the terms of the Creative Commons Attribution License 3.0 (CC BY 3.0), which permits unrestricted use, distribution, and reproduction in any medium, provided the original author and source are credited.

ABSTRACT

Medullary thyroid carcinoma (MTC) is a slow growing neuroendocrine (NE) tumor for which few treatment options are available. Its incidence is rising and mortality rates have remained unchanged for decades. Increasing the repertoire of available treatments is thus crucial to manage MTC progression. Scarcity of patient samples and of relevant animal models are two challenges that have limited the development of effective non-surgical treatments. Here we use a clinically accurate mouse model of MTC to assess the effects and mode of action of the tyrosine kinase inhibitor (TKI) Vandetanib, one of only two drugs currently available to treat MTC. Effects on tumor progression, histopathology, and tumorigenic signaling were evaluated. Vandetanib blocked MTC growth through an anti-angiogenic mechanism. Furthermore, Vandetanib had an apparent anti-angiogenic effect in a patient MTC sample. Vandetanib displayed minimal anti-proliferative effects *in vivo* and in human and mouse MTC tumor-derived cells. Based on these results, we evaluated the second-generation TKI, Nintedanib, alone and in combination with the histone deacetylase (HDAC) inhibitor, Romidepsin, as potential alternative treatments to Vandetanib. Nintedanib showed an anti-angiogenic effect while Romidepsin decreased proliferation. Mechanistically, TKIs attenuated RET-, VEGFR2- and PI3K/AKT/FOXO signaling cascades. Nintedanib alone or in combination with Romidepsin, but not Vandetanib, inhibited mTOR signaling suggesting Nintedanib may have broader anti-cancer applicability. These findings validate the MTC mouse model as a clinically relevant platform for preclinical drug testing and reveal the modes of action and limitations of TKI therapies.

INTRODUCTION

MTC is a rare indolent cancer derived from calcitonin secreting C-cells of the thyroid gland, which occurs either as a sporadic or hereditary disease [1]. Most MTC patients carry activating mutations in the Rearranged-during-transfection (RET) gene, which encodes a receptor tyrosine kinase [2, 3]. Therefore therapeutics that target RET have been developed [4]. Two TKIs, Vandetanib and Cabozantinib, have been approved for the treatment of advanced MTC patients [5–7]. Limited drug responses as well as drug-associated adverse events have limited the number of patients for which these treatments can be used [8]. Furthermore, resistance to TKIs is common and their efficacy in stopping disease progression is not ideal [9]. Thus expanding the repertoire of therapies available for the treatment of MTC and other NE cancers is essential. In particular, defining the mode of action of current MTC drugs would advance our understanding of relevant oncogenic signaling pathways and could suggest additional drugs or combinations to more effectively treat these cancers.

Vandetanib was the first drug approved for MTC treatment in 2011 [5, 10]. It is a first generation TKI with demonstrated cross-specificity for VEGF, RET and EGF receptors [3]. However, its modes of action in MTC have not been well defined. Earlier work in cultured MTC cells as well as preclinical MTC mouse and *Drosophila* models indicated that Vandetanib impedes MTC proliferation via RET inhibition [11–13]. Paradoxically, Vandetanib-response does not correlate clearly with patient's RET-mutational status, as indicated by a randomized phase III clinical trial [14]. Overall, the efficacy of Vandetanib appears to be limited to an undefined patient sub-population. Thus insight into the mechanisms of action of Vandetanib could guide the development of more effective therapeutic strategies.

Given the limitations of the drugs currently available for clinical application, it is understandable that alternative TKI therapies are the subject of active investigation. For example, the second generation TKI, Nintedanib is a multi-kinase inhibitor that has been approved for the treatment of idiopathic pulmonary fibrosis [15] and is currently undergoing phase 2 clinical trials for MTC in Europe (ClinicalTrials.gov Identifier: NCT01788982). Nintedanib targets VEGF, FGF, and PDGF receptors [16], and blocks angiogenesis, the process by which new blood vessels form within tumors, and does not exhibit the common adverse events associated TKI. Although Nintedanib shares common targets with Vandetanib, the anti-cancer effects of these two TKIs have not previously been compared.

We have recently developed a clinically relevant mouse model of MTC in which transgenic overexpression of p25-GFP, a cyclin-dependent kinase 5 (Cdk5) activator causes MTC. Oncogenic signaling pathways that are

downstream of Cdk5 and drive mouse MTC growth are also detected in sporadic MTC patients [17, 18]. In particular, p25 expression leads to inactivation of the tumor suppressor, retinoblastoma protein (Rb) and deregulated expression of cell cycle proteins, both in the mouse model tumors and in MTC patients. Here we use this animal model to characterize and compare the anti-cancer effect and modes of action of an established MTC drug, *i.e.*, Vandetanib, and that of two experimental TKI-based MTC treatments, Nintedanib alone and in combination with the HDAC inhibitor, Romidepsin, which has previously been co-administrated with TKIs.

RESULTS

***In vivo* monitoring of mouse tumor growth by magnetic resonance imaging (MRI)**

An animal model commonly used for preclinical testing of anti-cancer therapies is one in which human cells are injected subcutaneously in immunocompromised mice and tumor growth is followed manually by measurement with calipers. In contrast, NSE/p25-GFP mouse tumors are smaller and arise spontaneously within the thyroid gland, dorsal to the salivary glands [17]. Advanced *in vivo* imaging techniques such as MRI allow monitoring tumor progression in this model. To determine the optimal conditions at which to conduct preclinical drug testing, we monitored tumor volume *in vivo* by MRI starting 9 weeks after induction of p25-GFP expression (see Materials and Methods), when tumors become detectable (Figure 1A). Tumors developed from the thyroid gland as bilateral masses on each side of the trachea [17]. Initial tumor growth was slow, consistent with a neuroendocrine phenotype. Starting approximately 14 weeks after transgene induction, tumor growth accelerated and tumor volumes at least doubled over a 2-week period (Figure 1B). Average volumes increased from $18.8 \pm 6.8 \text{ mm}^3$ at week 14 to $47.5 \pm 15.9 \text{ mm}^3$ at week 16. Despite growth heterogeneity between littermates, tumor volumes doubled within a 2-week period in all animals when tumor volumes reached 5–10 mm^3 . Therefore, preclinical testing of anti-cancer drugs was started about 14 weeks after transgene induction and when tumor volume was at least 5–10 mm^3 .

Anti-cancer effects of Vandetanib are mediated by disruption of tumor vasculature

As an important first step, Vandetanib, a drug currently in clinical use to treat MTC, was used to treat MTC model mice. Initial tumor volume was determined and either Vandetanib or control vehicle were administered for 2 weeks. Tumor volumes increased by 3.2-fold in the vehicle-treated animals during this period, whereas tumor volumes increased only by 1.2-fold in the Vandetanib-treated animals (Figure 2A). Subjects treated

with vehicle alone exhibited severe signs of morbidity necessitating euthanasia. However, tumor progression remained minimal in animals subjected to an additional 2 weeks of Vandetanib treatment (4 weeks total, Figure 2B). Resumption of tumor growth was apparent upon discontinuation of Vandetanib administration.

We have previously demonstrated that mouse tumors and MTC patient samples were indistinguishable with regard to the activation of a number of oncogenic signaling pathways [17]. For example activated RET, a hallmark of MTC, is detected in mouse MTCs as evidenced by pY1062 RET immunoreactivity (Figure 2C). Also RET signaling was disrupted in Vandetanib-treated animals as evidenced by decreased phosphorylation of RET at Tyr-1062. Furthermore, VEGFR2 inactivation occurred, as determined by attenuation in phosphorylation of this receptor tyrosine kinase (RTK) at Tyr-1115. These effects were accompanied by reduced activating phosphorylation of ERK1/2. These effects were consistent with the established role of Vandetanib as a VEGFR2 and RET inhibitor [11]. These data demonstrate that the MTC mouse model is suitable to test and characterize the modes of action of Vandetanib as well as other RET inhibitors or alternative anti-cancer therapies.

Histological analysis of the tumors by H&E and Hoechst staining revealed numerous necrotic areas and reduced cellular density (Figure 2D). To better understand these effects, microvessel density was evaluated by staining CD31-positive endothelial cells within tumors. Microvessel density was reduced 3.5-fold in Vandetanib-treated animals compared to controls. These data indicate that Vandetanib invokes an anti-angiogenic response in MTC tumors as a major mode of action. This is consistent with the known spectrum of Vandetanib as a VEGFR2

inhibitor and the well-characterized role of that receptor in tumor angiogenesis.

Despite the anti-angiogenic effects revealed here, Vandetanib was initially developed as a RET inhibitor with anti-proliferative potential. To evaluate this mode of action, cell proliferation was assessed by Ki67 staining. Surprisingly, cell proliferation was unaffected by Vandetanib treatment compared to vehicle-treated controls (Figure 2D). Together these findings suggest that Vandetanib acts by disrupting tumor vasculature, resulting in tumor tissue necrosis, without directly affecting cell growth and total tumor volume.

To determine if this effect occurs in humans, we obtained very rare pathology samples from a single MTC patient biopsied before and after treatment with Vandetanib. Interestingly, microvessel density within these samples was reduced after treatment, which is similar to the effects observed in MTC model mice (Figure 2E). These results, albeit from a very rare single human case, support that Vandetanib may act primarily as an anti-angiogenic drug and, that our MTC mouse model is clinically relevant and can be used for the preclinical testing of anti-cancer therapies.

Given the lack of effect of Vandetanib on cell proliferation in mouse tumors, we examined how Vandetanib impacted the proliferation of cultured MTC cells derived from our mouse model (MTCp25OE) [17] as well as two cell lines derived from non-RET mutated sporadic human MTC (MTC-SK and SIN-J) (Figure 3A) [18, 19]. Previous studies showed the proliferation of these human cell lines to be Cdk5-dependent [17]. MTCp25OE cells were not inhibited by 1 μ M Vandetanib, although anti-proliferative effects were achieved at a concentration of 10 μ M. Effects at both 1 and 10 μ M were limited in

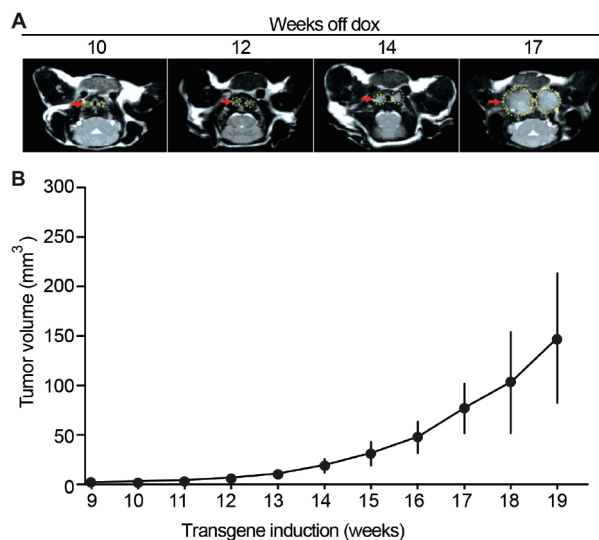


Figure 1: Mouse MTC tumor growth monitored *in vivo* by MRI. (A) Representative MRI images of tumors at 10, 12, 14 and 17 weeks after transgene induction (see Methods). (B) Quantification of tumor volumes shows tumor growth over time after transgene induction, N = 4.

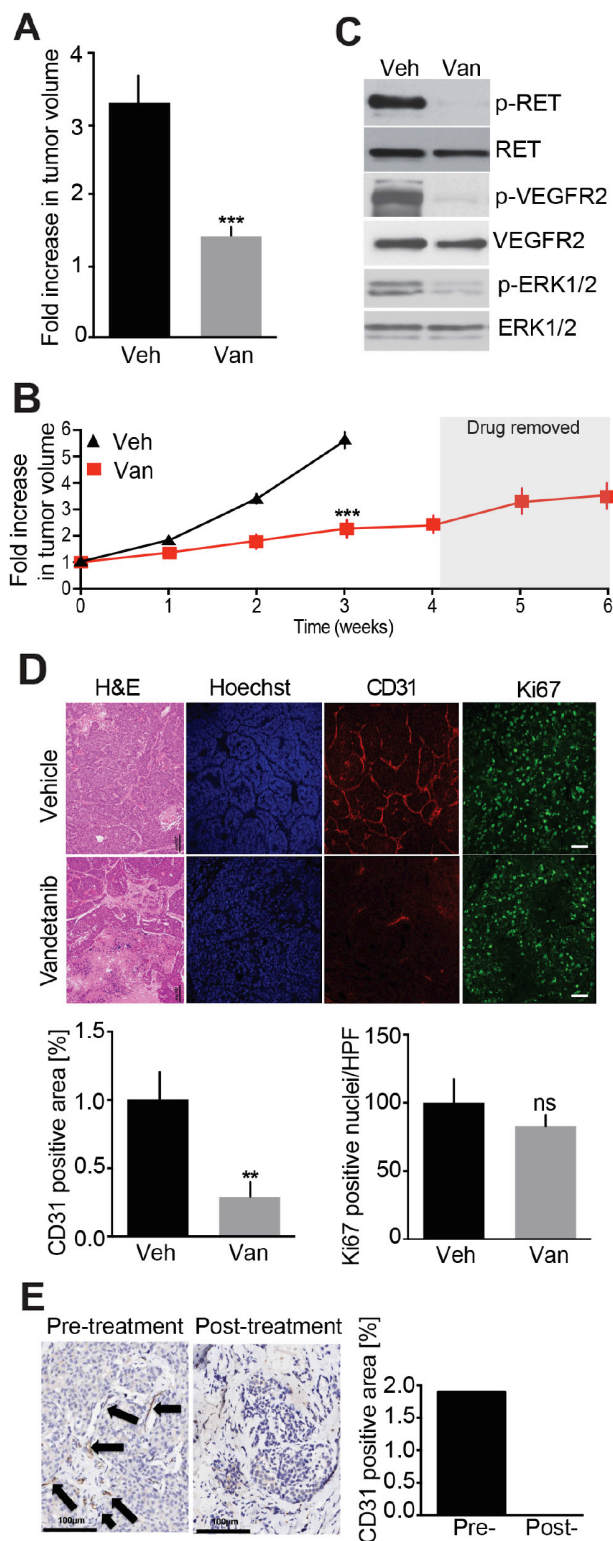


Figure 2: Evaluation of Vandetanib anti-tumor effect in a MTC mouse model. (A) Analysis of tumor volumes after a 2-week treatment with either Vandetanib (25 mg/kg/day, Van, o.g.) (N = 5) or vehicle (Veh, o.g.) (N = 6). (B) Monitoring of tumor volumes by MRI during 6-weeks. Mice were dosed with Vandetanib (25 mg/kg/day, i.p.) (N = 4) or vehicle (i.p.) (N = 4) for 4 weeks and treatment was stopped for the next 2 weeks. (C) Immunoblot analysis of tumor lysates after a 3-week Vandetanib or vehicle treatment. (N = 3) (D) Immunohistological analysis of tumors for CD31 and Ki67 and quantifications after a 3-week Vandetanib or vehicle treatment. (E) CD31 staining and quantification of a MTC patient tumor biopsy before and after Vandetanib treatment. Scale bars are 100 μ m. Arrows indicate microvessels.

both MTC-SK and SIN-J human sporadic MTC cell lines. These results further support that Vandetanib lacks strong anti-proliferative capacity toward sporadic forms of MTC, which depend upon aberrant Cdk5 activity for proliferation and do not harbor known RET mutations.

Mutations that constitutively activate RET are always detected in familial forms of MTC and Multiple Endocrine Neoplasia (MEN) 2A and the proliferation of MEN2 patient-derived MTC cell lines is inhibited by Vandetanib [20]. To determine if Vandetanib has stronger anti-proliferative effects in MTC cells harboring RET mutations, we compared the dose-dependent effects of Vandetanib on sporadic (MTC-SK) and familial (TT) MTC cell lines (Figure 3B). A concentration of 1 μM Vandetanib inhibited TT cell proliferation by >50% while it did not stop MTC-SK cell proliferation (Figure 3A, 3B). This observation indicates that Vandetanib exhibits

greater potency toward RET-mutated TT cells compared to sporadic MTC-SK cells. This suggests that Vandetanib anti-proliferative properties are dependent on the RET mutation status in cultured MTC cell lines. However the anti-angiogenic properties of the drug may predominate over anti-proliferative effects *in vivo*, given that RET mutational status in MTC patients does not correlate with responsiveness to Vandetanib treatment [14].

Evaluation of a second-generation TKI, Nintedanib as a treatment for MTC

Having found that Vandetanib acts via anti-angiogenesis and to expand the repertory of drugs available for MTC patient treatment, we decided to test a TKI with proven anti-angiogenic properties. Nintedanib antagonizes RET and VEGF receptors and blocks

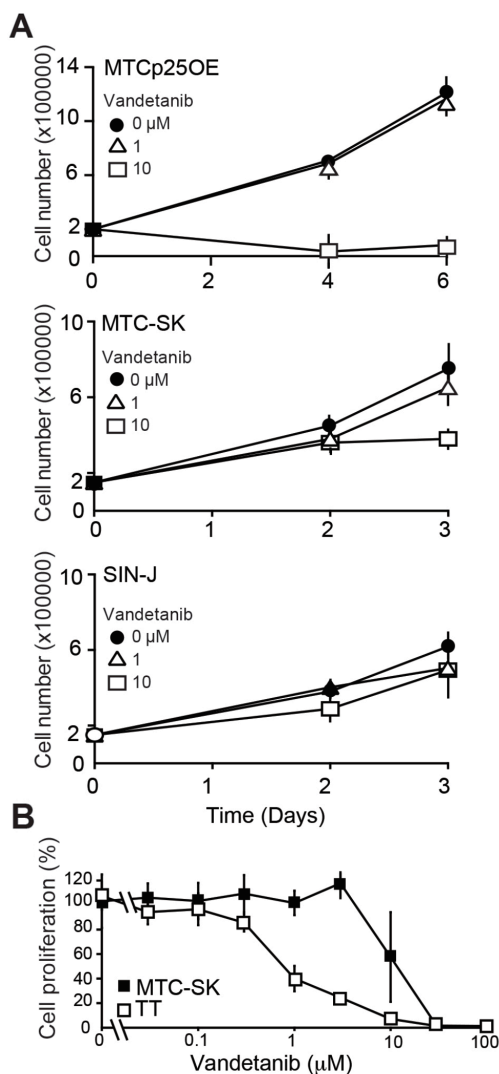


Figure 3: Analysis of Vandetanib anti-proliferative effect in cultured MTC cells. (A) Proliferation assay of MTC cell lines treated with Vandetanib. **(B)** Cell survival assay and dose-response curve of TT cells and MTC-SK cells after a 6-day Vandetanib treatment. N = 2 experiments, N = 3 replicates/experiment.

endothelial cell proliferation and tumor growth in mouse models of pancreatic and lung cancers [16, 21]. In our MTC animal model, Nintedanib arrested tumor growth across a 4-week treatment period compared to vehicle-treated controls (Figure 4A). Furthermore, Nintedanib showed the same tumor progression inhibition capability as Vandetanib across 3 weeks of treatment (Figure 4B). To determine if the Nintedanib inhibitory effect was dependent on continuous drug administration, treatment was interrupted for 2 weeks (Figure 4A). As previously seen for Vandetanib, tumors resumed growth once Nintedanib treatment was discontinued. Histological examination of tumors after a 3-week Nintedanib regimen revealed necrosis, tissue disorganization and a 5-fold reduction in CD31-positive cells (Figure 4C). Thus the anti-angiogenic effect of Nintedanib was greater than that of Vandetanib (Figure 2D) and was accompanied by a statistical significant attenuation in cancer cell proliferation as evidenced by a 1.5-fold reduction in Ki67 signal (Figure 4C). Consistent with its anti-angiogenic effects, Nintedanib therapy also reduced phosphorylation of RET, VEGFR2, and ERK1/2 in MTC tumors (Figure 4D).

To further characterize the anti-proliferative effect of Nintedanib, MTCp250E cells were treated with the drug for 2-4 days. Cell proliferation was inhibited by 1 μ M Nintedanib while 10 μ M drug caused cell death (Figure 4E), thereby confirming that Nintedanib exerts anti-proliferative effect on cancer cells. As a second set of experiments, the effects of Nintedanib on RET-mutated familial MTC-derived TT cell growth was compared to that of Vandetanib. In dose-response analysis, Nintedanib exhibited 10-fold greater anti-proliferation potency than Vandetanib (Supplementary Figure 1) with IC_{50} values (\pm SEM) of 0.12 (\pm 0.05) μ M for Nintedanib and 1.09 (\pm 0.28) μ M for Vandetanib. Thus Nintedanib has stronger anti-proliferative properties than Vandetanib in sporadic and RET-mutated familial cultured MTC cells and in our MTC mouse model. Overall our observations indicate that Nintedanib may have stronger anti-cancer effects than Vandetanib but with no improved outcome on decreasing tumor volume, which suggests that Nintedanib and Vandetanib may have distinct mechanisms of action.

Preclinical evaluation of a combination TKI/HDAC inhibitor therapy for MTC

Both Nintedanib and Vandetanib have strong anti-angiogenic effects *in vivo* while exhibiting no to moderate anti-proliferation properties. HDAC inhibitors are considered promising anti-mitotic agents, which may render solid tumors more vulnerable to other anti-cancer therapies. Romidepsin is an FDA approved HDAC inhibitor which exhibited synergistic inhibitory effects with TKIs in the treatment of non-small cell lung cancer (NSCLC) in preclinical models [22–24] and in clinical trials [25]. We tested the anti-proliferative effect

of Romidepsin on mouse MTC cells in culture. A 50% reduction in cell growth was achieved at a concentration of 100 nM (Figure 5A). We then evaluated the anti-tumor effects of Romidepsin alone and in combination with Nintedanib *in vivo*. Romidepsin treatment exhibited a trend toward reduction of MTC tumor growth (Figure 5B). Combinatorial treatment with Romidepsin and Nintedanib slowed tumor growth but showed no improved effect on measured tumor volume compared to Nintedanib alone. Romidepsin reduced Ki67 values by 1.5-fold (Figure 5C), which was comparable to Nintedanib effect on Ki67 values. Importantly, the combination caused a 2.7-fold decrease in this marker of cell proliferation, thereby showing a synergistic effect of combined treatments on cell proliferation. However, Romidepsin did not significantly reduce microvessel density while Nintedanib alone or in combination lowered CD31 staining.

Romidepsin had no effect on phosphorylation of RET, VEGFR2, or ERK1/2 while Nintedanib alone or in combination with Romidepsin lowered these signals, consistent with the previous results (Figure 5D). Importantly, the level of de-acetylated histone H4 was increased in tumors from Romidepsin and Romidepsin + Nintedanib treated animal but not in those treated with Nintedanib alone. These observations confirm that Romidepsin blocks HDAC activity as expected but not RTK signaling, while the combination of Romidepsin and Nintedanib blocked both HDAC and RTK signaling. While Romidepsin and Nintedanib synergized mechanistically, the combination therapy did not decrease tumor volume more efficiently than Nintedanib alone.

To better understand the relationship between drug administration and tumor response from the perspective of intermittent treatments, such as those experienced by patients, MTC model mice were treated for extended periods with cycles of drug treatment and removal (Supplementary Figure 2). After 3 cycles, tumors appeared to achieve resistance to the drug. Together with the other results presented here, these observations indicate that chronic Nintedanib treatment is necessary to block tumor growth but that tumors may eventually become resistant to the drug.

Nintedanib and Vandetanib inhibit PI3K/AKT signaling

Vandetanib and Nintedanib antagonize RET signaling, block tumor development but exhibit different anti-proliferative effects on tumor cells. These observations suggest that the mode of action of Vandetanib and Nintedanib are not identical and mediated not only via RET-dependent but also via RET-independent signaling pathways. The PI3K/AKT pathway is commonly deregulated in thyroid cancers, including MTC [26, 27]. Therefore, we examine how TKI- and HDAC-based treatments affect PI3K/AKT signaling

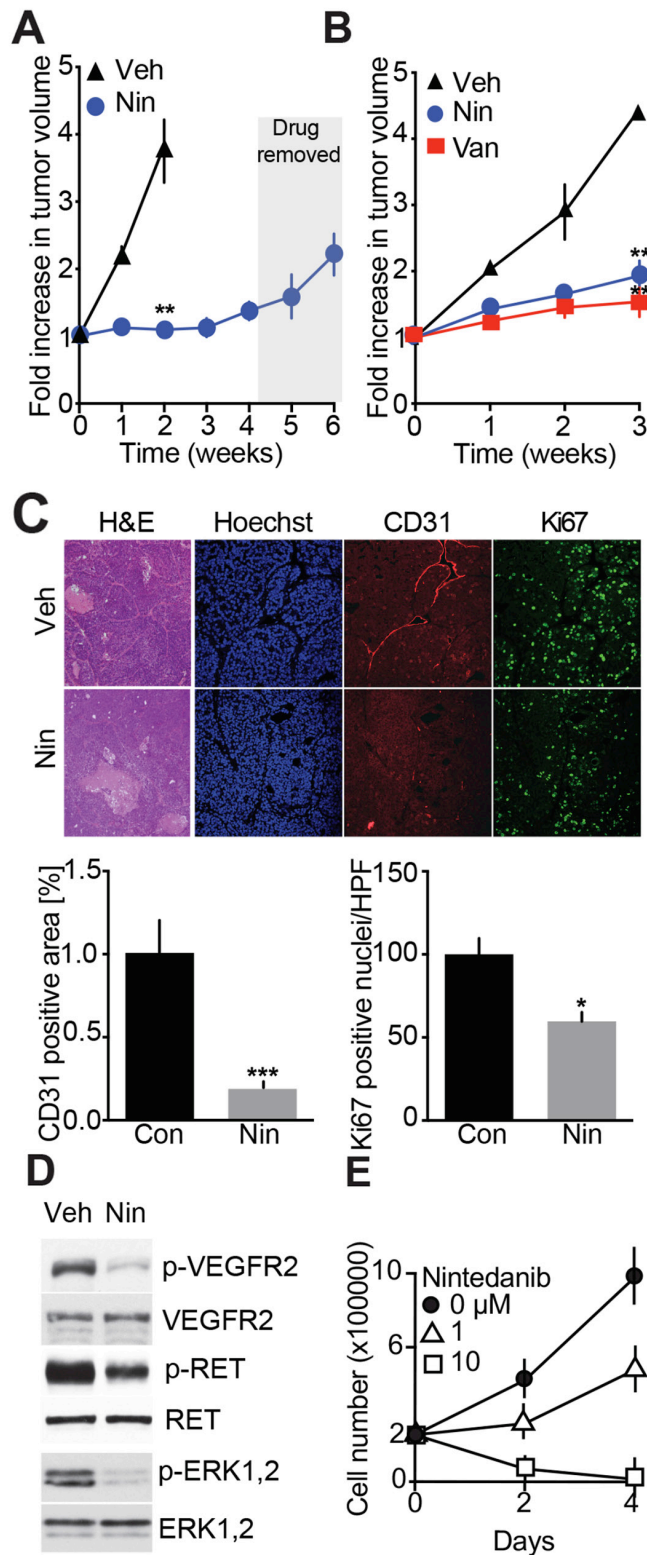


Figure 4: Evaluation of Nintedanib anti-MTC tumor and cell anti-proliferation effects. (A) Effects on tumor volume monitored by MRI over 6-weeks. Mice were dosed with Nintedanib (35 mg/kg/day, i.p., Nin) (N = 3) or vehicle for 4 weeks (N = 3) and treatment was stopped for the next 2 weeks. (B) MRI-monitoring of tumor growth during a 3-week treatment with either Vandetanib (25 mg/kg/day, o.g.) (N = 4), Nintedanib (100 mg/kg/day, o.g.) (N = 4) or vehicle (N = 3). (**p=0.0031, one-way ANOVA, Bonferroni's post hoc, week 3) (C) Immunohistological analysis of tumors for CD31 and Ki67 and quantifications after a 3-week Nintedanib or vehicle treatment. Scale bars are 100 μm, (N = 4). (D) Immunoblot analysis of tumors after a 3-week treatment with Nintedanib or vehicle (N = 3). (E) Proliferation assay of MTC cell lines treated with Nintedanib. N = 2 experiments, N = 3 replicates/experiment.

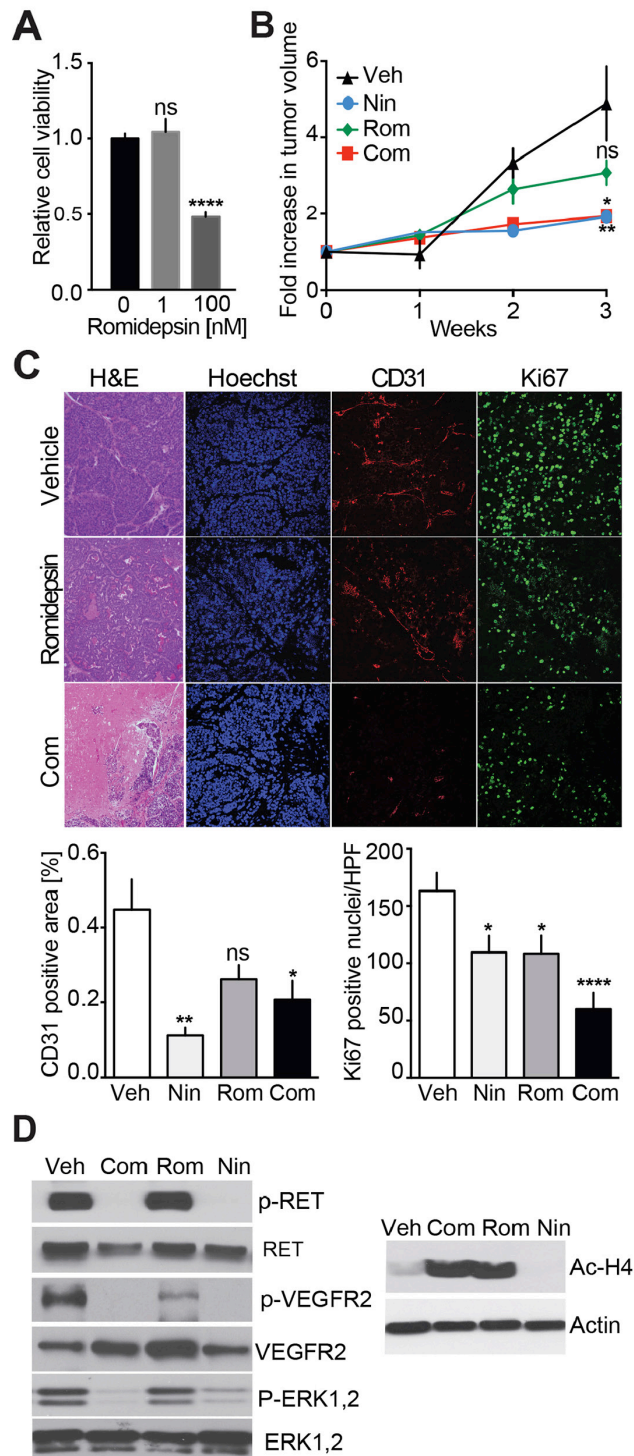


Figure 5: Analysis of Nintedanib/Romidepsin anti-tumor effect on MTC proliferation. (A) Cell survival analysis of MTCp25OE following treatment with increasing Romidepsin concentrations (**** $p < 0.0001$, one-way ANOVA, Bonferroni's post hoc) (B) Monitoring of tumor volumes by MRI during a 3-week treatment with Nintedanib (35 mg/kg/day i.p.) (N = 5), Romidepsin (0.78 mg/kg/day, i.p.) (N = 5), or Nintedanib (35 mg/kg/day, i.p.) + Romidepsin (0.38 mg/kg/day, i.p., Com) (N = 10) or vehicle (i.p.) (N = 11) (** $p < 0.005$, one-way ANOVA, Bonferroni's post hoc, week 3). (C) Immunohistological analysis of tumors for CD31 and Ki67 and quantifications after a 3-week treatment with either Romidepsin or Nintedanib + Romidepsin (Rom), or vehicle. Scale bars are 100 μm . (D) Immunoblot analysis of tumors after a 3-week treatment with vehicle, Nintedanib + Romidepsin, Romidepsin, or Nintedanib (N = 3).

cascades (Figure 6). AKT phosphorylation at Thr308 (phospho-Thr308) and Ser473 (phospho-Ser473) were detected in all mouse MTC tumors, demonstrating that the PI3K/AKT pathway is activated in these tumors, as observed in MTC patients [28, 29] (Figure 6A). Phospho-Thr308 AKT was reduced in tumors from Vandetanib, Nintedanib, and Nintedanib + Romidepsin treated mice, but not in mice treated with Romidepsin alone in comparison with vehicle-treated MTC mice. Phospho-Ser473 remained unchanged. These findings indicate that TKI-based treatments inhibited the PI3K/AKT pathway, and support the observation that phospho-Thr308 is a better marker of AKT activity than phospho-Ser473 [29]. Consistent with these effects, phosphorylation of FOXO1, an AKT downstream target, was reduced upon treatment with TKIs but not Romidepsin alone (Figure 6B). To investigate further the effect of TKI-based treatments on PI3K/AKT pathways, we examined the activation state of the mTOR signaling cascade, which is another well-characterized PI3K/AKT downstream target (Figure 6C). Nintedanib alone or in combination with Romidepsin inhibited mTOR signaling as evidenced by a decrease in the phosphorylation of mTOR downstream effectors, S6K and 4EBP-1. Interestingly, Vandetanib had no effects on mTOR. Together these findings indicate that Vandetanib

and Nintedanib use different mechanisms downstream of PI3K/AKT to stop MTC growth, although the two TKIs show several mechanistic similarities. These data also suggest that mTOR targeting is dependent on the type of TKI that is administered.

DISCUSSION

Here we conducted *in vivo* studies using a unique animal model of MTC to examine the anti-cancer effects of Vandetanib, one of only two drugs approved for MTC therapy. Biopsies and histological evaluations are rarely performed during or following chemotherapy treatment, and surprisingly few preclinical studies have examined the mode of action of TKIs in MTC. The MTC mouse model used here encompasses molecular and physical features related to sporadic MTC patients, which represent 75% of all MTC cases. The model exhibited responses to Vandetanib and histological effects consistent with those observed in human patients. Thus our mouse model of MTC appears valid for the preclinical testing of drug treatments for MTC. Investigations with this model could provide insight regarding the modes of action, doses, and administration schedules prior to testing in cancer patients [30].

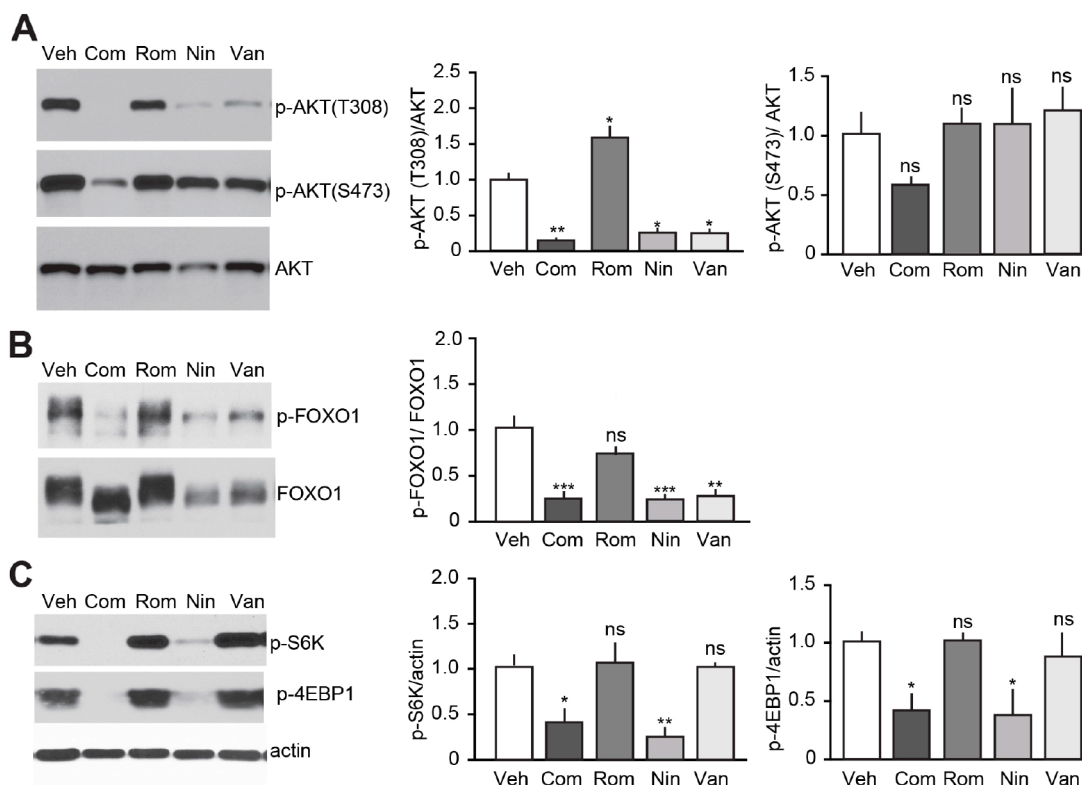


Figure 6: Effect of TKI-based therapies on the PI3K/AKT pathway. Immunoblot analysis of tumors after a 3-week treatment with either Vandetanib (25 mg/kg/day), Nintedanib (35 mg/kg/day), Romidepsin (0.78 mg/kg/day) or Nintedanib (35 mg/kg/day) + Romidepsin (0.38 mg/kg/day, Com) or vehicle for (A) AKT, (B) FOXO1 and (C) mTOR, (N = 3-4) (p-AKT(T308), ****p<0.0001; p-AKT(S473), ns p=0.1433; p-FOXO1, ***p<0.005; p-S6K, ***p<0.005; p-4EBP1, ***p<0.005, one-way ANOVA, Bonferroni's post hoc).

The impetus behind Vandetanib use as a MTC therapy stemmed from its inhibition profile which included antagonization of RET, the oncogene product often regarded as the main MTC driver [1, 11, 31]. Here we found that Vandetanib stopped tumor growth *in vivo* by causing necrosis, while having no effect on MTC cell proliferation. This observation indicates that the mode of action of Vandetanib is primarily through tumor associated-endothelial cells and subsequent blood vasculature reduction rather than via direct inhibition of RET in MTC tumor cells, as previously observed in preclinical model of colon cancers [30]. Likewise, the RET-targeting TKI, Sunitinib, mediates its renal cell carcinoma anti-tumor effect via tumor-associated endothelial cells and not tumor cells [32]. In neuroblastoma, Vandetanib exerts a dual action by targeting VEGF receptors on tumor endothelial cells and RET on tumor cells as demonstrated in neuroblastoma [33]. Together with our observations, these studies shows that TKIs do not always directly target tumor cells as may be expected from cell culture studies, but instead may target either the tumor microenvironment, tumor cells, or both. Characterizing the microenvironment of MTC tumors may help define markers and thus stratify patients so that those likely to benefit from Vandetanib treatment may be identified. It would also be of interest to determine if the recently developed and very specific RET inhibitors, BLU-667 and LOXO-292 [4] exhibit improved anti-angiogenic and antiproliferative properties compared to Vandetanib and Nintedanib *in vivo* and in cell culture conditions.

The PI3K/AKT pathway has emerged as a valid cancer drug target. In particular, targeting the PI3K/AKT/mTOR pathways using mTOR inhibitors improved progression-free survival in patients with advanced pancreatic neuroendocrine tumors [34]. Here we show that Vandetanib inhibits the PI3K/AKT/FOXO1 pathway but not the PI3K/AKT/mTOR pathway in MTC mouse tumors. These observations support the rationale of combining Vandetanib and an mTOR inhibitor to improve MTC treatment, an approach that is underway in current clinical trials (see clinicaltrials.gov Identifier NCT01582191). Preclinical studies in colon cancer mouse models have demonstrated that the doses and administration schedules (*e.g.*, sequential or concurrent) of Vandetanib or drug combination could change the treatment outcome [13, 30]. Furthermore, Nintedanib, which blocks VEGFR2, RET, ERK1,2 and PI3K/AKT/FOXO1 like Vandetanib, also inhibits PI3K/AKT/mTOR, but may still have limited long-term anti-tumor effects on MTC due to the development of resistance. Therefore determining the right doses and best schedule may be crucial for the success of a Vandetanib/mTOR inhibitor clinical trial. It may also be important to determine if a Vandetanib/mTOR inhibitor combination or a Nintedanib monotherapy is the most beneficial through future patient-centered studies. Regardless, targeted therapies other than TKIs that affects these pathways should be explored further. For

example, the inhibitor of the molecular chaperone HSP90 (AUY922) targets RET and mTOR signaling and inhibits the growth of cultured MTC cell lines [35].

While Vandetanib and Nintedanib both stopped tumor development, they had weaker effects than expected on tumor cell proliferation based on previously published studies [20]. We hypothesized that combining these TKIs with an antiproliferative drug could improve TKI efficacy on MTC mouse tumor development. We chose the cyclic HDAC inhibitor Romidepsin to test in combination with Nintedanib. Although tumor cell proliferation and microvessel density were decreased, synergistic effects of the two drugs *in vivo* did not occur under our experimental conditions. In fact the overall effect on tumor growth was similar to that observed for Nintedanib alone. Although HDACs have shown promise as combinatorial treatment components, they bring the added complication of potentially problematic side effects at the doses that may be required for efficacy when used in the context of other drug burdens.

The TKIs tested here caused histological changes in the tumors with large necrotic areas arising. However a survey of apoptotic markers in our mouse tumors yielded negative results (data not shown). This did not exclude necroptosis as an additional mode of action in these tumors. Our data suggests that the use of Nintedanib in combination with Romidepsin for MTC is unwarranted. However, other cytotoxic drugs might be combined with Vandetanib or Nintedanib administration. For example, irinotecan was used successfully in preclinical models of colon cancer [30]. Also, Aurora kinase inhibitors have shown strong anti-tumor effects in several types of cancer [36, 37]. Testing these drugs preclinically in our animal model will provide future insight into the potency of these combinations.

The limited effects of Vandetanib and Nintedanib on sporadic MTC cell proliferation suggest that targeted therapies other than TKIs should be further explored. Given the role of Cdk5 in MTC proliferation [17] and in angiogenesis [38], Cdk5 inhibitors might be considered as therapeutic drugs to be used alone or in combination with a TKI such as Nintedanib. In recent years, numerous therapies, including antibody-drug conjugates, immune checkpoint therapies and peptide receptor radionuclide therapy, which have potential applications for MTC treatment [4] have been developed. Some have been approved by the FDA for other clinical applications than MTC. Given the lack of therapeutic options available for MTC patients it will be important to determine if these drugs can be re-purposed and fast-track approved for MTC therapy.

MATERIALS AND METHODS

Mouse line

NSE-tTA/tetOp-p25-GFP bi-transgenic mice were derived by crossing NSE-tTA and the tetOp-p25-GFP mouse lines as previously described [17]. In this system,

p25-GFP expression is controlled by a tetracycline response element (TRE), which is activated by binding of a tetracycline transactivator (tTA). In presence of doxycycline (Dox), tTA binds to Dox instead of the TRE. Dox (100 mg/ml) is added to drinking water until weaning. Tumor growth is induced by removing Dox. All procedures were approved by the Institutional Animal Care and Use Committees of the University of Texas and University of Alabama Birmingham conducted in accordance with the applicable portions of the National Institute of Health Guide for the Care and Use of Laboratory Animals.

Human samples

Lymph node MTC metastasis were obtained after written informed consent from the patient was obtained.

Drugs

Vandetanib (#V-9402) and Nintedanib (#N-9077) were obtained from LC Laboratories. Romidepsin (#3515) was purchased from Tocris R&D.

Animal testing

Unless stated otherwise, drugs were administered by intra-peritoneal (i.p.) injections. Drug doses were determined based on published studies [39–41] (see also Supplementary Figure 3) and were as indicated in the Figure legends. Due to adverse events, Romidepsin was used at 0.78 mg/kg/day instead of 1.2 mg/kg/day [22] for monotherapy. Vandetanib and Nintedanib were administered initially by oral gavage (o.g.) 6 days/week for experiments lasting up to 3 weeks. TKI administration was switched to i.p. injections 6 days/week when treatment protocols were over 3-weeks. Before switching from o.g. to i.p. administration, we confirmed that the doses administered using the different routes led to comparable antitumor effects (Supplementary Figure 3). Romidepsin was always administered i.p. twice a week. For combinatorial treatment, Romidepsin was injected i.p. twice a week and Nintedanib 3 times a week. Romidepsin and Nintedanib were not injected on the same day. No drug was administered on the day that mice were imaged. Vandetanib and Nintedanib were solubilized in citrate buffer pH 6.2 and pH 4, respectively. Romidepsin was dissolved in DMSO and diluted in PBS.

Magnetic resonance imaging

All MRI studies were conducted in a 7T small-animal scanner with a 38-mm inner diameter radio frequency (RF) coil (Agilent, Palo Alto, Calif). Under anesthesia with 1-2% isoflurane (Aerrane; Baxter Health Care, Deerfield, Ill) mixed in 100% oxygen, all animals were placed supine with the thyroid centered with respect

to the center of the RF coil. Following initial localization, high-resolution axial T2W images were obtained to cover the entire thyroid with a fast spin-echo sequence. The imaging parameters were: repetition time = 2500 ms, effective echo time = 40 ms, field of view = 32² mm, matrix size = 256² (125 μm in-plane resolution), slice thickness = 1 mm, gapless, number of excitations = 8, affording a total scan time of 10 min 45 s. For analysis, the entire volume of the tumor was measured by means of manual segmentation on the T2W image in all slices. All image processing was conducted using an imaging processing software (ImageJ, version 1.50i).

Tissue collection

At the end of treatments, or if animals were in distress, animals were culled by asphyxia using CO₂ and perfused using PBS containing protease and phosphatase inhibitors as described [17]. One side of the tumor was fixed in 4% paraformaldehyde (PFA) for 48 h prior to paraffin embedding and the other side was frozen in dry-ice upon collection.

Immunoblotting

Quantitative immunoblot analyses were conducted using standard procedures [17]. Antibodies directed to ERK1/2 (#9102), phospho-ERK1/2 (#9101), VEGFR2 (#9698), phospho-VEGFR2 Tyr1115 (#3770), acetyl-histone H4 Lys8 (#2594), phospho-AKT Thr308 (#4056), phospho-AKT Ser473 (#3787), AKT (#4691), phospho-FOXO1 Ser256 (#9461), FOXO1 (#2880), phospho-4EBP1 Thr37/46 (#2855), phospho-S6K Ser235/236 (#4858) were purchased from Cell Signaling Technology and used at dilutions of 1:1000. Antibodies to RET (#ab134100) and phospho-RET Tyr 1062 (#ab51103) were purchased from Abcam and used at dilutions of 1:10,000 and 1:2000 respectively. Antibodies to Actin (#A2228) were from Sigma-Aldrich and used at dilution 1:10,000.

Immunostaining

Rat monoclonal CD31 (PECAM-1), Clone SZ31 (DIA-310) antibodies were from Dianova and rabbit polyclonal Ki-67 antibodies from Abcam (ab15580). Paraffin sections were boiled in citrate buffer pH 6.0 for antigen unmasking. Primary antibodies were used at a dilution of 1:100. Alexa Fluor®546 conjugated goat anti-rat secondary antibodies (for CD31) and Alexa Fluor®647 conjugated chicken anti-rabbit secondary antibodies (for Ki-67) were from Life Technologies and used at a dilution of 1:400. Sections were counterstained with Hoechst 33342 (5 mg/ml) for nuclear detection. Images were obtained with a Leica SP8SMD laser scanning confocal microscope using a 40x oil immersion lens, λ 561 nm and λ 563 nm laser lines for excitation and emission between 570 and 620 nm, and 650 and 700 nm, respectively. There was no overlap with

endogenous p25-EGFP signal from the bitransgenic animal. The 633 nm channel was pseudo-colored in green, 561 nm channel in red and Hoechst in blue. For each conditions, N=3 fields from N=4 animals were imaged. Image analyses were conducted using Fiji17. Values reported are %CD31 staining and Ki67 positive cells /field of view.

Cell culture, proliferation and survival assays

Mouse and human MTC cell lines, *i.e.* MTCp25OE, MTC-SK, SIN-J and TT cells have been previously described [17, 42, 43]. Briefly, MTC-SK cells were derived from sporadic patient primary tumor [44], SIN-J cells from a sporadic MTC patient lymph node metastasis [42]. TT cells were from an hereditary MTC patient needle biopsy [43]. Cells were maintained and proliferation assays were conducted using the WST-1 cell proliferation reagent (Roche Diagnostics) [17]. For cell survival assays and dose-response curves, cells were seeded onto 96-well TC plates, treated with Vandetanib or Nintedanib for 6 days, fed with 10% FBS media on day 3, then incubated with CyQuant Cell Proliferation Assay (Invitrogen) reagents per manufacturer's protocol and assayed using a BMG Optima Fluostar microplate reader. RFU from each well was normalized to control treated cells in order to determine percent effect on survival.

Statistical analysis

All quantitative data are expressed as means \pm S.E.M. Two-tailed, unpaired Student's *t*-test or one-way ANOVA followed by a Bonferroni's post-test were used to compare the different groups as needed. Probability values of 0.05 or lower were considered to indicate significant differences between groups. The symbols used to indicate p-values were * $p < 0.05$, ** $p < 0.01$, *** $p < 0.005$, with subject number (n) stated in the legend.

Abbreviations

Medullary Thyroid Carcinoma (MTC), Neuroendocrine (NE), Tyrosine Kinase Inhibitor (TKI), Receptor Tyrosine Kinase (RTK), Magnetic Resonance Imaging (MRI), oral gavage (o.g.), intra-peritoneal (i.p.).

Author contributions

Conception and design: K. Pozo, S. Oltmann and J. A. Bibb

Development of methodology: K. Pozo, A. M. Carter, S. Zahler, K. Ishimatsu, M. Takahashi

Acquisition of data: K. Pozo, K. Ishimatsu, A. M. Carter, R. Telange, C. Tan, S. Wang, J. Fujimoto, S. Zahler

Analysis and interpretation of data: K. Pozo, S. Zahler, K. Ishimatsu, A. M. Carter, R. Telange, C. Tan, S. Wang, J. Fujimoto

Writing: K. Pozo, A. M. Carter and J. A. Bibb

Administrative, technical, or material support: E. Gardner Grubbs, R. Pfragner, S. C. Oltmann
Study supervision: J. A. Bibb

ACKNOWLEDGMENTS

We acknowledge the help and guidance of Drs. Rolf Brekken, Shanrong Wang, Kim Kangasami, Koji Sagiya (UT Southwestern Medical Center, Dallas, TX).

CONFLICTS OF INTEREST

The authors declare that they have no conflicts of interest with the contents of this article.

FUNDING

This research was supported by a North American Neuroendocrine Tumor Society Fellowship (K.P.), an American Cancer Society Young Investigator Award (A.M.C.), a Chinese Council Scholarship (S.W.), a Dedman Family Scholar Award (S.C. O.), an American Thyroid Association Research Grant (S.C.O.) and an American Cancer Society MEN2 Thyroid Cancer Consortium research grant RSGM-11-190-01 (J.A.B.).

REFERENCES

1. Fagin JA, Wells SA, Jr. Biologic and clinical perspectives on thyroid cancer. *N Engl J Med.* 2016; 375:1054-1067.
2. Wells SA Jr, Santoro M. Targeting the RET pathway in thyroid cancer. *Clin Cancer Res.* 2009; 15:7119-7123.
3. Mulligan LM. RET revisited: expanding the oncogenic portfolio. *Nat Rev Cancer.* 2014; 14:173-186.
4. Nelkin B. Recent advances in the biology and therapy of medullary thyroid carcinoma. *F1000Research.* 2017; 6:2184.
5. Jr SAW, Robinson BG, Gagel RF, Dralle H, Fagin JA, Santoro M, Baudin E, Elisei R, Jarzab B, Vasselli JR, Read J, Langmuir P, Ryan AJ, et al. Vandetanib in patients with locally advanced or metastatic medullary thyroid cancer: a randomized, double-blind phase III trial. *Journal of Clinical Oncology.* 2012; 30:134-141.
6. Elisei R, Schlumberger MJ, Muller SP, Schoffski P, Brose MS, Shah MH, Licitra L, Jarzab B, Medvedev V, Kreissl MC, Niederle B, Cohen EE, Wirth LJ, et al. Cabozantinib in progressive medullary thyroid cancer. *J Clin Oncol.* 2013; 31:3639-3646.
7. Gild ML, Bullock M, Robinson BG, Clifton-Bligh R. Multikinase inhibitors: a new option for the treatment of thyroid cancer. *Nat Rev Endocrinol.* 2011; 7:617-624.
8. Cabanillas ME, Hu MI, Jimenez C, Grubbs EG, Cote GJ. Treating medullary thyroid cancer in the age of targeted therapy. *Int J Endocr Oncol.* 2014; 1:203-216.

9. Lin JJ, Shaw AT. Resisting resistance: targeted therapies in lung cancer. *Trends in cancer*. 2016; 2:350-364.
10. Robinson BG, Paz-Ares L, Krebs A, Vasselli J, Haddad R. Vandetanib (100 mg) in patients with locally advanced or metastatic hereditary medullary thyroid cancer. *J Clin Endocrinol Metab*. 2010; 95:2664-2671.
11. Carlomagno F, Vitagliano D, Guida T, Ciardiello F, Tortora G, Vecchio G, Ryan AJ, Fontanini G, Fusco A, Santoro M. ZD6474, an orally available inhibitor of KDR tyrosine kinase activity, efficiently blocks oncogenic RET kinases. *Cancer Res*. 2002; 62:7284-7290.
12. Vidal M, Wells S, Ryan A, Cagan R. ZD6474 suppresses oncogenic RET isoforms in a Drosophila model for type 2 multiple endocrine neoplasia syndromes and papillary thyroid carcinoma. *Cancer Res*. 2005; 65:3538-3541.
13. Johanson V, Ahlman H, Bernhardt P, Jansson S, Kolby L, Persson F, Stenman G, Sward C, Wangberg B, Stridsberg M, Nilsson O. A transplantable human medullary thyroid carcinoma as a model for RET tyrosine kinase-driven tumorigenesis. *Endocr Relat Cancer*. 2007; 14:433-444.
14. Wells SA, Jr., Robinson BG, Gagel RF, Dralle H, Fagin JA, Santoro M, Baudin E, Elisei R, Jarzab B, Vasselli JR, Read J, Langmuir P, Ryan AJ, Schlumberger MJ. Vandetanib in patients with locally advanced or metastatic medullary thyroid cancer: a randomized, double-blind phase III trial. *J Clin Oncol*. 2012; 30:134-141.
15. Richeldi L, du Bois RM, Raghu G, Azuma A, Brown KK, Costabel U, Cottin V, Flaherty KR, Hansell DM, Inoue Y, Kim DS, Kolb M, Nicholson AG, Noble PW, et al. Efficacy and safety of nintedanib in idiopathic pulmonary fibrosis. *N Engl J Med*. 2014; 370:2071-2082.
16. Awasthi N, Schwarz RE. Profile of nintedanib in the treatment of solid tumors: the evidence to date. *Onco Targets Ther*. 2015; 8:3691-3701.
17. Pozo K, Castro-Rivera E, Tan C, Plattner F, Schwach G, Siegl V, Meyer D, Guo A, Gundara J, Mettlach G, Richer E, Guevara JA, Ning L, Gupta A, et al. The role of Cdk5 in neuroendocrine thyroid cancer. *Cancer Cell*. 2013; 24:499-511.
18. Pozo K, Hillmann A, Augustyn A, Plattner F, Hai T, Singh T, Ramezani S, Sun X, Pfragner R, Minna JD, Cote GJ, Chen H, Bibb JA, et al. Differential expression of cell cycle regulators in CDK5-dependent medullary thyroid carcinoma tumorigenesis. *Oncotarget*. 2015; 6:12080-12093.
19. Eng C, Mulligan LM, Smith DP, Healey CS, Frilling A, Raue F, Neumann HP, Pfragner R, Behmel A, Lorenzo MJ and et al. Mutation of the RET protooncogene in sporadic medullary thyroid carcinoma. *Genes Chromosomes Cancer*. 1995; 12:209-212.
20. Vitagliano D, De Falco V, Tamburrino A, Coluzzi S, Troncone G, Chiappetta G, Ciardiello F, Tortora G, Fagin JA, Ryan AJ, Carlomagno F, Santoro M. The tyrosine kinase inhibitor ZD6474 blocks proliferation of RET mutant medullary thyroid carcinoma cells. *Endocr Relat Cancer*. 2011; 18:1-11.
21. Kutluk Cenik B, Ostapoff KT, Gerber DE, Brekken RA. BIBF 1120 (Nintedanib), a triple angiokinase inhibitor, induces hypoxia but not EMT and blocks progression of preclinical models of lung and pancreatic cancer. *American Association for Cancer Research*. 2013; 12:992-1001.
22. Zhang W, Peyton M, Xie Y, Soh J, Minna JD, Gazdar AF, Frenkel EP. Histone deacetylase inhibitor romidepsin enhances anti-tumor effect of erlotinib in non-small cell lung cancer (NSCLC) cell lines. *J Thorac Oncol*. 2009; 4:161-166.
23. Jaskula-Sztul R, Eide J, Tesfazghi S, Dammalapati A, Harrison AD, Yu XM, Scheinebeck C, Winston-McPherson G, Kupcho KR, Robers MB, Hundal AK, Tang W, Chen H. Tumor-suppressor role of Notch3 in medullary thyroid carcinoma revealed by genetic and pharmacological induction. *Mol Cancer Ther*. 2015; 14:499-512.
24. Jaskula-Sztul R, Xu W, Chen G, Harrison A, Dammalapati A, Nair R, Cheng Y, Gong S, Chen H. Thailandepsin A-loaded and octreotide-functionalized unimolecular micelles for targeted neuroendocrine cancer therapy. *Biomaterials*. 2016; 91:1-10.
25. Gerber DE, Boothman DA, Fattah FJ, Dong Y, Zhu H, Skelton RA, Priddy LL, Vo P, Dowell JE, Sarode V, Leff R, Meek C, Xie Y, et al. Phase 1 study of romidepsin plus erlotinib in advanced non-small cell lung cancer. *Lung Cancer*. 2015; 90:534-541.
26. Nozhat Z, Hedayati M. PI3K/AKT pathway and its mediators in thyroid carcinomas. *Mol Diagn Ther*. 2016; 20:13-26.
27. Manfredi GI, Dicitore A, Gaudenzi G, Caraglia M, Persani L, Vitale G. PI3K/Akt/mTOR signaling in medullary thyroid cancer: a promising molecular target for cancer therapy. *Endocrine*. 2015; 48:363-370.
28. Tamburrino A, Molinolo AA, Salerno P, Chernock RD, Raffeld M, Xi L, Gutkind JS, Moley JF, Wells SA Jr, Santoro M. Activation of the mTOR pathway in primary medullary thyroid carcinoma and lymph node metastases. *Clin Cancer Res*. 2012; 18:3532-3540.
29. Vincent EE, Elder DJE, Thomas EC, Phillips L, Morgan C, Pawade J, Sohail M, May MT, Hetzel MR, Tavaré JM. Akt phosphorylation on Thr308 but not on Ser473 correlates with Akt protein kinase activity in human non-small cell lung cancer. *British Journal of Cancer*. 2011; 104:1755-1761.
30. Troiani T, Serkova NJ, Gustafson DL, Henthorn TK, Lockerbie O, Merz A, Long M, Morrow M, Ciardiello F, Eckhardt SG. Investigation of two dosing schedules of vandetanib (ZD6474), an inhibitor of vascular endothelial growth factor receptor and epidermal growth factor receptor signaling, in combination with irinotecan in a human colon cancer xenograft model. *Clin Cancer Res*. 2007; 13:6450-6458.
31. Lian EY, Maritan SM, Cockburn JG, Kasaian K, Crupi MJ, Hurlbut D, Jones SJ, Wiseman SM, Mulligan LM. Differential roles of RET isoforms in medullary and papillary thyroid carcinomas. *Endocr Relat Cancer*. 2017; 24:53-69.

32. Huang D, Ding Y, Li Y, Luo WM, Zhang ZF, Snider J, Vandenbeldt K, Qian CN, Teh BT. Sunitinib acts primarily on tumor endothelium rather than tumor cells to inhibit the growth of renal cell carcinoma. *Cancer Res.* 2010; 70:1053-1062.
33. Beaudry P, Nilsson M, Rieth M, Prox D, Poon D, Xu L, Zweidler-Mckay P, Ryan A, Folkman J, Ryeom S, Heymach J. Potent antitumor effects of ZD6474 on neuroblastoma via dual targeting of tumor cells and tumor endothelium. *Mol Cancer Ther.* 2008; 7:418-424.
34. Yao JC, Lombard-Bohas C, Baudin E, Kvols LK, Rougier P, Ruzsiewicz P, Hoosen S, St Peter J, Haas T, Lebowitz D, Van Cutsem E, Kulke MH, Hobday TJ, O'Dorisio TM, Shah MH, Cadiot G, et al. Daily oral everolimus activity in patients with metastatic pancreatic neuroendocrine tumors after failure of cytotoxic chemotherapy: a phase II trial. *J Clin Oncol.* 2010; 28:69-76.
35. Gild ML, Bullock M, Pon CK, Robinson BG, Clifton-Bligh RJ. Destabilizing RET in targeted treatment of thyroid cancers. *Endocr Connect.* 2016; 5:10-19.
36. Tagal V, Wei S, Zhang W, Brekken RA, Posner BA, Peyton M, Girard L, Hwang T, Wheeler DA, Minna JD, White MA, Gazdar AF, Roth MG. SMARCA4-inactivating mutations increase sensitivity to Aurora kinase A inhibitor VX-680 in non-small cell lung cancers. *Nat Commun.* 2017; 8:14098.
37. Mollaoglu G, Guthrie MR, Bohm S, Bragelmann J, Can I, Ballieu PM, Marx A, George J, Heinen C, Chalishazar MD, Cheng H, Ireland AS, Denning KE, et al. MYC Drives progression of small cell lung cancer to a variant neuroendocrine subtype with vulnerability to aurora kinase inhibition. *Cancer Cell.* 2017; 31:270-285.
38. Merk H, Zhang S, Lehr T, Muller C, Ulrich M, Bibb JA, Adams RH, Bracher F, Zahler S, Vollmar AM, Liebl J. Inhibition of endothelial Cdk5 reduces tumor growth by promoting non-productive angiogenesis. *Oncotarget.* 2016; 7:6088-6104.
39. Yoshikawa D, Ojima H, Kokubu A, Ochiya T, Kasai S, Hirohashi S, Shibata T. Vandetanib (ZD6474), an inhibitor of VEGFR, EGFR signalling, as a novel molecular-targeted therapy against cholangiocarcinoma. *Br J Cancer.* 2009; 100:1257-1266.
40. Broutin S, Commo F, De Koning L, Marty-Prouvost B, Lacroix L, Talbot M, Caillou B, Dubois T, Ryan AJ, Dupuy C, Schlumberger M, Bidart JM. Changes in signaling pathways induced by vandetanib in a human medullary thyroid carcinoma model, as analyzed by reverse phase protein array. *Thyroid.* 2014; 24:43-51.
41. Hilberg F, Roth GJ, Krssak M, Kautschitsch S, Sommergruber W, Tontsch-Grunt U, Garin-Chesa P, Bader G, Zoepfel A, Quant J, Heckel A, Rettig WJ. BIBF 1120: triple angiokinase inhibitor with sustained receptor blockade and good antitumor efficacy. *Cancer Res.* 2008; 68:4774-4782.
42. Pfragner R, Wirnsberger G, Behmel A, Wolf G, Passath A, Ingolic E, Adamiker D, Schauenstein K. New continuous cell-line from human medullary-thyroid carcinoma - sinj - phenotypic analysis and *in vivo* carcinogenesis. *International journal of oncology.* 1993; 2:831-836.
43. Gagel RF, Palmer WN, Leonhart K, Chan L, Leong SS. Somatostatin production by a human medullary thyroid carcinoma cell line. *Endocrinology.* 1986; 118:1643-1651.
44. Pfragner R, Hofler H, Behmel A, Ingolic E, Walser V. Establishment and characterization of continuous cell line MTC-SK derived from a human medullary thyroid carcinoma. *Cancer Res.* 1990; 50:4160-4166.

Review

The Emerging Role of Cdk5 in Cancer

Karine Pozo^{1,2,*} and James A. Bibb^{3,4,*}

Cdk5 is an atypical cyclin-dependent kinase that is well characterized for its role in the central nervous system rather than in the cell cycle. However, Cdk5 has been recently implicated in the development and progression of a variety of cancers including breast, lung, colon, pancreatic, melanoma, thyroid, and brain tumors. This broad protumorigenic role makes Cdk5 a promising drug target for the development of new cancer therapies. In this review, we discuss the contribution of Cdk5 to molecular mechanisms that confer upon tumors the ability to grow, proliferate, and disseminate to secondary organs, as well as resistance to chemotherapies. We subsequently discuss existing and new strategies for targeting Cdk5 and its downstream mechanisms as anticancer treatments.

Cdk5: An Overlooked Player in the Cancer Field

Deregulation of the cell cycle is a fundamental process that underlies cancer proliferation [1]. Progression through the cell cycle is regulated by the coordinated actions of cyclin-dependent kinases (Cdks), which are, therefore, targets of interest for anticancer drugs. However, many cancers are currently not responsive to anti-Cdk therapies [2]. The protein kinase Cdk5 has long been overlooked in cancer-related studies because it is an atypical Cdk that is predominantly expressed in neurons and is mainly activated by the noncyclin activator p35 or its truncated product, p25 [3] (Box 1; Figure 1B, Key Figure). Nevertheless, Cdk5 is rapidly emerging as a new player in tumorigenesis with functions ranging from cell proliferation to metastatic invasion (Figure 1C) and angiogenesis. In this review, we present recent evidence demonstrating that Cdk5 plays a critical role in the molecular mechanisms driving tumor formation and development. We further examine new studies indicating a link between Cdk5 and radiotherapy/chemotherapy resistance as well as Cdk5 and immunotherapy. Finally, we discuss why Cdk5 may be a valid target for anticancer therapies.

Human Cancers Express Cdk5

Expanding evidence at the gene, mRNA, and protein levels supports a role for Cdk5 in human cancers (Table 1) and its expression and activity as biomarkers for the prediction of cancer severity. First, genetic variations such as the amplification of the *Cdk5* gene [4] or *p35/p39* genes [5,6] as well as single-nucleotide polymorphisms in the *Cdk5* gene promoter region [7] occur in several cancer populations. These are, for example, associated with higher lung cancer risks in the Korean population [4,7] and with aggressive forms of prostate cancers in African Americans [8]. Second, mRNA and protein expression levels of Cdk5 and its activators are increased, or decreased, in several forms of cancer and these alterations are correlated with cancer severity (Figure 1A, Table 1). For example, Cdk5 and p35/p25 are elevated in pulmonary neuroendocrine cancers [9–11], in sporadic and familial forms of medullary thyroid carcinoma (MTC) [12], and in pituitary adenoma [13]. In fact, Cdk5 and p35/p25 expressions appear to typify neuroendocrine cancer pathology. In tissues from nonsmall cell lung cancer (NSCLC), breast, brain, and nasopharyngeal cancer patients, increased Cdk5 and/or activator expression parallels

Trends

Cdk5 is not mutated in cancer tissues but its expression and activity are deregulated. Because discovery of the molecular causes of cancer is predominantly based on the identification of tumor-associated mutations, the role of Cdk5 in cancer has been overlooked until recently.

Cdk5 contributes to tumor proliferation, migration, angiogenesis, and is linked to chemotherapy resistance and antitumor immunity.

Strategies to target Cdk5 and downstream pathways include small molecules to block the kinase activity and peptides to disrupt Cdk5 binding to its activators or substrates.

Genetically modified animal models of cancer may be generated by deregulating Cdk5 via overexpression of its activator p25 in cancer cells. Such models may be clinically relevant and exhibit tumors that grow within a physiological microenvironment in an animal with an intact immune system.

¹Department of Neuroscience, The University of Texas Southwestern Medical Center, Dallas, TX, USA

²Department of Surgery, The University of Texas Southwestern Medical Center, Dallas, TX, USA

³Department of Surgery, The University of Alabama Birmingham Medical Center, Birmingham, AL, USA

⁴Comprehensive Cancer Center, The University of Alabama Birmingham Medical Center, Birmingham, AL, USA

*Correspondence:

Karine.Pozo@utsouthwestern.edu

(K. Pozo) and jbibb@uab.edu (J.A. Bibb).

Box 1. Cdk5, an Unconventional Cyclin-Dependent Kinase (Cdk)

Although Cdk5 exhibits approximately 60% amino acid sequence identity with Cdk1 and Cdk2 [3], it is highly expressed in the brain compared with other organs, and is therefore considered as a neuronal kinase. Cdk5 has been well characterized for brain development, function, and pathologies [3], while its roles in non-neuronal tissues have been underexplored until recently [22,63].

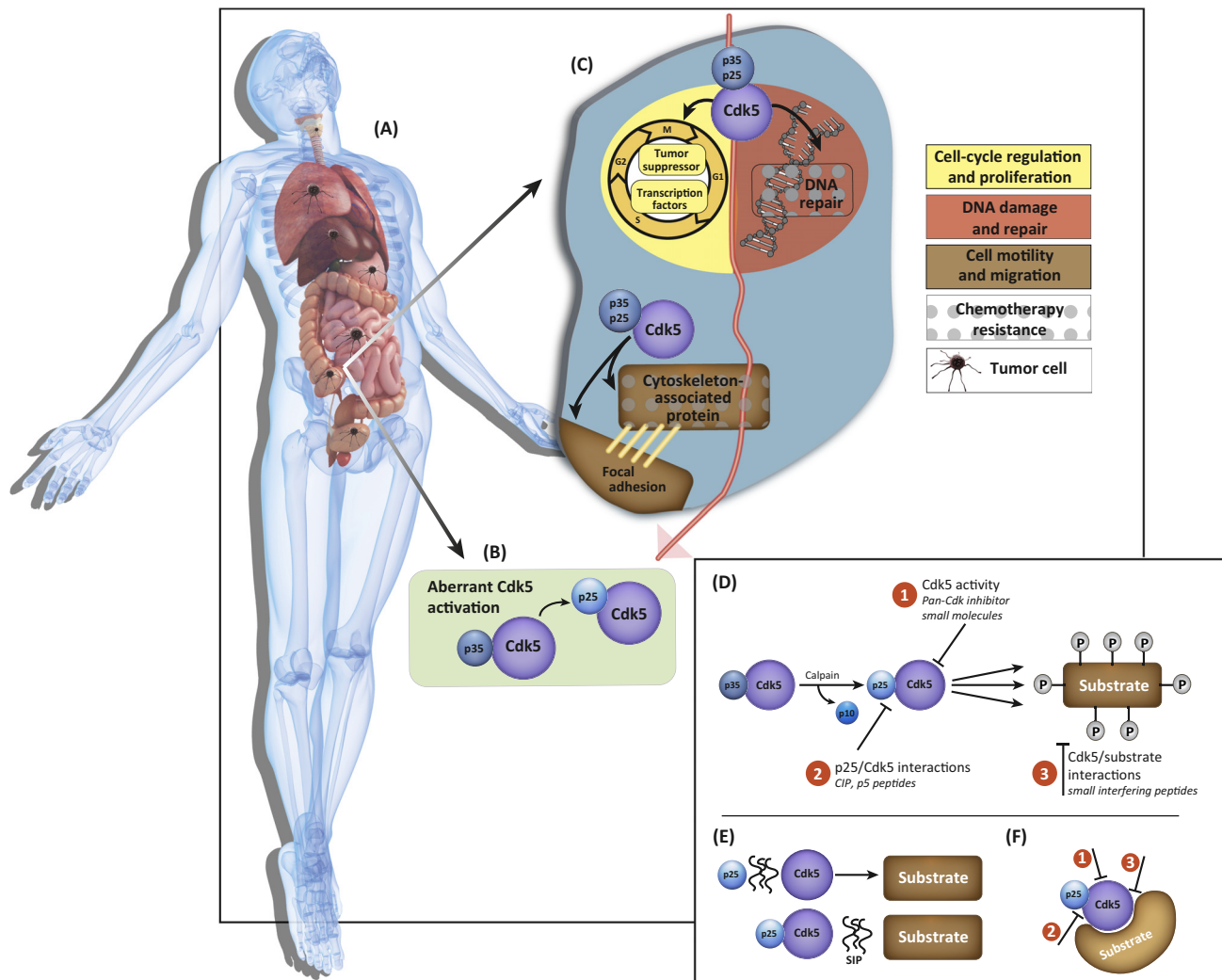
Control of Cdk5 activity is unlike that of any other Cdks [3]. It is activated by binding to the noncyclin activators, p35 or p39, and phosphorylates substrates on serine or threonine residues within the consensus motif S/TPXH/K/R (Figure 1B,D). Cdk5 activation by cyclins D, E, and G1, and the non-cyclin protein p67 has also been reported but the significance in tumorigenesis has not been elucidated yet [64]. Cdk5 can also be activated by binding to cyclin I [65] and in cervical cancer patients, the Cdk5/cyclin I complex is associated with resistance to cisplatin treatment [66]. Since the predominant Cdk5 activators are p35 and p39, these are discussed further here. Cdk5/p35 and Cdk5/p39 are constitutively active forms of the kinase, with relatively low catalytic efficiency compared with more acutely activated kinases, and are distributed throughout cells. Cleavage of Cdk5 cofactors by calpain removes the first 100 amino acids, to produce p25 or p29, which still contain the Cdk5 binding domain. The resulting Cdk5/p25 or Cdk5/p29 holoenzymes have longer half-lives and altered substrate specificity compared with Cdk5/p35 or Cdk5/p39. Cdk5/p35 is often docked to cell membranes due to a myristoylation in the p35 N-terminal region. Loss of this domain as a result of cleavage renders Cdk5/p25 more soluble, able to access cytoplasmic and nuclear substrates that are not in cellular membranes proximity [67] (Figure 1). Cdk5/p25 and Cdk5/p35 have been linked to tumorigenesis, however, Cdk5/p25 seems to be a more toxic form linked to neurodegenerative diseases and paradoxically, pro-cell cycle [22]. Regulation of calpain-mediated p35-to-p25 cleavage in cancer cells has not been studied. It can be speculated that environmental stresses cause changes in calcium concentration that activates the calpain protease activity. p35 also undergoes post-translational modifications in addition to proteolytic cleavage, including autophosphorylation, which may impact regulatory mechanisms [67]. The cytoskeleton protein, nestin, regulates the turnover of p35 into p25 in myoblasts [68]. A similar mechanism might occur in cancer cells. Getting a better insight of the mechanisms underlying the p35-to-p25 cleavage may offer new targets for Cdk5-driven cancer treatments.

Table 1. Expression of Cdk5 in Human Cancers

Cancer	Cdk5 function	Refs
Breast	Proliferation, survival, epithelial-to-mesenchymal transition, and metastasis	[15,16]
Colorectal	Proliferation	[78]
Gastric	Cell-cycle suppressor	[20]
Glioma, glioblastoma	Invasion	[17,18]
Hepatocellular carcinoma	Migration, angiogenesis, inflammation, and lymphatic development	[21,34]
Head and neck	Not known	[19]
Leukemia	Survival	[79]
Lung – small cell lung cancer, carcinoids	Proliferation and migration	[42]
Lung – nonsmall cell lung cancer	Proliferation, migration, and invasion	[4,14]
Mantle cell lymphoma	Proliferation	[80]
Medulloblastoma	Immune evasion	[62]
Melanoma	Proliferation and invasion	[45]
Multiple myeloma	Not known	[81]
Ovary	Migration	[19]
Pancreatic	Proliferation, migration, invasion, and metastasis	[6,44]
Pituitary adenoma	Migration and invasion	[13]
Prostate	Proliferation, migration, invasion, metastasis, and apoptosis	[43]
Thyroid – medullary thyroid carcinoma	Proliferation	[12]

Key Figure

Targeting Cdk5 in Cancer



Trends in Cancer

Figure 1. (A) Cdk5 contributes to carcinogenesis in several organs throughout the body. (B) Cdk5 activation is dependent on its binding to the cofactor p35 or its proteolytic cleavage product p25 (green box). (C) At a cellular level, Cdk5 is involved in the regulation of the cell cycle and cell proliferation by phosphorylating tumor suppressors and transcription factors, and in the DNA-damage response upon exposure to genotoxic agents such as chemotherapy and radiotherapy. Cdk5 plays a role in cell motility and migration by regulating the cytoskeleton and focal adhesions. The role of Cdk5 in the DNA-damage response and cytoskeleton remodeling has been linked to resistance to common chemotherapies. (D–F) Therapeutic targeting of Cdk5 is achieved either by (i) inhibiting Cdk5 kinase activity with a pan-Cdk inhibitor or small molecules (D); by (ii) preventing Cdk5 binding to p25 using peptides (E); or by (iii) interfering with Cdk5 association and phosphorylation of its substrate using peptides (F).

advanced cancer stages, occurrence of lymph node metastasis, and overall poor 5-year survival, while low Cdk5 levels correlates with metastatic-free disease [14–19]. Somewhat remarkably abnormal low Cdk5 or activator tumor levels are also indicative of poor prognosis as in advanced gastric cancer [20] or hepatocellular carcinoma (HCC) [21]. However, more

studies are needed to understand the molecular mechanisms by which Cdk5 and activators contribute to these cancers. In the following section, we discuss what is currently known about Cdk5 role in oncogenic pathways.

Molecular Links between Cdk5 and the Cell Cycle

Historically, Cdk5 has not been considered as a potential cell-cycle regulator because it is predominantly expressed in nondividing, postmitotic neurons [3]. However, it has been noted that Cdk5 facilitates amyloid β protein-induced cell-cycle re-entry in neurons of mouse models of Alzheimer's disease [22] and directly modulates the function of tumor suppressors and transcription factors (Figure 2A, Table 2). This raises the possibility that evolution of the central nervous system function occurred through adaption of cell-cycle mechanisms. Thus, Cdk5 may contribute to neurodegeneration and oncogenesis through overlapping or common pathways and especially those related to the cell cycle and cell proliferation (Figure 1C).

Cdk5 and the Retinoblastoma Protein/E2 Family of Transcription Factors Pathway

Cdk5 modulates the retinoblastoma protein (Rb)/E2 family of transcription factors (E2F) pathway by phosphorylating Rb [23], thereby promoting cancer cell proliferation as in MTC [12]. Rb controls the transition from the G₀/G₁ to S phase, and thus the initiation of the cell cycle by sequestering the transcription factor E2F [22] (Figure 2A). It is well accepted that upon Rb phosphorylation by Cdk4–6/cyclin D, E2F is released and activates the transcription of genes required for cell-cycle progression. In MTC, phosphorylation of Rb by Cdk5 results in E2F target genes expression, including Cdk2, p15^{INK4b}, and p21^{CIP/WAF1} with cancer proliferation ensuing

Table 2. Cdk5 Substrates Implicated in Cancer

Substrate	Site	Protein type/cellular function	Refs
Akt	Ser-473	Kinase/proliferation	[30]
AR	Ser-81, Ser-308	Transcription factor/proliferation	[82] [30]
Ape1	Thr-232	Endonuclease/DNA-damage response	[83]
ATM		Kinase/DNA-damage response	[37]
Caldesmon	Ser-527	Cytoskeletal protein/migration	[75]
DLC-1	Ser-120, Ser-205, Ser-422, and Ser-509	Tumor suppressor/proliferation	[84]
FAK	Ser-732	Cytoskeletal protein/migration/EMT	[15,85]
Girdin	Ser-1674	GTPase/Migration	[41]
Hu antigen R	Ser-202	mRNA binding protein/proliferation	[86]
Noxa	Ser-15	Proapoptotic factor/apoptosis	[79]
PAK1	Thr-212	Cytoskeletal protein/migration	[87]
p53	Ser-15, Ser-33, and Ser-46	Tumor suppressor/apoptosis	[88] [89]
PIKE-A	Ser-279	GTPase/migration, invasion	[90]
Rb	Ser-780, Ser-795, and Ser-807/811	Tumor suppressor/proliferation	[91] [23]
STAT3	Ser-727	Transcription factor/proliferation	[26]
Talin	Ser-425	Cytoskeletal protein/migration	[74]
VEGFR2	Ser-229	Tyrosine kinase receptor/invasion	[92]

AR, androgen receptor; ATM, ataxia-telangiectasia mutated; DLC-1, deleted in liver cancer 1; EMT, epithelial-to-mesenchymal transition; FAK, focal adhesion kinase; PAK1, p21-activated kinase 1; PIKE-A, PI 3-kinase enhancer A; STAT3, signal transducer and activator of transcription 3; VEGFR2, vascular endothelial growth factor receptor 2.

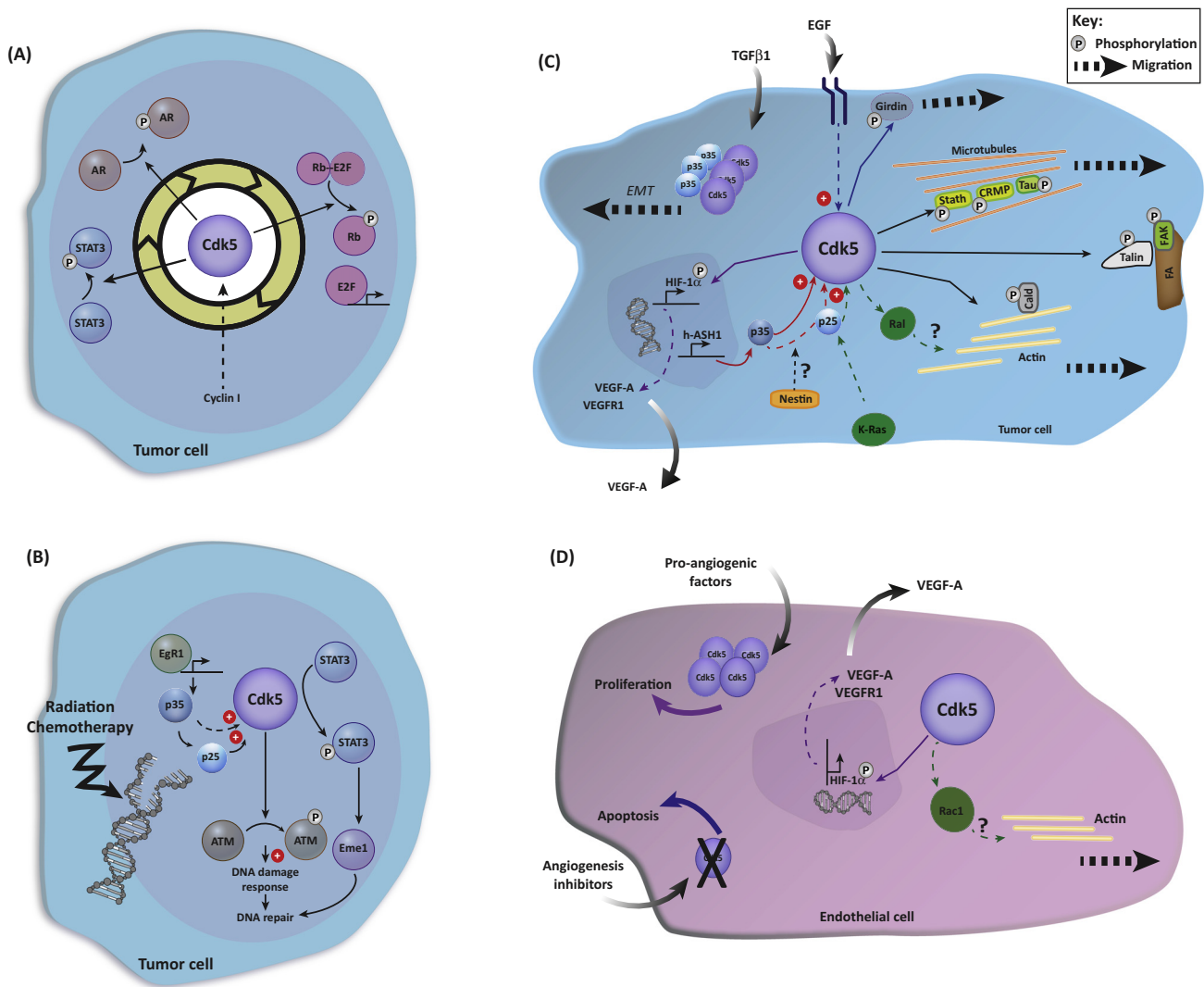


Figure 2. Cdk5-Driven Mechanisms in Cancer Progression. (A) Schematic representation of Cdk5 contribution to cell cycle and proliferation. Cdk5 phosphorylates tumor suppressors and transcription factors involved in cell-cycle progression. Cyclin I may bind and activate Cdk5 during the cell cycle. The phases at which Cdk5 regulates each transcription factor have not been clearly defined. (B) Proposed role for Cdk5 in the DNA-damage response and DNA-repair processes. Cdk5 becomes activated in tumor cells exposed to DNA-damaging agents (i.e., radiation and chemotherapy). EgR1 induces p35 expression, which binds and activates Cdk5. p35 can be cleaved to produce p25, which activates Cdk5, as in brain cancers. Upon activation, Cdk5 phosphorylates the checkpoint kinase ataxia-telangiectasia mutated (ATM) and the transcription factor signal transducer and activator of transcription 3 (STAT3) to transduce DNA-damage responses and facilitate DNA repair. (C) Cdk5 in cell motility and migration. Cdk5 becomes activated upon stimulation with transforming growth factor β (TGF β) or epithelial growth factor (EGF) and phosphorylates components of the cytoskeleton and focal adhesions to induce cell motility and migration. Cdk5 may facilitate neoplasia and angiogenesis through hypoxia-inducible factor 1 α (HIF1 α) and vascular endothelial growth factor (VEGF) signaling. Induction of human Achaete-scute homolog 1 (hASH1) and subsequent expression of p35 may be a mechanism by which Cdk5 is activated as it occurs in lung cancer. The intermediate filament protein, nestin, is a Cdk5 substrate and might regulate the cleavage of p35-to-p25 by an autoregulatory process. (D) Role of Cdk5 in endothelial cell proliferation and migration. Cdk5 is expressed in endothelial cells, is activated by proangiogenic factors, and regulates angiogenesis by facilitating the migration of endothelial cells via a Rac-dependent mechanism. Cald, caldesmon; CRMP, collapsin response mediator protein-2; E2F, E2 family of transcription factors; EgR1, early growth response protein; Eme1, DNA endonuclease; EMT, epithelial-to-mesenchymal transition; FA, focal adhesion; FAK, focal adhesion kinase; P, Cdk5-mediated phosphorylation; Rb, Retinoblastoma protein; Stath, stathmin; VEGF-A, vascular endothelial growth factor A; VEGFR1, vascular endothelial growth factor receptor 1.

[12]. All these events are prevented by Cdk5 inhibition, supporting a key role for Cdk5 activity in MTC via Rb dysregulation. These provocative findings also raise the intriguing possibility that Cdk5 is capable of replacing Cdk4/6 in certain cancer types, providing a molecular basis for why some cancers are resistant to Cdk4/6 inhibitors. Whether Cdk5 regulates the function of Rb-like proteins, p107 and p130, which are also E2F-binding tumor suppressors, in Rb-negative tumors remains to be determined. Moreover, it would be interesting to find out if Cdk5 can modulate cell-cycle progression by associating with E2F in a p35-dependent manner, thereby interfering its function as observed in neurons [22]. Finally, understanding the cell-cycle progression effects of Cdk5 phosphorylation of E2F targets genes, p19^{INK4d}, and the Cdc25 family of dual-specific phosphatases, Cdc25A-C, on [24,25] would yield more insights into the role of Cdk5 in the cell cycle and tumorigenesis.

Cdk5 and Signal Transducer and Activator of Transcription 3

Besides Rb/E2F, Cdk5 has been associated with the dysregulation of signal transducer and activator of transcription 3 (STAT3) in cancer cells. This transcription factor integrates a variety of signaling pathways and controls the expression of cell-cycle genes such as cyclin D1 and c-Fos [26] (Figure 2A). In normal cells, STAT3 becomes activated following cell stimulation by a cytokine or growth factor, while in cancer cells STAT3 is often deregulated. Cdk5 interacts with and phosphorylates STAT3 at Ser-727, which is necessary for MTC and prostate cancer cells proliferation [27,28]. STAT3-target genes are indeed induced upon Cdk5 activation. Importantly, prostate cancer cells and prostate cancer patient tumors express Cdk5, p35, and phosphorylated Ser-727 STAT3 [28,29]. It would be interesting to define the determinants for Cdk5-dependent phosphorylation of Rb versus STAT3.

Cdk5 and the Androgen Receptor

In prostate cancer, Cdk5 can also phosphorylate the transcription factor androgen receptor (AR; Figure 2A). Cdk5 interacts with AR and phosphorylates it at Ser-308, thereby stabilizing the receptor and enabling transcription of AR-induced genes in early stage prostate cancer cells [30]. AR phosphorylation at Ser-81 by Cdk5 also promotes the growth of prostate cancer cells and prostate tumor xenografts [28]. AR may also be stabilized by interacting with a Cdk5-phosphorylated form of STAT3, that is, Ser-727 STAT3 in prostate cancer cells, thus providing a mechanism linking Cdk5–STAT3–AR in prostate cancer tumorigenesis [28]. Interestingly, AR gene expression in hormone therapy-resistant prostate cancers is driven by the Rb/E2F pathway upon Rb genetic inactivation. It would be interesting to determine if Cdk5 plays a role in the signaling mechanisms underlying advanced forms of prostate cancers by regulating AR or E2F function.

Overall, Cdk5 appears to modulate the function of cell-cycle proteins, including tumor suppressors and transcription factors, thereby regulating cancer cell proliferation. Interestingly, Cdk5 has previously been proposed as a cell-cycle suppressor in neurons [22]. Indeed, in gastric cancer cells, Cdk5 accumulation in the nucleus has an antitumor effect, while decrease in nuclear Cdk5 correlates with cancer progression [20]. We speculate that for some malignancies, Cdk5 may have a protective effect and act as a cell suppressor as found in neurons, while in others, dysregulated Cdk5 promotes tumorigenesis.

Cdk5 in DNA Repair and Drug Resistance

Increasing evidence indicates that Cdk5 contributes to the initiation of the DNA-damage response (DDR) and DNA repair. Upon exposure to environmental stressors such as UV, genotoxic agents, or radiation, these mechanisms are activated and ensure maintenance of genome integrity during cell division by preventing the transmission of damaged DNA. Deregulation of the DDR and DNA repair have been associated with tumorigenesis and resistance to conventional DNA-damaging agent-based cancer treatments, such as chemotherapies and radiation therapies [31]. As will be discussed in the following section, Cdk5's role in the DDR and

DNA repair is leading to the exciting hypothesis that Cdk5 inhibition may be a valid strategy to bypass chemotherapy and radiation therapy resistance.

DNA-Damaging Agents Induce Cdk5

Cdk5 is activated in cancer cells or tissues exposed to conventional DNA-damaging therapies including ionizing radiations (IRs) or genotoxic agents, such as topoisomerase inhibitors and DNA crosslinkers [16,32–35] (Figure 2B). Upregulation of p35 expression, via the early growth response protein 1 (EgR1) promoter, and formation of p25 may underlie increases in Cdk5 activity in IR-exposed glioblastoma and genotoxic agent-treated neuroblastoma [17,36,37]. IR/genotoxic agent-induced Cdk5 activation likely contributes to DNA repair as DNA double-strand breaks are more abundant following pharmacological inhibition of Cdk5 or siRNA/short hairpin RNA-mediated knockout of Cdk5 in cancer cells exposed to DNA-damaging agents [33–35].

Cdk5 and the Regulation of the DDR and DNA Repair

Cdk5 is known to activate cell-cycle checkpoints, which is a prerequisite to DNA repair (Figures 1C and 2B). First, Cdk5 phosphorylates the checkpoint-activating kinase ataxia-telangiectasia mutated at Ser-794 to switch on its kinase activity [34,35,37] in some cancer cells. Consistent with these findings, Cdk5 activity blockade in HCC cell lines prevents ataxia-telangiectasia mutated phosphorylation and the initiation of the downstream DDR signaling cascade, while the formation of double-strand breaks is increased [34]. Second, Cdk5 phosphorylates and activates replication protein A-32, which is a necessary step for the induction of the intra-S-phase checkpoint and DNA repair [16]. Finally, Cdk5 transduces the signals necessary for the expression of DNA-repair molecules. For example, expression of the DNA-repair endonuclease Eme1 in genotoxic agent-treated colorectal cancer cell lines is dependent on the activation of STAT3 by Cdk5 [33,38]. It will be useful to determine if Cdk5's role in the initiation and transduction of the DDR is dependent on the cancer type, the type of DNA-damaging method, or the severity of the DNA damage, as this might influence potential treatment strategies.

Cdk5 and Clinical Implications of Resistance to DNA-Damaging Therapies

Cdk5 function in the DDR and DNA repair may be linked to resistance to DNA-damaging anticancer therapies. Cdk5 has indeed been implicated in resistance to poly(ADP-ribose) polymerase inhibitors [16,32,34,39], topoisomerase inhibitors, and DNA crosslinkers. In line with these observations, treatment of the NSCLC cell line A549, the proliferation of which is driven by Cdk5 [11], with the Cdk5 inhibitor roscovitine enhanced its sensitivity to IR [40]. In all cases, Cdk5 inhibition or Cdk5 knockdown restored chemotherapeutics sensitivity. Likewise, the antitumor response to the chemotherapeutic in a xenograft mouse model of HCC was improved when roscovitine was coadministered [34]. These observations all suggest that effective Cdk5 inhibitors could be administered in combination with DNA-damaging agents to improve conventional anticancer treatments.

Cdk5 and Cancer Dissemination

During tumorigenesis, malignant cells can acquire phenotypic features enabling them to leave the primary tumor and transit via the blood and lymphatic circulation to secondary sites, in which they will grow into macrometastases [1]. In addition to tumor proliferation, Cdk5 is involved in the signaling pathways that underlie cancer cell migration to metastatic sites. Cdk5 has been linked to different components of the cancer dissemination process (Figure 2C).

Cdk5 and 'Migration-Proliferation Dichotomy'

Cdk5 contributes to the early events that decide whether tumor cells will continue growing or migrate toward secondary tumor sites for metastatic invasion [41]. When breast cancer cells are stimulated with epidermal growth factor, Cdk5 becomes activated and phosphorylates the G α -interacting vesicle-associated protein Girdin, which in turn activates traditional downstream

G-coupled receptor-dependent signaling mechanisms that promote cell migration. Thus, Cdk5 activity may be key in determining whether cells maintain a strictly proliferative versus invasive agenda.

Cdk5 and Epithelial-to-Mesenchymal Transition

Acquisition of the invasive phenotype requires cancer cells to change their cell–cell adhesion properties and acquire a motility phenotype, a process called epithelial-to-mesenchymal transition (Figure 2C). In breast cancer, Cdk5 is essential for initiation of metastatic invasion upon stimulation with transforming growth factor β 1 (TGF β 1) [15]. Depleting Cdk5 is sufficient to abolish TGF β 1-induced epithelial-to-mesenchymal transition. Interestingly, expression of Cdk5 and p35 in breast cancer cells is enhanced upon TGF β 1 stimulation. It will be useful to determine how TGF β 1 regulates the transcription of Cdk5 and p35.

Cdk5 and Cancer Cell Migration

Cdk5 activity drives the migration and metastatic invasion of some forms of lung [42], prostate [29,43], pancreas [6,44], melanoma [45], pituitary [13], and thyroid [27] cancers. The migration of these cancer cells in culture or *in vivo* is stopped upon Cdk5 inhibition (Figure 2C). Mechanistically, Cdk5 activity is dependent on p35 expression, which is controlled by the transcription factor human Achaete-scute homolog 1 in migrating neuroendocrine lung cancer cells [42].

In pancreatic cancer, Cdk5 is downstream of K-Ras [6,44]. In fact, K-Ras promotes the generation of p25 and activation of Cdk5, which subsequently turns on the Ral pathway and causes changes in cell morphology favoring cell migration. Pancreatic ductal adenocarcinoma cells exhibit shorter processes and become flat upon Cdk5 inhibition downstream of Ras [6]. In fact, Cdk5 activity is associated with the invasive cellular phenotype, including the remodeling of the actin cytoskeleton, the formation of invadopodia, and the regulation of focal adhesions, which are protein complexes involved in cell extracellular matrix adhesions and motility (Box 2). Whether Cdk5 involvement in cancer cell migration is dependent on cancer context or is common to all cancer types remains to be elucidated.

An Unexpected Role for Cdk5 in Tumor Angiogenesis

One of the least suspected functions for Cdk5 is its critical contribution to angiogenesis. This process by which blood vessels form from pre-existing ones to ensure the delivery of oxygen and nutrients to growing tumors allows removal of metabolic wastes and, together with lymphatic vessels, provide an escape route for cancer cells migration to metastatic sites. Evidence is rapidly

Box 2. Cdk5 Role in Cytoskeleton Regulation and Paclitaxel Resistance

Cdk5 is implicated in the acquisition of the invasive phenotype via regulation of actin and microtubule cytoskeleton as well as focal adhesions, which underlie the formation of invadopodia for cell motility (Table 2). Cdk5 regulates the formation of F-actin bundles in breast cancer cells [15]. Furthermore, Cdk5 modifies actin dynamics regulators such as caldesmon, an actin- and calmodulin-binding protein that participates in the migration and metastatic invasion of melanoma and breast cancer cells [45]. Cdk5 has long been implicated in the regulation of microtubule complexes that are essential for cell motility. For example, the microtubule-associated proteins Tau [69,70] and collapsin response mediator protein-2 [71], which promote microtubule assembly, as well as the microtubule-disassembly protein stathmin [72,73] are well-characterized Cdk5 substrates implicated in cancer progression. Finally, Cdk5 contributes to the formation and stabilization of focal adhesions, which serve as anchor for the migration process, by phosphorylating talin and focal adhesion kinase in migrating cells [6,15,74].

Cdk5s role in cytoskeleton remodeling may underlie resistance mechanisms to paclitaxel, a common chemotherapy agent that acts by preventing microtubule depolymerization and thus mitosis. Paclitaxel resistance is common and is associated with an invasive phenotype, which can be prevented by blocking Cdk5 activity [75]. Consistently, the sensitivity of ovary cancer cells to paclitaxel is enhanced upon Cdk5 depletion [76]. Remarkably, this drug induces Cdk5 expression, thereby promoting cell migration [61]. Thus, combinatorial treatments with a Cdk5 inhibitor and paclitaxel may prevent paclitaxel resistance [61]. Interestingly, Tau was identified as a potential predictive biomarker of the response of breast and gastric cancer patients to paclitaxel [70,77] with Tau-negative patients likely to have a better response to the drug.

implicating Cdk5 as a master regulator of angiogenesis at least in some cancers [46]. In addition to tumor cells, Cdk5 is expressed in endothelial cells lining of blood vessels that are usually quiescent [47] and regulates their proliferative and migratory properties [48,49] (Figure 2C).

Cdk5 and Endothelial Cell Survival

Cdk5 is critical for endothelial cell proliferation and disruption of Cdk5 expression causes apoptosis. Cdk5 protein levels are elevated in proliferating cultured bovine aortic endothelial cells while Cdk5 expression is lower in quiescent cells [47]. Consistently, overexpression of Cdk5 (and Cdk2) triggers cell proliferation and angiogenesis, whereas Cdk5/2 inhibition with roscovitine arrests both processes and leads to apoptosis [47,50].

Cdk5 and Endothelial Cell Migration

Cdk5 also contributes to endothelial cell migration [48,49]. Cdk5 regulates lamellipodia formation, and thus endothelial cell migration by remodeling the actin cytoskeleton via regulation of the monomeric GTPase Rac1 [48,51]. In melanoma xenograft mouse models, Cdk5 inhibition prevents formation of functional blood vessels and consequently tumor growth [49].

Cdk5 and Angiogenic Molecules

Several lines of evidence suggest there is an intricate relationship between Cdk5 and angiogenic molecules. First, Cdk5 expression in endothelial cell is induced by proproliferative, angiogenic factors, including basic fibroblast growth factor, that are secreted by tumor cells [50], while angiogenesis inhibitors such as angiostatin prevent Cdk5 expression and cause apoptosis [47]. Second, Cdk5 regulates the expression and activity of the transcription factor hypoxia-inducible factor 1 α (HIF1 α) in both HCC tumor and endothelial cells (Figure 2C,D). Thus, Cdk5 exerts direct control over expression of the HIF1 α target gene, vascular endothelial growth factor (VEGF)-A, and VEGF receptor 1, which are essential for the formation of new blood vessels in tumors [46]. Interestingly, Cdk5 can also act at the tumor cell level, inducing secretion of proangiogenic molecules. It will be critical in the future to determine if a regulatory loop between tumor and endothelial cells exists to control angiogenesis and how Cdk5 fits into it.

Cdk5 As an Antiangiogenic Drug Target

The apparent role of Cdk5 in endothelial cell physiology and tumor angiogenesis suggests it as a target for antiangiogenic treatment. New anti-Cdk5 drugs are being developed for this purpose [51]. Furthermore, other potential downstream targets of Cdk5 with function in angiogenesis, such as HIF1 α and Notch, are being identified [46,49]. With the recent discovery that Cdk5 is involved in the development of lymphatic vessels [52], it is becoming clear that Cdk5 plays a more important role than suspected in the tumor vasculature and in supporting tumor development and spread.

Current Strategies for Cdk5 Targeting

From pan-Cdk inhibitors to pathway-specific blocking peptides, the repertoire of Cdk5-targeting drugs is increasing [2,53] (Figure 1D–F). While currently available compounds and agents have limitations, there is now renewed interest in the therapeutic targeting of Cdk5 or its pathogenic effectors.

Small Molecules Inhibitors

Inhibition of kinase activity using pan-Cdk small molecules inhibitors is the most common strategy currently on hand to target Cdk5 in preclinical studies. For some of these drugs, clinical trials have been conducted with mixed results [2]. Roscovitine is widely used to inhibit Cdk5 in cell lines and mouse models. This purine analog competes for ATP binding to Cdk5, but also inhibits Cdk1, 2, 9, and 7 [54]. Roscovitine has no effects on Cdk4/6, rendering it useful to study Cdk5 effects on Rb and the cell cycle. Although roscovitine exhibits anticancer properties

preclinically, clinical trials have been inconclusive to date [2]. By contrast, dinaciclib, which has improved potency for Cdk5 and Cdk1, 2, and 9, exhibits antiproliferative effects on hematological cancers during clinical trials [2,53]. Thus, targeting Cdk5 along with Cdk1, 2, and 9 may be a valid anticancer strategy. Other small molecule inhibitors CP681301 [55], indolinone A [56], and *N*-(5-isopropylthiazol-2-yl)-3-phenylpropanamide (PJB) [45] exhibit increased selectivity for Cdk5 and Cdk2 over other Cdks and anticancer activity in cell lines [12,45], but *in vivo* preclinical studies remain to be conducted. Thus, more inhibitors are available to target Cdk5 more specifically.

A Peptide for the Disruption of Cdk5/Activator Binding

A peptide derived from p35/p25 that selectively blocks Cdk5/p25 interactions has been used to rescue the Cdk5/p25-induced pathological phenotypes [53] (Figure 1E). However, the anticancer effect of this peptide remains to be determined. A peptide that disrupts Cdk5/p35 binding would be a useful tool to target Cdk5 in tumor cells or animal models because both holoenzymes, Cdk5/p35 and Cdk5/p25, appear to be tumorigenic.

Small Interfering Peptides: Targeting Cdk5/Substrate Interactions

An alternative approach for preventing Cdk5-induced pathogenesis consists in using short peptides to selectively block Cdk5-dependent phosphorylation of aberrant substrate within a given pathogenic pathway (Figure 1E). These approximately 20-amino acid peptides, designed based on the Cdk5 phosphorylation site on the substrate, were successful in selectively preventing Cdk5 phosphorylation of Rb, *N*-methyl-D-aspartate receptor subunit, and phosphodiesterase 4 (PDE4) to impair molecular processes leading, respectively, to cancer progression, loss of cognition, or depression [12,57,58]. Using pathway-specific peptides has the advantage of limiting side effects due to mechanistic specificity, although size and stability issues are of concern. Rigorous preclinical studies will be necessary to confirm the possibility of using these peptides or peptidelike molecules as anticancer treatments.

Drug Combinations

Combining Cdk5 inhibitors with other drugs is appearing as an attractive strategy for improving existing therapies. Co-treatment of roscovitine and irinotecan arrests HCC growth in mouse models [34]. Combining Cdk5 inhibition with the antiviral agent tilorone selectively inhibited growth, proliferation, and invasive phenotype of prostate cancer cells [59], while using the Cdk5 inhibitor AC1MMYR2 in combination with the chemotherapy agent paclitaxel may prevent resistance associated with the use of paclitaxel [60,61].

Concluding Remarks

Cdk5 appears to play a central role in tumorigenic pathways, and therefore may be a valid target for anticancer drugs. Yet, many challenges remain (see Outstanding Questions). In particular, current clinical trials with pan-Cdk inhibitors have not been entirely conclusive. Developing more potent Cdk5 inhibitors and targeting Cdk5 downstream pathways in addition to Cdk5 may be a more effective strategy to stop cancer progression and limit adverse events.

Generating animal models of different cancers will be crucial to pinpoint the neoplastic roles of Cdk5 and identify targets for the treatment of Cdk5-driven cancers as well as for preclinical testing new therapies. Conditional expression of p25 under the appropriate promoter appears as a valid strategy to develop clinically relevant Cdk5-driven cancers that recapitulate the human disease. In this new era of immunotherapy, using animals in which tumor grows in a physiological microenvironment and in the context of a functional immune system may be crucial to obtain results that can be reproducible in patients.

Identifying the population of patients who could benefit from Cdk5-based treatments may also improve the outcomes of clinical trials. Defining a panel of biomarkers that includes Cdk5,

Outstanding Questions

Cdk5 can exist as both p35/Cdk5 and p25/Cdk5 complexes in cancer tissues. These two holoenzymes have different enzymatic properties with p25/Cdk5 being apparently more pathogenic. How is p25 generated in cancer cells? What cues activate calpain cleavage of p35 into p25 in cancer cells? What is the contribution of nestin in the p35-to-p25 turnover? Can the p35/Cdk5 over p25/Cdk5 ratio determine cancer prognosis? What are the exact roles of Cdk5/p35 and Cdk5/p25 in angiogenesis? How do they affect the secretion of proangiogenic growth factors by tumors and in which conditions?

Cdk5 is involved in many tumorigenic processes in different type of cancers. Are all cancers somehow dependent on Cdk5 activity at one stage of their development?

Given that Cdk5 is linked to resistance to DNA-damaging cancer drugs and paclitaxel, can Cdk5, p35, p25, or downstream signaling effectors be used as biomarkers to predict patient response to conventional cancer therapies and to stratify cancer patient population for personalized medicine treatments?

New potent and specific targeted therapies are being developed to inhibit Cdk5 or its downstream effectors and display antitumor effects in cell culture and preclinical models. Will these compounds have anticancer effects in clinical trials when used as mono or combinatorial therapies? Will combinatorial treatments of Cdk5 inhibitor and DNA-damaging agents/paclitaxel sensitize drug-resistant tumors in humans as observed preclinically? What will be the adverse events?

Cdk5 regulates the expression of the immune checkpoint programmed cell death-ligand 1 in medulloblastoma. Will targeting Cdk5 be a valid immunotherapy strategy in other cancers?

Drugs targeting epigenetic mechanisms are showing promising results in cancer treatments. Would targeting Cdk5 epigenetic regulation be a better anticancer strategy than targeting Cdk5 kinase activity?

activators, and phosphorylation sites on pro-neoplastic effectors would allow stratification of the patient population, facilitating more precise treatments.

Knowledge gained in the field of neuroscience over the past two to three decades has given cancer researchers hints on the oncogenic functions of Cdk5 and have led to potential translational applications that may benefit cancer patients. For example, the links between Cdk5 and resistance to conventional therapies, that is, DNA-damaging and microtubule-stabilizing agents, open new treatment opportunities. An important next challenge will be to determine in the clinic if combining Cdk5 inhibitors can improve tumor-resistant patient responses to conventional treatments, as observed in cell culture and preclinical models. Furthermore, the groundbreaking finding that Cdk5 regulates the expression of the immune checkpoint programmed cell death-ligand 1 (PD-L1) [62] may offer new applications for Cdk5-targeting drugs in the immunotherapy.

Recent efforts have focused on targeting Cdk4/6 [2] and have led to the development and Food and Drug Administration approval of potent inhibitors for the treatment of some breast cancers. However, resistance to these drugs is frequently observed. Based on the newly discovered role of Cdk5 in Rb regulation, the question is arising as whether Cdk5 acts as an alternate driver in Cdk4/6-resistant cancers, broadening the spectrum for treatment strategies while increasing the urgency for moving Cdk5-specific anticancer drugs into the clinical arsenal. In this upcoming era of personalized medicine, defining a set of biomarkers that differentiate Cdk5- from Cdk4/6-driven cancers will be crucial to match cancer patients with the appropriate treatment.

Acknowledgments

This work was supported by a North American Neuroendocrine Tumor Society fellowship (K.P.), U.S. National Institutes of Health Grants (MH79710, MH083711, DA016672, DA033485, and NS073855) and American Cancer Society MEN2 Thyroid Cancer Consortium Research Grant (RSGM-11-190-01) to J.A.B. We thank Erik Knudsen and Florian Plattner for helpful discussions and Kate Mackley for graphic art. We apologize to authors whose work was not cited due to space limitations. Some images are used under license from Shutterstock.com. Credits to S. Kaulitzki/S.K. Chavan/M. Vaculikova/J. Vitanovski/Shutterstock.

Supplemental Information

Supplemental information associated with this article can be found online at [doi:10.1016/j.trecan.2016.09.001](https://doi.org/10.1016/j.trecan.2016.09.001).

References

- Hanahan, D. and Weinberg, R.A. (2011) Hallmarks of cancer: the next generation. *Cell* 144, 646–674
- Asghar, U. *et al.* (2015) The history and future of targeting cyclin-dependent kinases in cancer therapy. *Nat. Rev. Drug Discov.* 14, 130–146
- Dhavan, R. and Tsai, L.H. (2001) A decade of CDK5. *Nat. Rev. Mol. Cell Biol.* 2, 749–759
- Lockwood, W.W. *et al.* (2008) DNA amplification is a ubiquitous mechanism of oncogene activation in lung and other cancers. *Oncogene* 27, 4615–4624
- Harada, T. *et al.* (2008) Genome-wide DNA copy number analysis in pancreatic cancer using high-density single nucleotide polymorphism arrays. *Oncogene* 27, 1951–1960
- Eggers, J.P. *et al.* (2011) Cyclin-dependent kinase 5 is amplified and overexpressed in pancreatic cancer and activated by mutant K-Ras. *Clin. Cancer Res.* 17, 6140–6150
- Choi, H.S. *et al.* (2009) Single-nucleotide polymorphisms in the promoter of the CDK5 gene and lung cancer risk in a Korean population. *J. Hum. Genet.* 54, 298–303
- Kibel, A.S. *et al.* (2016) Genetic variants in cell cycle control pathway confer susceptibility to aggressive prostate carcinoma. *Prostate* 76, 479–490
- Wei, K. *et al.* (2016) An immunohistochemical study of cyclin-dependent kinase 5 (CDK5) expression in non-small cell lung cancer (NSCLC) and small cell lung cancer (SCLC): a possible prognostic biomarker. *World J. Surg. Oncol.* 14, 34
- Meder, L. *et al.* (2016) NOTCH, ASCL1, p53 and RB alterations define an alternative pathway driving neuroendocrine and small cell lung carcinomas. *Int. J. Cancer* 138, 927–938
- Liu, J.L. *et al.* (2015) Cyclin-dependent kinase 5 regulates the proliferation, motility and invasiveness of lung cancer cells through its effects on cytoskeletal remodeling. *Mol. Med. Rep.* 12, 3979–3985
- Pozo, K. *et al.* (2013) The role of Cdk5 in neuroendocrine thyroid cancer. *Cancer Cell* 24, 499–511
- Xie, W. *et al.* (2016) Phosphorylation of kinase insert domain receptor by cyclin-dependent kinase 5 at serine 229 is associated with invasive behavior and poor prognosis in prolactin pituitary adenomas. *Oncotarget*. Published online July 12, 2016. <http://dx.doi.org/10.18632/oncotarget.10550>
- Liu, J.L. *et al.* (2011) Expression of CDK5/p35 in resected patients with non-small cell lung cancer: relation to prognosis. *Med. Oncol.* 28, 673–678
- Liang, Q. *et al.* (2013) CDK5 is essential for TGF- β 1-induced epithelial-mesenchymal transition and breast cancer progression. *Sci. Rep.* 3, 2932
- Chiker, S. *et al.* (2015) Cdk5 promotes DNA replication stress checkpoint activation through RPA-32 phosphorylation, and

- impacts on metastasis free survival in breast cancer patients. *Cell Cycle* 14, 3066–3078
17. Catania, A. *et al.* (2001) Expression and localization of cyclin-dependent kinase 5 in apoptotic human glioma cells. *Neuro. Oncol.* 3, 89–98
 18. Yushan, R. *et al.* (2015) Insights into the clinical value of cyclin-dependent kinase 5 in glioma: a retrospective study. *World J. Surg. Oncol.* 13, 223
 19. Zhang, X. *et al.* (2015) Aberrant expression of CDK5 infers poor outcomes for nasopharyngeal carcinoma patients. *Int. J. Clin. Exp. Pathol.* 8, 8066–8074
 20. Cao, L. *et al.* (2015) Cyclin-dependent kinase 5 decreases in gastric cancer and its nuclear accumulation suppresses gastric tumorigenesis. *Clin. Cancer Res.* 21, 1419–1428
 21. Lu, J.W. *et al.* (2011) Decreased expression of p39 is associated with a poor prognosis in human hepatocellular carcinoma. *Med. Oncol.* 28 (Suppl 1), S239–S245
 22. Lopes, J.P. and Agostinho, P. (2011) Cdk5: multitasking between physiological and pathological conditions. *Prog. Neurobiol.* 94, 49–63
 23. Futatsugi, A. *et al.* (2012) Cyclin-dependent kinase 5 regulates E2F transcription factor through phosphorylation of Rb protein in neurons. *Cell Cycle* 11, 1603–1610
 24. Ogara, M.F. *et al.* (2014) CDK5-mediated phosphorylation of p19INK4d avoids DNA damage-induced neurodegeneration in mouse hippocampus and prevents loss of cognitive functions. *Biochim. Biophys. Acta* 1843, 1309–1324
 25. Chang, K.H. *et al.* (2012) Deregulated Cdk5 triggers aberrant activation of cell cycle kinases and phosphatases inducing neuronal death. *J. Cell Sci.* 125, 5124–5137
 26. Fu, A.K. *et al.* (2004) Cyclin-dependent kinase 5 phosphorylates signal transducer and activator of transcription 3 and regulates its transcriptional activity. *Proc. Natl. Acad. Sci. U. S. A.* 101, 6728–6733
 27. Lin, H. *et al.* (2007) Cdk5 regulates STAT3 activation and cell proliferation in medullary thyroid carcinoma cells. *J. Biol. Chem.* 282, 2776–2784
 28. Hsu, F.N. *et al.* (2013) Cyclin-dependent kinase 5 modulates STAT3 and androgen receptor activation through phosphorylation of Ser(7)(2)(7) on STAT3 in prostate cancer cells. *Am. J. Physiol. Endocrinol. Metab.* 305, E975–E986
 29. Lin, H. *et al.* (2004) Involvement of Cdk5/p25 in digoxin-triggered prostate cancer cell apoptosis. *J. Biol. Chem.* 279, 29302–29307
 30. Lindqvist, J. *et al.* (2015) Cyclin-dependent kinase 5 acts as a critical determinant of AKT-dependent proliferation and regulates differential gene expression by the androgen receptor in prostate cancer cells. *Mol. Biol. Cell* 26, 1971–1984
 31. Goldstein, M. and Kastan, M.B. (2015) The DNA damage response: implications for tumor responses to radiation and chemotherapy. *Annu. Rev. Med.* 66, 129–143
 32. Turner, N.C. *et al.* (2008) A synthetic lethal siRNA screen identifying genes mediating sensitivity to a PARP inhibitor. *EMBO J.* 27, 1368–1377
 33. Courapied, S. *et al.* (2010) The cdk5 kinase regulates the STAT3 transcription factor to prevent DNA damage upon topoisomerase I inhibition. *J. Biol. Chem.* 285, 26765–26778
 34. Ehrlich, S.M. *et al.* (2015) Targeting cyclin dependent kinase 5 in hepatocellular carcinoma – a novel therapeutic approach. *J. Hepatol.* 63, 102–113
 35. Yu, H.P. *et al.* (2015) TIGAR regulates DNA damage and repair through pentosephosphate pathway and Cdk5-ATM pathway. *Sci. Rep.* 5, 9853
 36. Lee, J.H. and Kim, K.T. (2007) Regulation of cyclin-dependent kinase 5 and p53 by ERK1/2 pathway in the DNA damage-induced neuronal death. *J. Cell Physiol.* 210, 784–797
 37. Tian, B. *et al.* (2009) Phosphorylation of ATM by Cdk5 mediates DNA damage signalling and regulates neuronal death. *Nat. Cell Biol.* 11, 211–218
 38. Vigneron, A. *et al.* (2008) The EGFR-STAT3 oncogenic pathway up-regulates the Eme1 endonuclease to reduce DNA damage after topoisomerase I inhibition. *Cancer Res.* 68, 815–825
 39. Bolin, C. *et al.* (2012) The impact of cyclin-dependent kinase 5 depletion on poly(ADP-ribose) polymerase activity and responses to radiation. *Cell Mol. Life Sci.* 69, 951–962
 40. Zhang, F. *et al.* (2008) Enhancement of radiosensitivity by roscovitine pretreatment in human non-small cell lung cancer A549 cells. *J. Radiat. Res.* 49, 541–548
 41. Bhandari, D. *et al.* (2015) Cyclin-dependent kinase 5 activates guanine nucleotide exchange factor GIV/Girdin to orchestrate migration-proliferation dichotomy. *Proc. Natl. Acad. Sci. U. S. A.* 112, E4874–E4883
 42. Demelash, A. *et al.* (2012) Achaete-scute homologue-1 (ASH1) stimulates migration of lung cancer cells through Cdk5/p35 pathway. *Mol. Biol. Cell* 23, 2856–2866
 43. Strock, C.J. *et al.* (2006) Cyclin-dependent kinase 5 activity controls cell motility and metastatic potential of prostate cancer cells. *Cancer Res.* 66, 7509–7515
 44. Feldmann, G. *et al.* (2011) Cyclin-dependent kinase inhibitor Dinaciclib (SCH727965) inhibits pancreatic cancer growth and progression in murine xenograft models. *Cancer Biol. Ther.* 12, 598–609
 45. Bisht, S. *et al.* (2015) Cyclin-dependent kinase 5 (CDK5) controls melanoma cell motility, invasiveness, and metastatic spread – identification of a promising novel therapeutic target. *Transl. Oncol.* 8, 295–307
 46. Herzog, J. *et al.* (2016) Cyclin-dependent kinase 5 stabilizes hypoxia-inducible factor-1alpha: a novel approach for inhibiting angiogenesis in hepatocellular carcinoma. *Oncotarget* 7, 27108–27121
 47. Sharma, M.R. *et al.* (2004) Angiostatin-induced inhibition of endothelial cell proliferation/apoptosis is associated with the down-regulation of cell cycle regulatory protein cdk5. *J. Cell Biochem.* 91, 398–409
 48. Liebl, J. *et al.* (2010) Cyclin-dependent kinase 5 regulates endothelial cell migration and angiogenesis. *J. Biol. Chem.* 285, 35932–35943
 49. Merk, H. *et al.* (2016) Inhibition of endothelial Cdk5 reduces tumor growth by promoting non-productive angiogenesis. *Oncotarget* 7, 6088–6104
 50. de Nigris, F. *et al.* (2013) Osteosarcoma cells induce endothelial cell proliferation during neo-angiogenesis. *J. Cell. Physiol.* 228, 846–852
 51. Weitensteiner, S.B. *et al.* (2013) Trisubstituted pyrazolopyrimidines as novel angiogenesis inhibitors. *PLoS One* 8, e54607
 52. Liebl, J. *et al.* (2015) Cdk5 controls lymphatic vessel development and function by phosphorylation of Foxc2. *Nat. Commun.* 6, 7274
 53. Peyressat, M. *et al.* (2015) Targeting cyclin-dependent kinases in human cancers: from small molecules to peptide inhibitors. *Cancers (Basel)* 7, 179–237
 54. Cicen, J. *et al.* (2015) Roscovitine in cancer and other diseases. *Ann. Transl. Med.* 3, 135
 55. Karran, E. and Palmer, A.M. (2007) Neurodegenerative disorders and their treatment. *Drug News Perspect.* 20, 407–412
 56. Weishaupt, J.H. *et al.* (2003) Inhibition of CDK5 is protective in necrotic and apoptotic paradigms of neuronal cell death and prevents mitochondrial dysfunction. *Mol. Cell Neurosci.* 24, 489–502
 57. Plattner, F. *et al.* (2014) Memory enhancement by targeting Cdk5 regulation of NR2B. *Neuron* 81, 1070–1083
 58. Plattner, F. *et al.* (2015) The role of ventral striatal cAMP signaling in stress-induced behaviors. *Nat. Neurosci.* 18, 1094–1100
 59. Wissing, M.D. *et al.* (2014) Small-molecule screening of PC3 prostate cancer cells identifies tilorone dihydrochloride to selectively inhibit cell growth based on cyclin-dependent kinase 5 expression. *Oncol. Rep.* 32, 419–424
 60. Shi, Z. *et al.* (2013) AC1MMYR2, an inhibitor of dicer-mediated biogenesis of oncomir miR-21, reverses epithelial-mesenchymal transition and suppresses tumor growth and progression. *Cancer Res.* 73, 5519–5531
 61. Ren, Y. *et al.* (2015) AC1MMYR2 impairs high dose paclitaxel-induced tumor metastasis by targeting miR-21/CDK5 axis. *Cancer Lett.* 362, 174–182
 62. Dorand, R.D. *et al.* (2016) Cdk5 disruption attenuates tumor PD-L1 expression and promotes antitumor immunity. *Science* 353, 399–403

63. Liebl, J. *et al.* (2011) Twice switched at birth: cell cycle-independent roles of the "neuron-specific" cyclin-dependent kinase 5 (Cdk5) in non-neuronal cells. *Cell Signal*. 23, 1698–1707
64. Arif, A. (2012) Extraneuronal activities and regulatory mechanisms of the atypical cyclin-dependent kinase Cdk5. *Biochem. Pharmacol.* 84, 985–993
65. Brinkkoetter, P.T. *et al.* (2009) Cyclin I activates Cdk5 and regulates expression of Bcl-2 and Bcl-XL in postmitotic mouse cells. *J. Clin. Investig.* 119, 3089–3101
66. Li, R. *et al.* (2015) Cyclin I promotes cisplatin resistance via Cdk5 activation in cervical cancer. *Eur. Rev. Med. Pharmacol. Sci.* 19, 4533–4541
67. Hisanaga, S. and Saito, T. (2003) The regulation of cyclin-dependent kinase 5 activity through the metabolism of p35 or p39 Cdk5 activator. *Neurosignals* 12, 221–229
68. Lindqvist, J. *et al.* (2016) Studying nestin and its interrelationship with Cdk5. *Methods Enzymol.* 568, 509–535
69. Takashima, A. *et al.* (2001) Involvement of cyclin dependent kinase5 activator p25 on tau phosphorylation in mouse brain. *Neurosci. Lett.* 306, 37–40
70. Rouzier, R. *et al.* (2005) Microtubule-associated protein tau: a marker of paclitaxel sensitivity in breast cancer. *Proc. Natl. Acad. Sci. U. S. A.* 102, 8315–8320
71. Grant, N.J. *et al.* (2015) Phosphorylation of a splice variant of collapsin response mediator protein 2 in the nucleus of tumour cells links cyclin dependent kinase-5 to oncogenesis. *BMC Cancer* 15, 885
72. Hayashi, K. *et al.* (2006) Phosphorylation of the tubulin-binding protein, stathmin, by Cdk5 and MAP kinases in the brain. *J. Neurochem.* 99, 237–250
73. Nie, W. *et al.* (2015) Overexpression of stathmin 1 is a poor prognostic biomarker in non-small cell lung cancer. *Lab. Invest.* 95, 56–64
74. Huang, C. *et al.* (2009) Talin phosphorylation by Cdk5 regulates Smurf1-mediated talin head ubiquitylation and cell migration. *Nat. Cell Biol.* 11, 624–630
75. Quintavalle, M. *et al.* (2011) A cell-based high-content screening assay reveals activators and inhibitors of cancer cell invasion. *Sci. Signal.* 4, ra49
76. Zhang, S. *et al.* (2015) CDK5 regulates paclitaxel sensitivity in ovarian cancer cells by modulating AKT activation, p21Cip1- and p27Kip1-mediated G₁ cell cycle arrest and apoptosis. *PLoS One* 10, e0131833
77. Mimori, K. *et al.* (2006) Reduced tau expression in gastric cancer can identify candidates for successful paclitaxel treatment. *Br. J. Cancer* 94, 1894–1897
78. Kim, E. *et al.* (2006) CDK5 is a novel regulatory protein in PPARgamma ligand-induced antiproliferation. *Int. J. Oncol.* 28, 191–194
79. Lowman, X.H. *et al.* (2010) The proapoptotic function of Noxa in human leukemia cells is regulated by the kinase Cdk5 and by glucose. *Mol. Cell* 40, 823–833
80. Leshchenko, V.V. *et al.* (2010) Genomewide DNA methylation analysis reveals novel targets for drug development in mantle cell lymphoma. *Blood* 116, 1025–1034
81. Levacque, Z. *et al.* (2012) Level of cdk5 expression predicts the survival of relapsed multiple myeloma patients. *Cell Cycle* 11, 4093–4095
82. Hsu, F.N. *et al.* (2011) Regulation of androgen receptor and prostate cancer growth by cyclin-dependent kinase 5. *J. Biol. Chem.* 286, 33141–33149
83. Huang, E. *et al.* (2010) The role of Cdk5-mediated apurinic/apyr-imidinic endonuclease 1 phosphorylation in neuronal death. *Nat. Cell Biol.* 12, 563–571
84. Tripathi, B.K. *et al.* (2014) CDK5 is a major regulator of the tumor suppressor DLC1. *J. Cell. Biol.* 207, 627–642
85. Xie, Z. *et al.* (2003) Serine 732 phosphorylation of FAK by Cdk5 is important for microtubule organization, nuclear movement, and neuronal migration. *Cell* 114, 469–482
86. Filippova, N. *et al.* (2012) Phosphoregulation of the RNA-binding protein Hu antigen R (HuR) by Cdk5 affects centrosome function. *J. Biol. Chem.* 287, 32277–32287
87. Rashid, T. *et al.* (2001) Phosphorylation of Pak1 by the p35/Cdk5 kinase affects neuronal morphology. *J. Biol. Chem.* 276, 49043–49052
88. Lee, J.H. *et al.* (2007) Stabilization and activation of p53 induced by Cdk5 contributes to neuronal cell death. *J. Cell Sci.* 120, 2259–2271
89. Ajay, A.K. *et al.* (2010) Cdk5 phosphorylates non-genotoxically overexpressed p53 following inhibition of PP2A to induce cell cycle arrest/apoptosis and inhibits tumor progression. *Mol. Cancer* 9, 204
90. Liu, R. *et al.* (2008) Cdk5-mediated regulation of the PIKE-A-Akt pathway and glioblastoma cell invasion. *Proc. Natl. Acad. Sci. U. S. A.* 105, 7570–7575
91. Lee, K.Y. *et al.* (1997) Neuronal Cdc2-like kinase (Nclk) binds and phosphorylates the retinoblastoma protein. *J. Biol. Chem.* 272, 5622–5626
92. Xie, W. *et al.* (2014) CDK5 and its activator P35 in normal pituitary and in pituitary adenomas: relationship to VEGF expression. *Int. J. Biol. Sci.* 10, 192–199

Differential expression of cell cycle regulators in CDK5-dependent medullary thyroid carcinoma tumorigenesis

Karine Pozo¹, Antje Hillmann¹, Alexander Augustyn^{2,3}, Florian Plattner¹, Tao Hai⁴, Tanvir Singh¹, Saleh Ramezani⁵, Xiankai Sun⁵, Roswitha Pfragner⁶, John D. Minna^{2,3,7}, Gilbert J. Cote⁴, Herbert Chen⁸, James A. Bibb^{1,5,9,*} and Fiemu E. Nwariaku^{10,*}

¹ Department of Psychiatry, The University of Texas Southwestern Medical Center, Dallas, TX, USA

² Hamon Center for Therapeutic Oncology Research, The University of Texas Southwestern Medical Center, Dallas, TX, USA

³ Harold C. Simmons Comprehensive Cancer Center, The University of Texas Southwestern Medical Center, Dallas, TX, USA

⁴ Department of Endocrine Neoplasia and Hormonal Disorders, The University of Texas MD Anderson Cancer Center, Houston, TX, USA

⁵ Department of Radiology, The University of Texas Southwestern Medical Center, Dallas, TX, USA

⁶ Institute of Pathophysiology and Immunology, Medical University of Graz, Graz, Austria

⁷ Department of Pharmacology, The University of Texas Southwestern Medical Center, Dallas, TX, USA

⁸ Endocrine Surgery Research Laboratory, The University of Wisconsin Carbone Cancer Center, Madison, WI, USA

⁹ Department of Neurology and Neurotherapeutics, The University of Texas Southwestern Medical Center, Dallas, TX, USA

¹⁰ Department of Surgery, The University of Texas Southwestern Medical Center, Dallas, TX, USA

* These authors have contributed equally to this work

Correspondence to: James A. Bibb, *email:* james.bibb@utsouthwestern.edu

Karine Pozo, *email:* karine.pozo@utsouthwestern.edu

Keywords: Cdk5, retinoblastoma protein, neuroendocrine, medullary thyroid carcinoma, cell cycle

Received: August 26, 2014

Accepted: March 03, 2015

Published: April 14, 2015

This is an open-access article distributed under the terms of the Creative Commons Attribution License, which permits unrestricted use, distribution, and reproduction in any medium, provided the original author and source are credited.

ABSTRACT

Medullary thyroid carcinoma (MTC) is a neuroendocrine cancer of thyroid C-cells, for which few treatment options are available. We have recently reported a role for cyclin-dependent kinase 5 (CDK5) in MTC pathogenesis. We have generated a mouse model, in which MTC proliferation is induced upon conditional overexpression of the CDK5 activator, p25, in C-cells, and arrested by interrupting p25 overexpression. Here, we identify genes and proteins that are differentially expressed in proliferating versus arrested benign mouse MTC. We find that downstream target genes of the tumor suppressor, retinoblastoma protein, including genes encoding cell cycle regulators such as CDKs, cyclins and CDK inhibitors, are significantly upregulated in malignant mouse tumors in a CDK5-dependent manner. Reducing CDK5 activity in human MTC cells down-regulated these cell cycle regulators suggesting that CDK5 activity is critical for cell cycle progression and MTC proliferation. Finally, the same set of cell cycle proteins was consistently overexpressed in human sporadic MTC but not in hereditary MTC. Together these findings suggest that aberrant CDK5 activity precedes cell cycle initiation and thus may function as a tumor-promoting factor facilitating cell cycle protein expression in MTC. Targeting aberrant CDK5 or its downstream effectors may be a strategy to halt MTC tumorigenesis.

INTRODUCTION

Neuroendocrine tumors (NETs) are rare cancers

originating from hormone-secreting neuroendocrine (NE) cells. These slow-growing neoplasms affect both genders equally and their incidence is rising [1, 2]. NETs are often

diagnosed at late metastatic stages due to the absence of specific symptoms and are therefore often fatal. MTC arises from the thyroid parafollicular cells (C-cells), which secrete calcitonin. Most MTC cases (75%) are sporadic and about 40% are caused by somatic mutations in the *RET* proto-oncogene, 15% by mutation in the *RAS* gene, 10% by mutations in other genes and 35% by unknown causes [3-5]. Overall the etiology of sporadic MTC is poorly understood. Hereditary forms of MTC represent about 25% of cases and result from germline mutation in the *RET* proto-oncogene [6]. These genetic forms of MTC are often associated with other types of NE cancers and they are referred to as Multiple Endocrine Neoplasia of Type 2 (MEN 2). Surgical resection of the thyroid is the best treatment currently available for early stage disease but recurrence is common, particularly in sporadic MTC. The prognosis for advanced forms of MTC is poor with a five-year survival rate of 30%. FDA-approved drugs include the tyrosine kinase inhibitors, Vandetanib [7] and Cabozantinib [8], however their efficacy is limited [8, 9]. Therefore a better understanding of the drivers of MTC progression, especially in the absence of *RET* or *RAS* mutations, is needed to develop more effective treatment strategies. Toward this goal, it is paramount to elucidate additional molecular mechanisms underlying MTC and identify new targets for therapy development.

We recently reported that cyclin-dependent kinase 5 (CDK5) was involved in MTC pathogenesis [10, 11]. CDK5 is a serine/threonine kinase that is highly expressed in the brain and regulates neuronal function [12] but its role in cell cycle and cancer has not been well explored. CDK5 is activated by interaction with its cofactor, p35 [13], which can be cleaved by the calcium-dependent protein kinase, calpain, to produce p25. The resulting p25-CDK5 complex engenders aberrant activity with a different range of substrates. CDK5, p35 and p25 are expressed in other tissues besides brain and have been implicated in various forms of neoplasms, including thyroid [10, 11], pancreatic [14, 15], pituitary [16], breast [17], prostate [18, 19], and lung [20] cancers. In particular, CDK5 contributes to MTC by inactivating the tumor suppressor retinoblastoma protein (Rb), which is a 'gatekeeper' of the cell cycle [10], thereby suggesting a crucial role for CDK5 in the regulation of the cell cycle.

We have generated a novel conditional MTC mouse model in which overexpression of p25 (p25OE) in mouse thyroid C-cells invokes aberrant CDK5 activity and MTC tumorigenesis [10, 21]. Importantly, in these mice, arrest of p25OE completely halts MTC growth, thereby transforming tumors from a malignant to benign state. Mice harboring arrested tumors exhibit normal survival rates, whereas mice with proliferating MTC die within 30 weeks of transgene induction. A comparison of genes and proteins that are differentially expressed between malignant and benign tumors can help unravel the molecular basis for MTC tumorigenesis. Therefore in

this study we investigate further the role of CDK5 in MTC pathogenesis by using an integrated approach including the novel MTC mouse model, human MTC cell lines and patient samples.

RESULTS

Differential gene expression analysis of tumors from an inducible medullary thyroid carcinoma mouse model

We have previously described a novel mouse model for MTC in which tumor progression and arrest are induced by overexpressing, and interrupting, green fluorescent protein-tagged p25 (p25-GFP) in thyroid C-cells [10]. Proliferating tumors display abnormally elevated CDK5 activity and are malignant. In contrast, arrested tumors are benign and exhibit much lower levels of CDK5 activity. Consistent with elevated cell proliferation, PET/CT imaging revealed 2.7-fold elevation in metabolic activity for proliferating malignant thyroid tumors compared to arrested benign tumors (Figure 1A). To gain more understanding of the molecular mechanisms underlying p25-CDK5-induced MTC proliferation, we conducted a microarray study of the differential mRNA expression in malignant versus benign tumors. Unsupervised clustering analyses identified 116 genes that were up-regulated, while 7 genes were down-regulated in malignant MTC compared to benign tumors (Figure 1B, Tables S1 and S2). Gene ontology analyses revealed a significant up-regulation of genes involved in cell cycle, cellular assembly and organization, DNA replication, DNA recombination, DNA repair, cellular movement, cellular death and cell survival (Figure 1C).

We previously showed that p25-CDK5-induced tumorigenesis was associated with elevated Rb phosphorylation, which inactivates Rb and leads to increased transcription of E2F target genes [10]. Consistent with these observations, differential gene analysis showed that the expression of E2F target genes such as those encoding Aurora kinase 1, Polo-like kinase 1, Survivin (BIRC5) and the cell cycle regulators CDK1, cyclin-A1 and cyclin-E2 were 3- to 4-fold up-regulated in malignant tumors (Figures 1D - 1E, Table S1).

To validate the results of the differential gene expression analyses, *eGFP* was used as an internal control, as *eGFP* mRNA levels increase in proliferating tumors due to tetOp-tTA-mediated p25-GFP transgene overexpression. Consistent with its targeted regulation, the *eGFP* gene exhibited the highest differential expression level ($\log_2 = 6.88$, Table S1). Reverse transcription real time PCR (RT-qPCR) analysis confirmed this increased *eGFP* mRNA expression (Figure S1A).

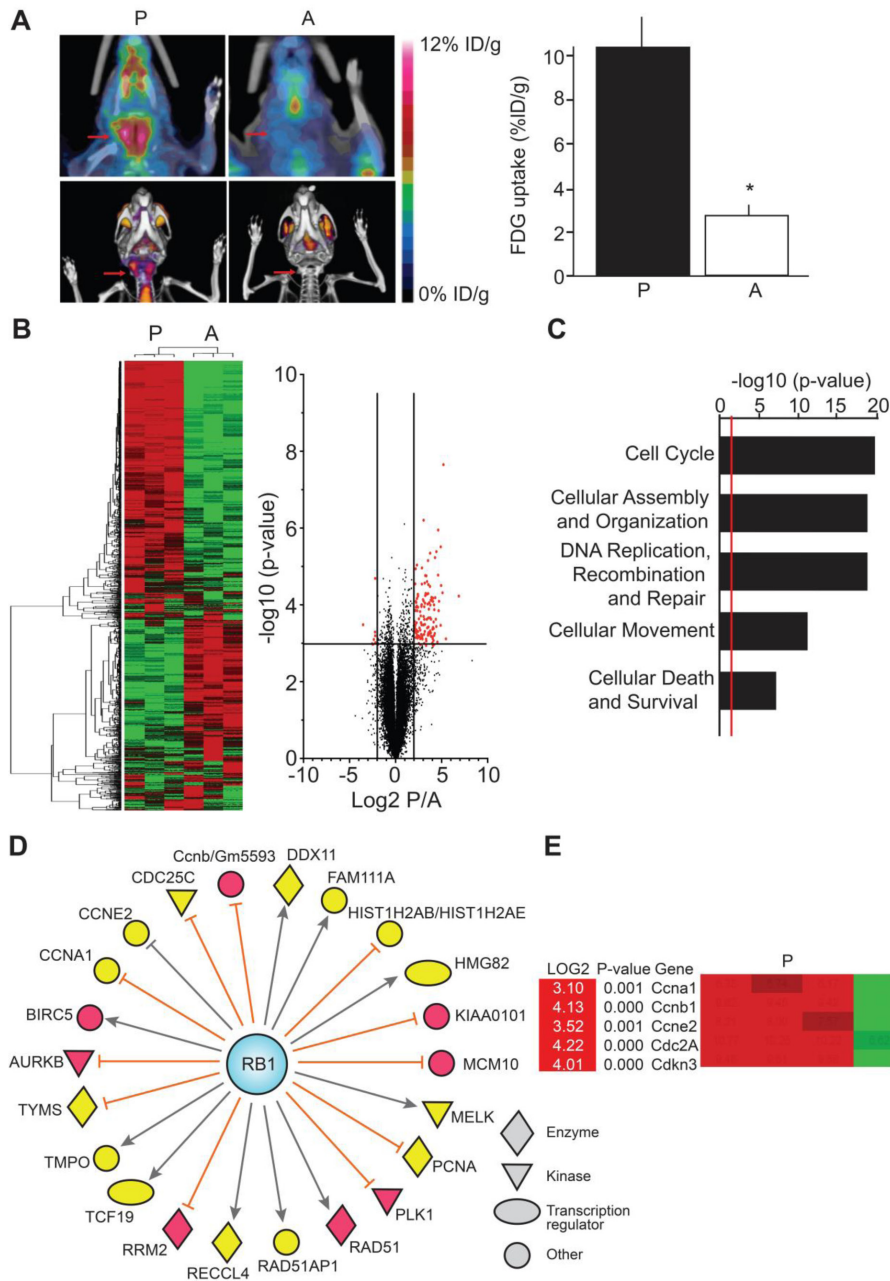


Figure 1: Differential gene expression analysis of the conditional MTC mouse tumors. A) PET/CT scans show increased thyroid metabolism in mice with proliferating malignant tumors (P) compared to mice with arrested benign tumors (A) (N = 3 for each condition, $p = 0.0139$, Student's t-test), arrows show the thyroid area. B, C and D) Expression array analyses. B) Heat map and volcano plot representations of differentially regulated mRNA in proliferating malignant versus arrested benign mouse tumors. Heat map shows segregation of arrested and proliferating tumors using unsupervised clustering analysis of gene expression data. Green color indicates down-regulated genes and red color, up-regulated genes. The X-axis on volcano plot represents expression of all genes in the microarray, with cutoffs displayed at $\pm \log_2 = 2.00$. The Y-axis plots a t-test transform, representing the significance of the gene expression difference for each gene. The line represents the boundary for p-values above $-\log_{10} = 3.00$. Red points represent genes of interest, which exceeded both indicated cutoffs. C) Pathway analysis of up-regulated genes in proliferating tumors. The X-axis represents the p-value associated with each gene category identified from Ingenuity Pathway Analysis (IPA). The higher the value, the less likely that the gene group appears in the proliferating tumors by chance. The red line represents a standard cutoff value of $p = 0.01$. D) IPA analysis showing the relationship between retinoblastoma protein (RB1) and up-regulated downstream molecules that were identified in the gene expression array analysis. Yellow color indicates moderate levels of expression and red color indicates high levels of expression. Relations between Rb and downstream molecules are as follows: orange lines indicate molecules that are inhibited when Rb is in an active, hypophosphorylated state; grey lines indicate that the effect of Rb on the molecule is not predicted. E) Examples of cell cycle regulators with quantitation from proliferating vs. arrested tumors. Data are represented as mean \pm SEM.

Table 1: A Table summarizing cell cycle protein expression in mouse MTC tumors, human MTC-SK cells and human MTC tissues. To determine the role of CDK5 activity in the expression of cell cycle regulators, we assessed the changes in protein level of cyclins, CDKs, and CKI in mouse tumors and in MTC-SK cells following blockade of CDK5 activity. We have indeed previously demonstrated that CDK5 activity is reduced in arrested tumors by stopping p25-GFP transgene expression and in MTC-SK cells by overexpressing a kinase-dead CDK5 construct [10]. The changes in expression of cell cycle regulators in human MTC tumors compared to normal thyroid tissues are also reported

	Mouse model		Human cell line		Patient tissues	
	Arrested vs proliferating MTC	vs	Kd-Cdk5-transfected cells vs control cells	Sporadic control thyroid	MTC vs Hereditary MTC	vs control thyroid
Cdk2	↓		↓	↑		↓
Cdk4	-		↓	-		-
Cdk6	-		↓	-		-
cyclin A1	↓		↓	-		-
cyclin B1	↓		↓	n.d.		n.d.
cyclin D1	-		n.d.	↑		-
cyclin E2	↓		↓	-		-
p15 ^{INK4b}	↓		↓	↑		↑
p16 ^{INK4a}	-		-	↑		↑
p18 ^{INK4c}	↓		-	↑		-
p19 ^{INK4d}	↓		↓	↑		-
p21 ^{CIP/WAF1}	↓		↓	(↑)		-
p27 ^{KIP1}	-		-	-		-

Gene expression analysis of cell cycle regulators in malignant and benign mouse MTC

While CDK5 is well characterized for its role in the central nervous system, less is known about its role in the cell cycle. We and others have found that CDK5 could regulate the activation state of the tumor suppressor Rb, thereby implicating CDK5 in the regulation of cell cycle progression [10, 22, 23]. Here, the gene expression analysis revealed a significant up-regulation of genes encoding cell cycle proteins, including CDKs, cyclins and endogenous cyclin-dependent kinase inhibitors (CKI), in malignant mouse MTC, suggesting that p25-CDK5-dependent MTC tumorigenesis is associated with alterations in cell cycle regulation.

To validate the expression array data and investigate further the role of CDK5 in the cell cycle, we measured the relative expression of genes encoding CDK, cyclins and CKI by RT-qPCR analyses. Elevated *Cdk1*, *Cdk2* and *Cdk4* mRNA levels were detected in proliferating malignant tumors. *Cdk5* mRNA levels remained unchanged despite

p25 overexpression. Somewhat unexpectedly, *Cdk6* mRNA expression was increased in arrested benign tumors (Figure 2A). Similarly, cyclin-D1 and p35 gene products, *Ccnd1* and *Cdk5r1*, were up-regulated in benign tumors (Figure 2B). In contrast, the genes encoding cyclin-A1, -B1, -E1 and -E2, *i.e.* *Ccna1*, *Ccnb1*, *Ccne1* and *Ccne2*, were up-regulated in malignant tumors. Finally, CKI gene expression analysis revealed elevated mRNA expression in malignant tumors for p16^{INK4a}, p18^{INK4c}, p19^{INK4d} and p21^{CIP/WAF1} encoding genes, *i.e.* *Cdkn2a*, *Cdkn2c*, *Cdkn2d* and *Cdkn1a*, while p15^{INK4b} and p27^{KIP1} encoding genes, *i.e.* *Cdkn2b* and *Cdkn1b* mRNA levels were unchanged between conditions (Figure 2C). Thus there is an overall elevation in the expression of several mRNAs encoding CDK, cyclins and CKI in proliferating malignant tumors compared to arrested benign MTC, thereby suggesting a role for CDK5 activity in the cell cycle.

Protein expression analysis of cell cycle regulators in malignant and benign mouse MTC

To further confirm the effects of p25-CDK5 up-regulation on expression of cell cycle regulators, we evaluated protein expression levels in proliferating malignant versus arrested benign mouse MTC (Figure 3). Quantification of immunoblots revealed CDK2 protein levels were elevated in proliferating tumors as previously observed [10]. However, CDK4 expression was unchanged between conditions (Figure 3A). CDK6 levels were more

variable from sample to sample and thus no significant change in CDK6 was detected between malignant and benign MTC (Figure 3A). Consistent with mRNA findings, protein levels of cyclin-A1 [10], cyclin-B1 and cyclin-E2 were all up-regulated in malignant MTC (Figure 3B). Cyclin-D1 protein expression was also variable from sample to sample and overall its expression was not significantly altered (Figure 3B). As observed at the mRNA levels, CKI protein expression was predominantly up-regulated in malignant mouse tumors. In particular, the expression of p15^{INK4b}, p18^{INK4c}, p19^{INK4d} and p21^{CIP/WAF1} was elevated in proliferating tumors compared to those in

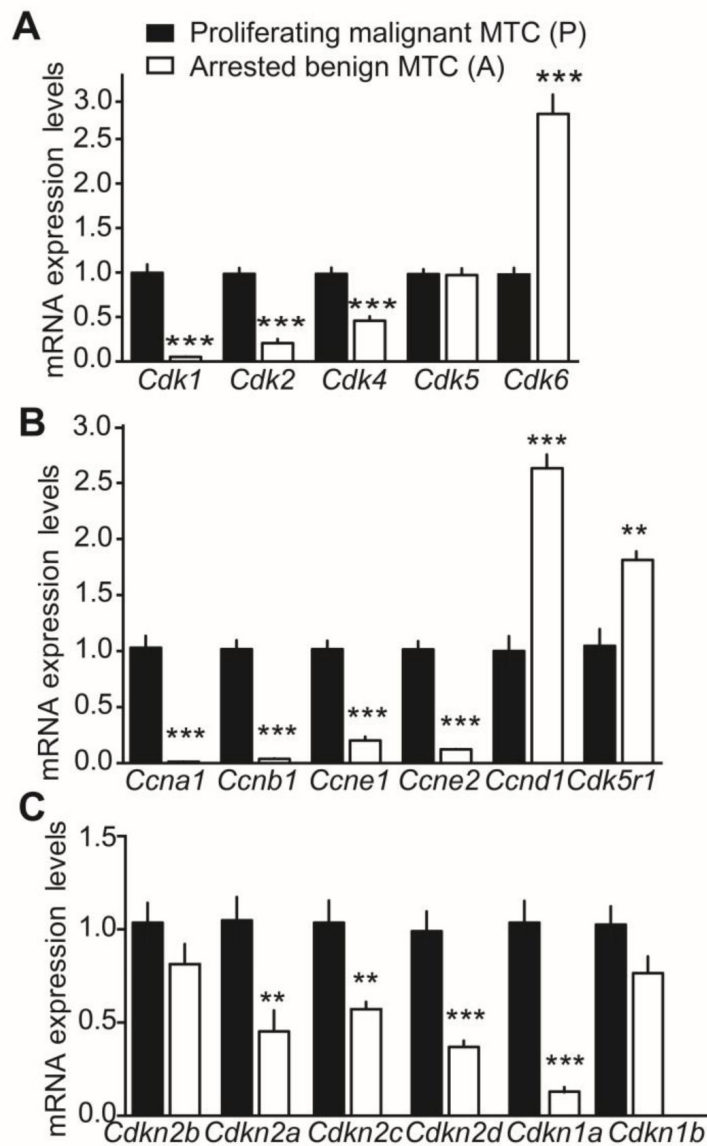


Figure 2: Gene expression analysis of cell cycle regulators in malignant and benign mouse MTC by RT-qPCR. Relative mRNA expression of A) CDK genes, *Cdk1*, *Cdk2*, *Cdk4*, *Cdk5* and *Cdk6*; B) cyclin genes, *Ccn1*, *Ccnb1*, *Ccne1*, *Ccne2*, *Ccnd1*, and *Cdk5r1* and C) CKI genes, *Cdkn2a*, *Cdkn2c*, *Cdkn2d*, *Cdkn1a*, *Cdkn1b* and *Cdkn2b* in proliferating malignant (P) versus arrested benign NSE/p25-GFP mouse tumors. P-values are $p < 0.0001$ for *Cdk1*, *Cdk2*, *Cdk4*, *Cdk6*, $p = 0.9838$ for CDK5; $p < 0.0001$ for *Ccn1*, *Ccnb1*, *Ccnd1*, *Ccne1* and *Ccne2*, $p = 0.0057$ for *Cdk5r1*; $p = 0.1754$ for *Cdkn2b*, $p = 0.005$ for *Cdkn2a*, $p = 0.0052$ for *Cdkn2c*, $p = 0.0003$ for *Cdkn2d*, $p < 0.0001$ for *Cdkn1a* and $p = 0.0811$ for *Cdkn1b*. Data are represented as mean \pm SEM, N = 6 -7 for each condition.

the arrested state (Figure 3C). In contrast, the expression of p16^{INK4a} and p27^{KIP1} was not significantly changed between conditions. Overall, these results are consistent with the observations from the differential gene expression analysis.

Evaluation of the relationship between CDK5 activity and cell cycle protein expression levels

The gene and cell cycle protein expression analyses described above indicate a possible relationship between CDK5 activity and the regulation of cell cycle protein expression in proliferating versus arrested mouse MTC tumors. To directly assess the effect of CDK5 activity on the expression of cell cycle regulators in human MTC, we compared cell cycle protein expression in a human sporadic, non-RET mutated MTC cell line, MTC-SK [24], which was transfected with either a construct encoding kinase-dead CDK5 (Kd-CDK5) or with a control plasmid.

We previously demonstrated that overexpressing kinase-dead CDK5 in MTC-SK cells abrogates CDK5 activity and stops cell proliferation [10].

As a prerequisite observation, most of the CDKs, cyclins and CKI that were detected in the mouse tumors were also expressed in MTC-SK cells transfected with a control plasmid (Figure 4). The only exception was cyclin-D1 which was not detected in MTC-SK cells and was unaffected by CDK5 activity in growing versus arrested mouse tumors. Interestingly, the expression of CDK2, CDK4 and CDK6 was diminished following Kd-CDK5 overexpression (Figure 4A). Moreover, the protein levels of cyclin-A1, cyclin-B1 and cyclin-E2 were all reduced in Kd-CDK5-transfected cells (Figure 4B). Finally, the expression of p15^{INK4b}, p19^{INK4d} and p21^{CIP/WAF1} was decreased in transfected MTC-SK cells, whereas the protein levels of p16^{INK4a}, p18^{INK4c} and p27^{KIP1} were not significantly changed (Figure 4C). These observations are consistent with the analysis of cell cycle protein

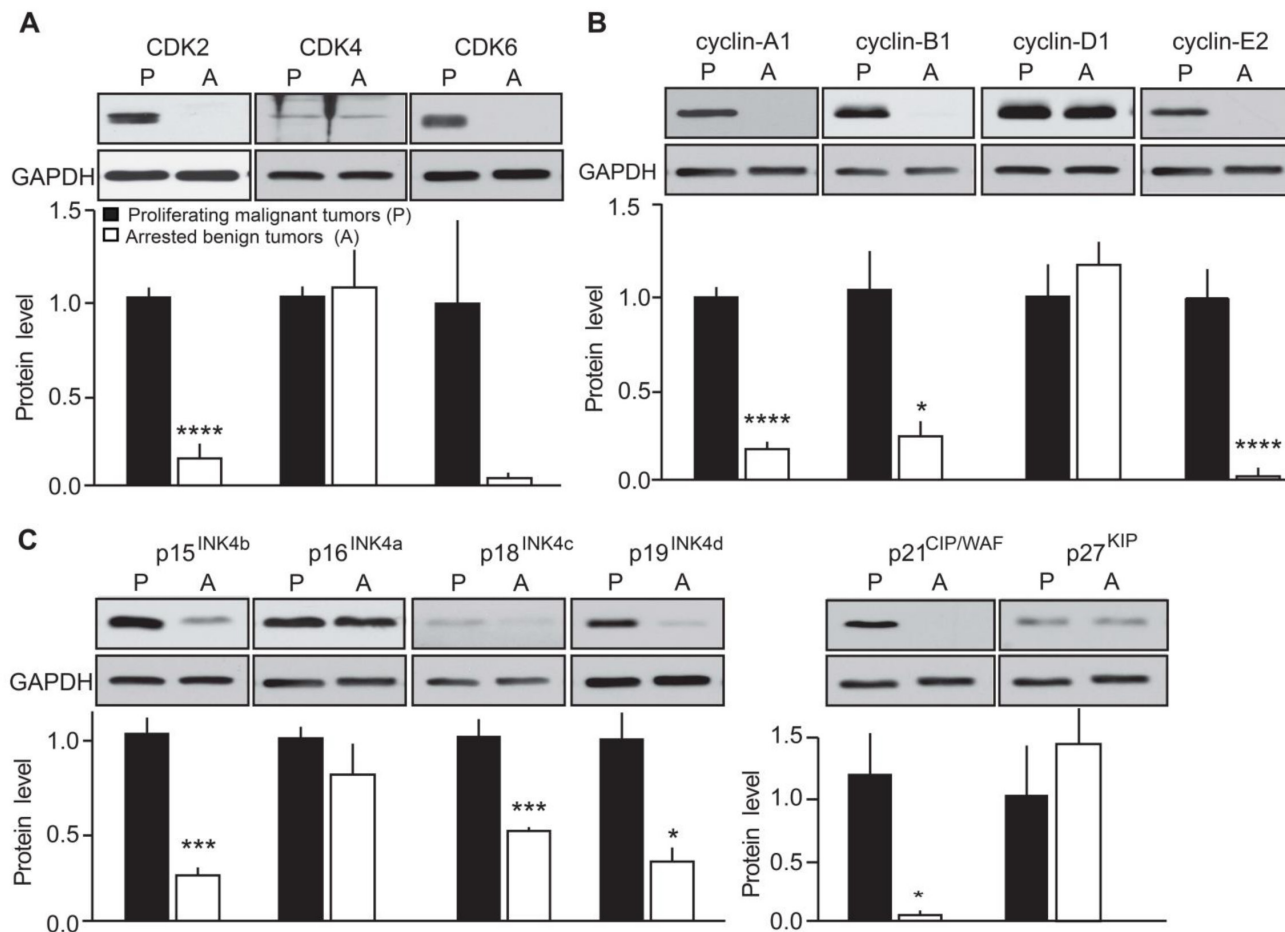


Figure 3: Evaluation of the effects of p25-GFP overexpression on cell cycle protein expression in malignant versus benign mouse MTC. Immunoblots of lysates from proliferating malignant (P) and arrested benign (A) mouse MTC for A) CDK2, CDK4 and CDK6; B) cyclins A1, B1, D1, E2 and C) p15^{INK4b}, p16^{INK4a}, p18^{INK4c}, p19^{INK4d}, p21^{CIP/WAF1} and p27^{KIP1}. P-values are p < 0.0001 for CDK2, p = 0.6974 for CDK4, p = 0.0633 for CDK6; p < 0.0001 for cyclin-A1, p = 0.0194 for cyclin-B1, p = 0.3416 for cyclin-D1, p < 0.0001 for cyclin-E2; p = 0.0002 for p15^{INK4b}, p = 0.291 for p16^{INK4a}, p = 0.0006 for p18^{INK4c}, p = 0.0054 for p19^{INK4d}, p = 0.02 for p21^{CIP/WAF1} and p = 0.67 for p27^{KIP1}. Data are represented as mean +/- SEM, N = 6 for each condition.

expression in the mouse MTC. Together these results suggest that CDK5 activity regulates the expression of CDK2, cyclin-A1, cyclin-B1, cyclin-E2, p15^{INK4b}, p19^{INK4d} and p21^{CIP/WAF1} but not p16^{INK4a} and p27^{KIP1} (Table 1). It is not clear whether CDK5 modulates the expression of CDK4, CDK6 and p18^{INK4c}. Overall, these findings are in agreement with CDK5 regulating the expression of Rb-E2F target genes.

Analysis of cell cycle protein expression in human MTC tissue

While hereditary MTC is mainly caused by RET proto-oncogene mutations and consequent deregulation of the RET signaling pathway, the molecular basis for

sporadic MTC is not well understood. Some sporadic MTC cases harbor mutations in the *RET* or *Ras* genes, but others do not. We previously reported that CDK5 was involved in MTC tumorigenesis, and found that high levels of CDK5 and its activators, p35 and p25, occur predominantly in the sporadic compared to the hereditary form of the disease [10]. Having established that CDK5 activity correlates with elevated cell cycle protein expression levels in proliferating mouse MTC and in a human sporadic MTC cell line, we compared protein levels of CDKs, cyclins and CKI in sporadic and hereditary MTC patient tissues (Figure 5). Sporadic specimen did not exhibit RET mutations (see method section). We found that CDK2 levels were elevated in sporadic cases, but decreased in hereditary forms of MTC. In contrast,

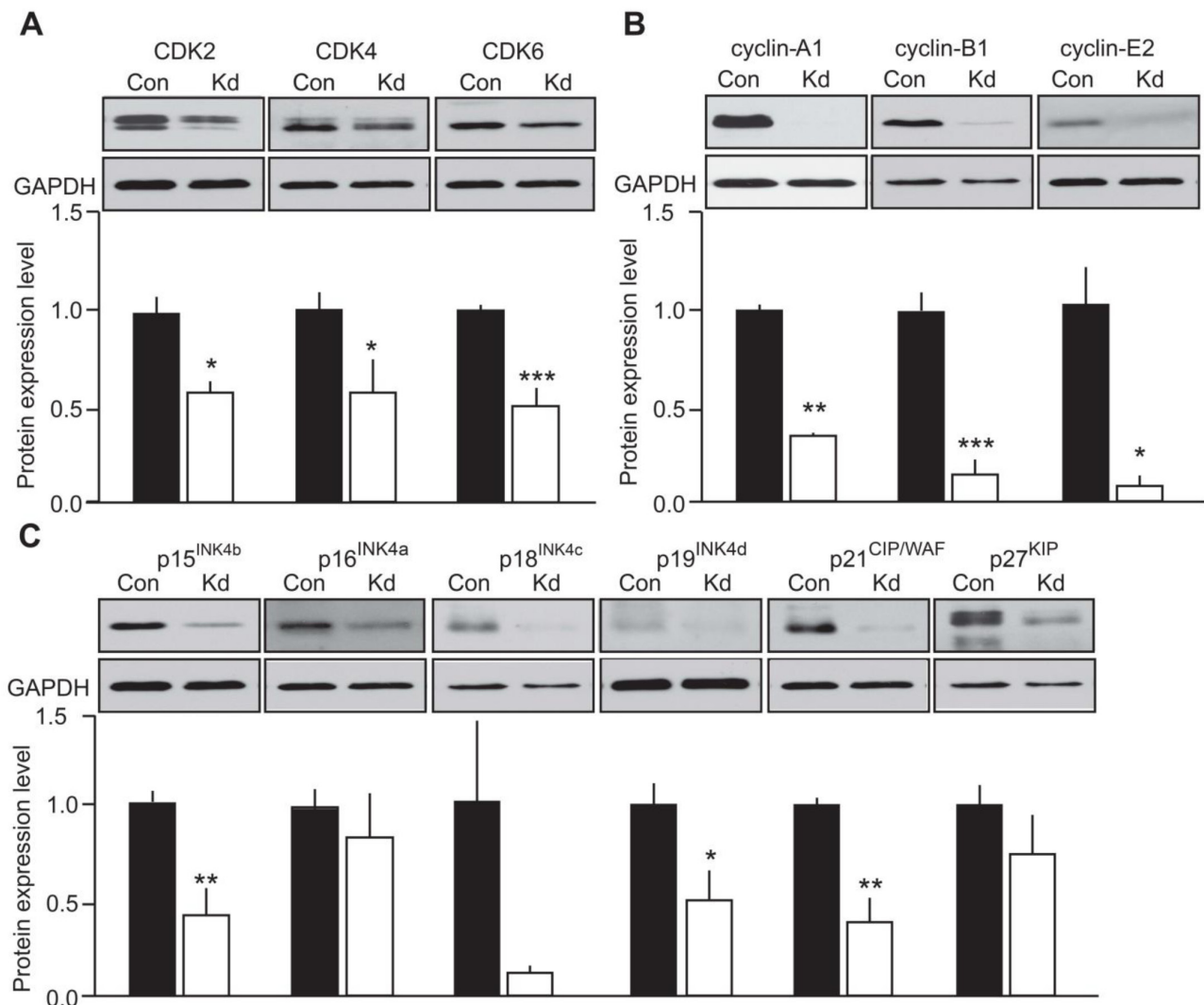


Figure 4: Evaluation of the effect of CDK5 activity on cell cycle protein expression in human MTC cells. Immunoblots of lysates from MTC-SK cells transfected with either a control plasmid (Con) or a kinase-dead (Kd) CDK5 encoding plasmid for A) CDK2, CDK4 and CDK6; B) cyclin-A1,-B1,-E2 and C) p15^{INK4b}, p16^{INK4a}, p18^{INK4c}, p19^{INK4d}, p21^{CIP/WAF1} and p27^{KIP1}. P-values are p = 0.0244 for CDK2, p = 0.038 for CDK4, p = 0.009 for CDK6; p < 0.0001 for cyclin-A1, p = 0.0005 for cyclin-B1, p = 0.0116 for cyclin-E2; p = 0.0044 for p15^{INK4b}, p = 0.4687 for p16^{INK4a}, p = 0.1032 for p18^{INK4c}, p = 0.0195 for p19^{INK4d}, p = 0.0022 for p21^{CIP/WAF1} and p = 0.2674 for p27^{KIP1}. Data are represented as mean ± SEM, N = 4-6 for each condition.

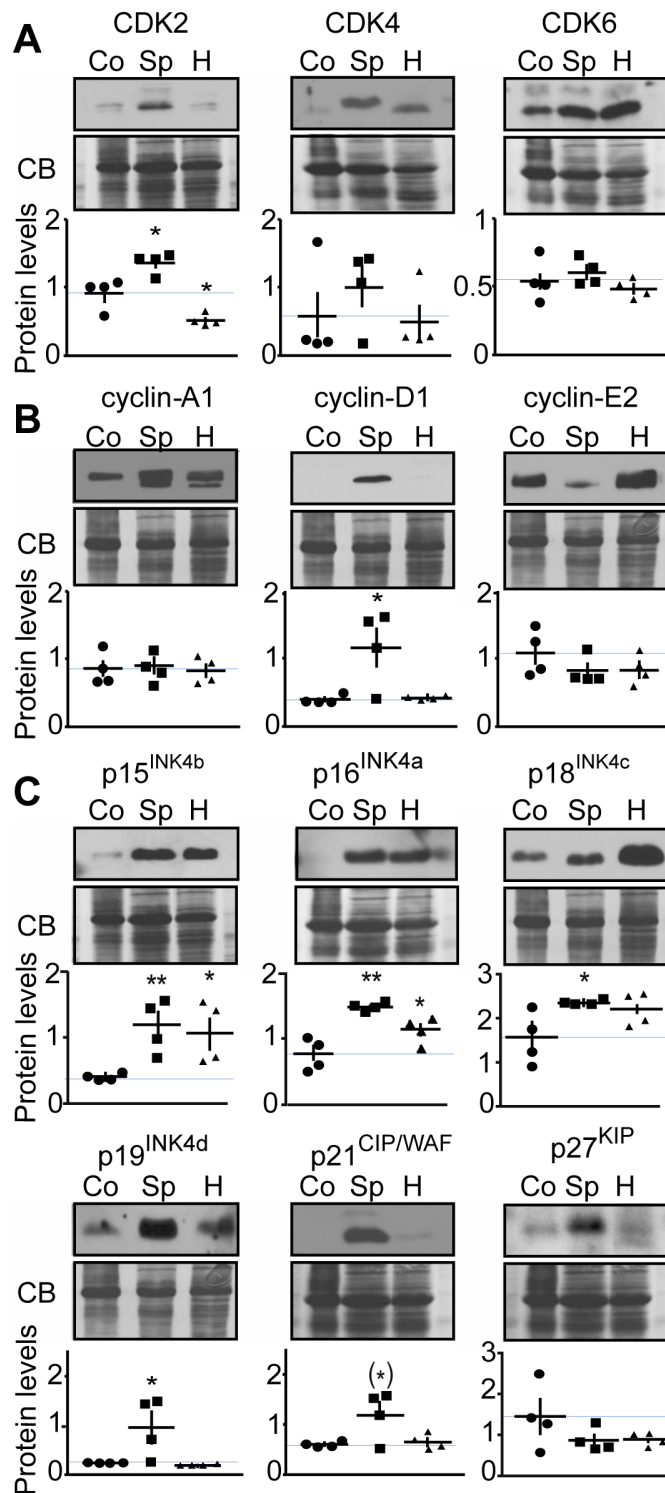


Figure 5: Analysis of cell cycle protein expression in human MTC samples. Representative immunoblots of lysates from control thyroid tissue (Co), sporadic (Sp) and hereditary (H) human MTC tumors with antibodies as indicated are shown with quantification. Protein levels were normalized to Coomassie blue (CB) signal. Immunoblots were probed with antibodies to A) CDK2, CDK4 and CDK6; B) cyclins-A1, -D1, -E2; C) in p15^{INK4b}, p16^{INK4a}, p18^{INK4c}, p19^{INK4d}, p21^{CIP/WAF1} and p27^{KIP}. P-values were for CDK2, Sp, p = 0.0168 and H, p = 0.0140; for CDK4, Sp, p = 0.4072 and H, p = 0.8576; for CDK6, Sp, p = 0.5484 and H, p = 0.4916; for cyclin-A1, Sp, p = 0.9923 and H, p = 0.7017; for cyclin-D1, Sp, p = 0.0307 and H, p = 0.6883; for cyclin-E2, Sp, p = 0.2645 and H, p = 0.3070; for p15^{INK4b}, Sp, p = 0.0088 and H, p = 0.0310; for p16^{INK4a}, Sp, p = 0.0014 and H, p = 0.0496; for p18^{INK4c}, Sp, p = 0.0309 and H, p = 0.1054; for p19^{INK4d}, Sp, p = 0.0484 and H, p = 0.3560; for p21^{CIP/WAF}, Sp, p = 0.0554 and H, p = 0.6807; for p27^{KIP1}, Sp, p = 0.2149 and H, p = 0.2131. Data are represented as mean +/- SEM, N = 4 for each condition.

CDK4 and CDK6 showed no significant changes in any of the groups analyzed (Figure 5A). Cyclin-D1 levels were increased in sporadic MTC, while cyclin-A1 and cyclin-E2 were unchanged in MTC compared to control thyroid samples (Figure 5B). Cyclin-B1 could not be detected in control thyroid or MTC specimens. p15^{INK4b} and p16^{INK4a} expression was increased in both, sporadic and hereditary MTC. The levels of p18^{INK4c}, p19^{INK4d} and p21^{CIP/WAF1} were elevated in sporadic but not hereditary MTC. Finally p27^{KIP1} expression was unchanged in MTC samples compared to control samples. Proliferating Cell Nuclear Antigen was expressed at the same level in sporadic and hereditary tumors, thereby confirming that the observed changes were not just a measure of growth fraction (Figure S1B). The changes in cell cycle regulator expression that were observed in sporadic MTC tissues are consistent with those observed in the human MTC cell line and in mouse tumors (Table 1). The results suggest that the MTC mouse model may more accurately model the molecular mechanisms underlying sporadic MTC than hereditary forms. Thus CDK5 may play a more important role in sporadic than familial MTC tumorigenesis.

To characterize further CDK5 activity in human tumors, we compared the phosphorylation state of the known CDK5 substrates, inhibitor-1 (Ser-6) [25], Tau (Thr205) [26] and STAT-3 (Ser727) [27] between sporadic and hereditary tumors (Figure 6). We found these substrates were phosphorylated at their respective CDK5 sites, equally in both forms of MTC. Thus CDK5 activity is not uniformly elevated in response to p25 overexpression, and as p35 expression remains normal in both forms of MTC [10], the phosphorylation state of physiological CDK5 substrates may be unaffected.

Together the analysis of human tumors, cell line and mouse MTC suggests that up-regulation of cell cycle protein expression via a CDK5-mediated mechanism may contribute to sporadic MTC pathogenesis. The role of CDK5 in hereditary MTC tumorigenesis such as those arising from familial mutations in RET is less clear. These findings also suggest that cell cycle proteins may serve as useful biomarkers for sporadic forms of neuroendocrine thyroid cancer.

DISCUSSION

MTC is a devastating disease for which new treatments are urgently needed. Having generated a novel, inducible animal model for MTC, we set to elucidate the molecular mechanisms underlying this cancer. Array-based transcriptome analysis comparing proliferating malignant and arrested benign mouse MTC revealed deregulation of cell cycle regulator expression (Figure 1). A focused examination uncovered a CDK5-dependent increase in expression of genes encoding cell cycle regulators, including CDK2, cyclin-D1, p15^{INK4b}, p16^{INK4a}, p18^{INK4c}, p19^{INK4d} and p21^{CIP/WAF1}. RT-qPCR and protein expression analyses confirmed their up-regulation at mRNA and protein level in p25-overexpressing malignant mouse MTC. Furthermore, the same set of cell cycle proteins are down-regulated in human MTC cells lacking CDK5 activity, suggesting aberrant CDK5 activity is necessary and sufficient to drive expression of these markers. Importantly, there was no difference in levels of CDK5 itself, thereby underlining that it is the aberrant activity of the kinase that is critical to these malignancy-associated effects rather than its expression

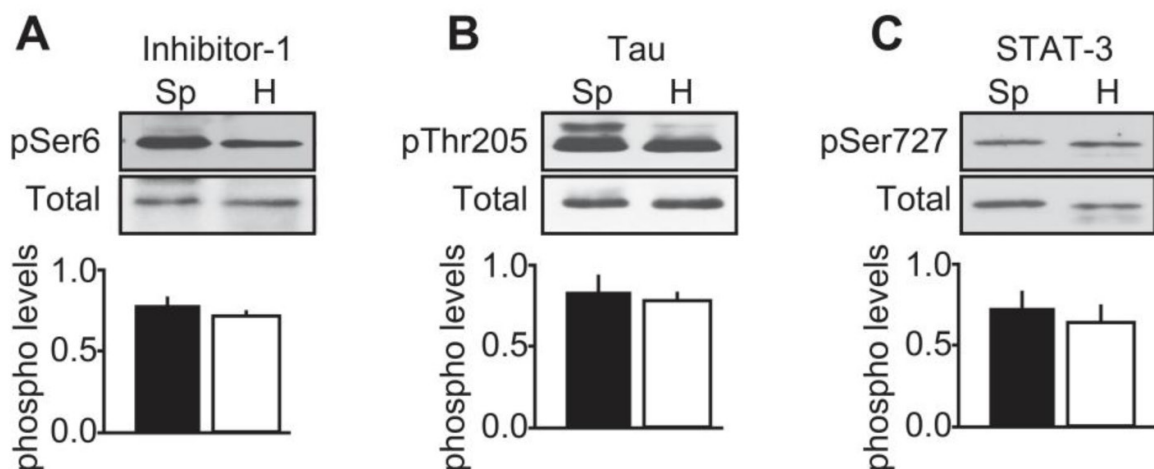


Figure 6: Characterization of CDK5 activity in human MTC tissues. Representative immunoblots of lysates from sporadic (Sp) and hereditary (H) MTC tumors with antibodies to A) inhibitor-1 and phospho-Ser6 Inhibitor-1; B) Tau and phospho-Thr205 Tau and C) STAT-3 and phospho-Ser727 STAT-3. Phosphorylated levels were normalized to total levels. P-values were $p = 0.2061$ for inhibitor-1; $p = 0.8545$ for Tau and $p = 0.6740$ for STAT-3. Data are represented as mean \pm SEM, $N = 4$ for each condition.

level. Analysis of human MTC tissues from sporadic and hereditary cases showed that the cell cycle proteins, CDK2, cyclin-D1, p18^{INK4c}, p19^{INK4d} and p21^{CIP/WAF1} were consistently overexpressed in human sporadic, but not hereditary, forms of MTC (Table 1). Although we could not demonstrate that CDK5 activity is higher in sporadic than in hereditary tumors, the integrated analysis of mouse tumors, the human cell line and patient samples suggest that CDK5 activity may be responsible for the increase in cell cycle protein expression that is detected in sporadic, non-RET MTC tissues. Our observations do not allow excluding a role for CDK5 in RET-dependent hereditary MTC. Cdk5 and its activators are indeed expressed in some hereditary tumors [10] and CDK5 has also been suggested to contribute to the proliferation of TT cells, which are derived from a hereditary form of MTC (RET mutation on codon 634) [28]. It will be important in the future to determine whether CDK5 is involved in RET-mediated MTC pathogenesis and how.

Here we find that all the members of the INK4 family of CKI, which are four ankyrin-repeat domains proteins inhibiting only cyclin-D-CDK4/6 function [29], are up-regulated in MTC patients. In particular p15^{INK4b} and p16^{INK4a} expression is increased in non-RET sporadic and RET-mutated, hereditary MTCs while p18^{INK4c} and p19^{INK4d} levels are elevated in non-RET sporadic MTC only. Interestingly p18^{INK4c} and p19^{INK4d} have potential CDK5 phosphorylation sites whereas p15^{INK4b} and p16^{INK4a} do not [30], thereby supporting our hypothesis that CDK5 may be more important for sporadic than hereditary MTC. The INK4 family members have previously been related to MTC. Base pair change mutations in exon 2 of the p15^{INK4b}-encoding gene were found in some MTC cases [31]. Somatic mutations in exon 3 of the p18^{INK4c}-encoding gene disrupting p18^{INK4c} interaction with CDK4 or CDK6 were also detected in MTC and pheochromocytoma patients [32]. In addition, mutations in other exons of the p18^{INK4c}-encoding gene or within p19^{INK4d}-encoding gene have been reported in MTC patients [33]. Mutant mice carrying deletions of p18^{INK4c}-encoding gene as well as the p27^{KIP1}-encoding gene develop multiple endocrine tumors including MTC and pheochromocytoma [34, 35]. Finally, deletion of the p18^{INK4c}-encoding gene and/or the p27^{KIP1}-encoding gene amplifies the tumorigenic effect of RET mutations causing hereditary forms of MTC as studied in mouse models and cell culture [35, 36]. Together with our findings, these observations lead us to propose that inactivation or loss of p18^{INK4c} and p19^{INK4d} might be a feature of RET-dependent hereditary MTC, while overexpression of these proteins might characterize non-RET sporadic MTC. Analysis of large cohorts of RET and non-RET MTC specimen will be necessary to validate this hypothesis.

In this study, we present compelling evidence that CDK5 functions in the regulatory mechanisms that govern cell cycle progression and contribute to MTC

tumorigenesis. The fact that a given set of cell cycle proteins display the same expression profile in three different MTC models, namely mouse model tissues, human sporadic MTC cell lines, and MTC patient samples, serves to underscore the relevance of our observations to mechanisms underlying this disease.

The cell cycle is initiated after the restriction point, or step of no-return, at which cells irreversibly commit to DNA replication. Bypassing the restriction point requires phosphorylation of Rb by CDKs, namely cyclin-D1-CDK4/6. Thereafter, cell cycle progression is reliant on coordinated action of cyclin-CDK complexes at defined phases throughout the cell cycle. Based on our current and previous studies, we propose that the aberrant activity of CDK5 may facilitate bypass of the restriction point through initial deactivation of Rb, via phosphorylation, which in turn promotes E2F target gene expression. In support of this notion, we show here that E2F target genes, including CDK2, p15^{INK4b}, p19^{INK4d} and p21^{CIP/WAF1} [37, 38] are up-regulated in p25-overexpressing malignant mouse MTCs, while the expression of these proteins is reduced following inhibition of CDK5 activity.

In summary, this study suggests that aberrant CDK5 activity promotes sporadic forms of MTC by modulating the expression of cell cycle proteins and points to these as possible biomarkers or targets for the development of new therapies.

MATERIALS AND METHODS

Human samples

Medullary thyroid cancer specimens and control thyroid samples (goiters) were obtained through a human subject institutional-review-board-approved protocol UT Southwestern IRB 052004-044, “Molecular Analysis of Endocrine Tumors”.

Sequencing of human MTC tumors and of the MTC-SK cell line

MTC tumors and MTC-SK cells were examined for ‘hot spot’ somatic RET mutations (exons 10, 11, 13, 14, 15 and 16) by direct sequencing of DNA extracted from tumor specimens using a QIAamp DNA FFPE Tissue Kit (QIAGEN) or extracted from cultured MTC-SK cells using DNAeasy Blood and Tissue Kit (QIAGEN) according to the manufacturer’s instructions. Sequencing was performed as previously described with some modification of primer sequences and conditions [39]. See supplemental methods for detailed information regarding primer sequences and reaction conditions. Sporadic MTC tumors (n = 4) had no mutations in RET exons. Hereditary MTC samples exhibited either a RET C634R mutation (n = 2) or a RET

C618S mutation (n = 1), or RET L790F (n = 1). Because of the low number of available samples, tumors were classified as either sporadic (non-RET) or hereditary (RET-mutated). No RET mutations were detected in MTC-SK cells.

Animals

The NSE/p25-GFP line is a bitransgenic mouse model of MTC based on a tetracycline transactivator system and has been described in detail [10, 21]. Briefly the neuron specific enolase (NSE) promoter controls expression of a tetracycline transactivator that is inhibited by dietary doxycycline (i.e., Dox off). Thus removing doxycycline (100 mg/L) from drinking water induces p25-GFP expression and MTC development. Subsequent re-addition of doxycycline stops p25-GFP overexpression and arrests tumor growth.

Tumor collection and lysate preparation

Proliferating tumors were obtained by inducing p25-GFP expression in NSE/p25-GFP mice for 16 weeks. For arrested tumors, NSE/p25-GFP mice were deprived from doxycycline for 16 weeks and exposed to doxycycline for 4 weeks. Tumors were collected and lysates were prepared as described in [40].

Positron Emission Tomography (PET)/Computed Tomography (CT) imaging

Mouse PET/CT imaging was performed using a Siemens Inveon PET/CT Multi Modality system (Siemens Medical Solutions, Knoxville, TN) with effective spatial resolution of 1.4 mm at the center of field of view (FOV). All animals were fasted for 12 h prior to PET imaging. Each mouse received 140 μ Ci of 2-deoxy-2-(18F)fluoro-D-glucose (FDG) in 150 μ L in saline intravenously via tail vein injection. The mice were placed on a heat pad before and during image acquisition. PET images were acquired 1h post-injection (p.i.), for 15 min, with animals under 2.5% isoflurane. PET images were reconstructed into a single frame using the 3D Ordered Subsets Expectation Maximization (OSEM3D/MAP) algorithm. CT images were acquired immediately after PET with the FOV centered at the shoulder of the mouse. CT projections (360 steps/rotation) were acquired with a power of 80 kVp, current of 500 μ A, exposure time of 145 ms, binning of 4, and effective pixel size of 102 μ m. The CT reconstruction protocol used a downsample factor of 2, was set to interpolate bilinearly, and used a Shepp-Logan filter. PET and CT images were co-registered in Inveon Acquisition Workplace (Siemens Medical Solutions) for analysis. Regions of interest (ROI) were drawn manually,

encompassing the thyroid in all planes containing the organ. The target activity was calculated as percentage injected dose per gram.

Microarray and pathway analyses

For microarray analysis, total RNA from arrested and proliferating tumors was isolated using RNeasy kit (QIAGEN, Hilden, Germany). Gene expression profiling on each sample was performed using Illumina Mouse WG-6 V3 BeadArrays (San Diego, CA, USA). Bead-level data were obtained and pre-processed using the R package “mbcb” for background correction and probe summarization. Pre-processed data were then quartile-normalized and log-transformed. Class comparison and unsupervised hierarchical clustering was performed using in-house MATRIX 1.48 (Girard, L. Manuscript in preparation). The volcano plot was developed by transforming p-values obtained in the *t*-test and plotting the transformed p-value versus the log₂ expression value obtained following microarray data processing in MATRIX 1.48. The networks and functional analyses were generated through the use of QIAGEN’s Ingenuity Pathway Analysis (IPA® QI Redwood City, www.qiagen.com/ingenuity).

Reverse transcription real time PCR (RT-qPCR)

Tissues of proliferating malignant (n = 7) and arrested benign tumors (n = 6) were collected as described above and homogenized in Trizol reagent (Life Technologies). RNA was extracted using QIAGEN RNeasy Kit according to the supplier’s protocol. Purified RNA was treated with RNase-free recombinant DNase I (Roche Diagnostics GmbH). Reverse transcription was performed using iScript select cDNA Synthesis Kit with provided random primers according to manufacturer’s instructions (Biorad Laboratories, Hercules, CA, USA). The SYBR-green based DyNAmo Flash SYBR Green qPCR Kit (Thermo scientific, Waltham, MA, USA) containing ROX as an internal reference dye was used for amplification. Real-time PCR reactions were run on an AB 7500 Real-time PCR system (Applied Biosystems, Foster City, CA, USA) and the specificity of each reaction was controlled by melt curve analysis. Primers were purchased from Integrated DNA Technologies (Coralville, IA, USA) and designed as intron-spanning pairs when possible (Table S4). Relative expression levels were calculated according to the 2- $\Delta\Delta$ Ct method [41]. Expression levels were normalized to Beta-2 microglobulin as endogenous control and calibrated to average expression level of proliferating tumors for each gene. Unpaired t-tests were used to compare changes in expression for each gene.

Cell culture, transfections and cell lysate preparation

MTC-SK cells were used for cell culture experiments. Those cells were derived from sporadic (non MEN) tumors and do not harbor RET mutations. MTC-SK cells were maintained in culture media containing Ham's F12 (Lonza Group Ltd, Basel, Switzerland), Medium 199 (Sigma, St. Louis, MO, USA) 1:1 v/v and 10% FBS as described in [24]. For transfections, cells were plated at a density of 2.5×10^5 cells/ml and transfected with either 1 μ g pCMV-Kd-CDK5 [34] or 1 μ g pCMV-EGFP (Clontech Laboratories, Inc., Mountain View, CA, USA) using X-tremeGene HP DNA transfection reagent (Roche Diagnostics GmbH, Mannheim, Germany). Cells were harvested 24 h post-transfection and lysate was prepared as previously described in [42].

Immunoblotting

Immunoblotting was conducted as previously described [43]. Membranes were probed with antibodies to p16^{INK4a} (PA5-20379, Pierce, Rockford, IL; USA), p15^{INK4b} (4822, Cell Signaling Technology (CST), Danvers, MA, USA), p18^{INK4c} (39-3400, Life Technologies, Carlsbad, CA, USA), p19^{INK4d} (PA5-26413, Pierce), p21^{CIP/WAF} (2946, CST), p27^{KIP} (2552, CST), CDK2 (sc-163, Santa Cruz Biotechnology (scbt), Santa Cruz, CA, USA), CDK4 (ab7955, Abcam, Cambridge, MA, USA), CDK6 (ABC275, Millipore, Temecula, CA, USA), Cyclin-A1 (sc-596, scbt), Cyclin-B1 (4135, CST), Cyclin D1 (ab134175, Abcam), Cyclin-E2 (4132, CST), GAPDH (G8795, Sigma), Tubulin (T5168, Sigma), STAT-3 (9132, CST) and pS727-STAT-3 (9134, CST), Tau (DAKO), pThr205-Tau (T6694, Sigma). Antibodies to Inhibitor-1 and pS6-inhibitor-1 were generated and characterized in-house [25]. The same membrane was probed for several proteins of different molecular weights after stripping in buffer containing 61 mM Tris-Base, 2%SDS and 7% β -mercaptoethanol at 50°C for 30 min. Immunoblots were quantified using Quantity One (BioRad). Samples were normalized to GAPDH (Figures 3 and 4) or to total protein levels as determined by Coomassie blue (CB) staining (Figure 5).

Statistical analysis

Results are presented as mean values and error bars represent \pm SEM. Statistical analyses were conducted using two-tailed Student's *t*-test in GraphPad Prism 6.0 (GraphPad Software, Inc., La Jolla, CA, USA) and *p*-values < 0.05 were considered as statistically significant.

ACKNOWLEDGMENTS

We thank Xiao-Min Yu (The University of Wisconsin) for help in obtaining human tumors, G. Mettlach for expert maintenance of the mouse colony and S. Hisanaga (University of Tokyo) for kinase-dead Cdk5 construct.

FUNDING

This research was supported by a North American Neuroendocrine Tumor Society fellowship (KP), U.S. National Institutes of Health Grants to H.C. (CA121115 and CA109053), F.E.N. (GM067674), and J.A.B. (MH79710, MH083711, DA016672, DA033485, and NS073855) and American Cancer Society MEN2 Thyroid Cancer Consortium Research Grants (RSGM-11-182-01, RPM-11-080-01 H.C.; RSGM-11-190-01, J.A.B.). The MD Anderson Cancer Center Sequencing and Microarray Facility is funded by NCI Grant CA016672 (SMF).

CONFLICT OF INTERESTS

The authors have no conflict of interests to declare

REFERENCES

1. Chen H, Sippel RS, O'Dorisio MS, Vinik AI, Lloyd RV and Pacak K. The North American Neuroendocrine Tumor Society consensus guideline for the diagnosis and management of neuroendocrine tumors: pheochromocytoma, paraganglioma, and medullary thyroid cancer. *Pancreas*. 2010; 39:775-783.
2. Yao JC, Hassan M, Phan A, Dagohoy C, Leary C, Mares JE, Abdalla EK, Fleming JB, Vauthey JN, Rashid A and Evans DB. One hundred years after "carcinoid": epidemiology of and prognostic factors for neuroendocrine tumors in 35,825 cases in the United States. *Journal of clinical oncology : official journal of the American Society of Clinical Oncology*. 2008; 26:3063-3072.
3. Hofstra RM, Landsvater RM, Ceccherini I, Stulp RP, Stelwagen T, Luo Y, Pasini B, Hoppener JW, van Amstel HK, Romeo G and et al. A mutation in the RET proto-oncogene associated with multiple endocrine neoplasia type 2B and sporadic medullary thyroid carcinoma. *Nature*. 1994; 367:375-376.
4. Moura MM, Cavaco BM, Pinto AE and Leite V. High prevalence of RAS mutations in RET-negative sporadic medullary thyroid carcinomas. *The Journal of clinical endocrinology and metabolism*. 2011; 96:E863-868.
5. Agrawal N, Jiao Y, Sausen M, Leary R, Bettegowda C, Roberts NJ, Bhan S, Ho AS, Khan Z, Bishop J, Westra WH, Wood LD, Hruban RH, Tufano RP, Robinson B, Dralle H, et al. Exomic sequencing of medullary thyroid cancer reveals dominant and mutually exclusive oncogenic

- mutations in RET and RAS. *The Journal of clinical endocrinology and metabolism*. 2013; 98:E364-369.
6. Mulligan LM, Kwok JB, Healey CS, Elsdon MJ, Eng C, Gardner E, Love DR, Mole SE, Moore JK, Papi L and et al. Germ-line mutations of the RET proto-oncogene in multiple endocrine neoplasia type 2A. *Nature*. 1993; 363:458-460.
 7. Wells SA, Jr., Robinson BG, Gagel RF, Dralle H, Fagin JA, Santoro M, Baudin E, Elisei R, Jarzab B, Vasselli JR, Read J, Langmuir P, Ryan AJ and Schlumberger MJ. Vandetanib in patients with locally advanced or metastatic medullary thyroid cancer: a randomized, double-blind phase III trial. *Journal of clinical oncology : official journal of the American Society of Clinical Oncology*. 2012; 30:134-141.
 8. Elisei R, Schlumberger MJ, Muller SP, Schoffski P, Brose MS, Shah MH, Licitra L, Jarzab B, Medvedev V, Kreissl MC, Niederle B, Cohen EE, Wirth LJ, Ali H, Hessel C, Yaron Y, et al. Cabozantinib in progressive medullary thyroid cancer. *Journal of clinical oncology : official journal of the American Society of Clinical Oncology*. 2013; 31:3639-3646.
 9. Sherman SI. Lessons learned and questions unanswered from use of multitargeted kinase inhibitors in medullary thyroid cancer. *Oral oncology*. 2013; 49:707-710.
 10. Pozo K, Castro-Rivera E, Tan C, Plattner F, Schwach G, Siegl V, Meyer D, Guo A, Gundara J, Mettlach G, Richer E, Guevara JA, Ning L, Gupta A, Hao G, Tsai LH, et al. The role of Cdk5 in neuroendocrine thyroid cancer. *Cancer cell*. 2013; 24:499-511.
 11. Pozo K, Nwariaku FE and Bibb JA. Breaking Bad: how does a neuronal protein cause neuroendocrine cancer? *Oncotarget*. 2014; 5:5-6.
 12. Angelo M, Plattner F and Giese KP. Cyclin-dependent kinase 5 in synaptic plasticity, learning and memory. *Journal of neurochemistry*. 2006; 99:353-370.
 13. Hisanaga S and Saito T. The regulation of cyclin-dependent kinase 5 activity through the metabolism of p35 or p39 Cdk5 activator. *Neuro-Signals*. 2003; 12:221-229.
 14. Eggers JP, Grandgenett PM, Collisson EC, Lewallen ME, Tremayne J, Singh PK, Swanson BJ, Andersen JM, Caffrey TC, High RR, Ouellette M and Hollingsworth MA. Cyclin-dependent kinase 5 is amplified and overexpressed in pancreatic cancer and activated by mutant K-Ras. *Clinical cancer research : an official journal of the American Association for Cancer Research*. 2011; 17:6140-6150.
 15. Feldmann G, Mishra A, Hong SM, Bisht S, Strock CJ, Ball DW, Goggins M, Maitra A and Nelkin BD. Inhibiting the cyclin-dependent kinase CDK5 blocks pancreatic cancer formation and progression through the suppression of Ras-Ral signaling. *Cancer research*. 2010; 70:4460-4469.
 16. Xie W, Wang H, He Y, Li D, Gong L and Zhang Y. CDK5 and its activator P35 in normal pituitary and in pituitary adenomas: relationship to VEGF expression. *International journal of biological sciences*. 2014; 10:192-199.
 17. Liang Q, Li L, Zhang J, Lei Y, Wang L, Liu DX, Feng J, Hou P, Yao R, Zhang Y, Huang B and Lu J. CDK5 is essential for TGF-beta1-induced epithelial-mesenchymal transition and breast cancer progression. *Scientific reports*. 2013; 3:2932.
 18. Strock CJ, Park JI, Nakakura EK, Bova GS, Isaacs JT, Ball DW and Nelkin BD. Cyclin-dependent kinase 5 activity controls cell motility and metastatic potential of prostate cancer cells. *Cancer research*. 2006; 66:7509-7515.
 19. Hsu FN, Chen MC, Chiang MC, Lin E, Lee YT, Huang PH, Lee GS and Lin H. Regulation of androgen receptor and prostate cancer growth by cyclin-dependent kinase 5. *The Journal of biological chemistry*. 2011; 286:33141-33149.
 20. Demelash A, Rudrabhatla P, Pant HC, Wang X, Amin ND, McWhite CD, Naizhen X and Linnola RI. Achaete-scute homologue-1 (ASH1) stimulates migration of lung cancer cells through Cdk5/p35 pathway. *Molecular biology of the cell*. 2012; 23:2856-2866.
 21. Meyer DA, Richer E, Benkovic SA, Hayashi K, Kansy JW, Hale CF, Moy LY, Kim Y, O'Callaghan JP, Tsai LH, Greengard P, Nairn AC, Cowan CW, Miller DB, Antich P and Bibb JA. Striatal dysregulation of Cdk5 alters locomotor responses to cocaine, motor learning, and dendritic morphology. *Proceedings of the National Academy of Sciences of the United States of America*. 2008; 105:18561-18566.
 22. Hamdane M, Bretteville A, Sambo AV, Schindowski K, Begard S, Delacourte A, Bertrand P and Buee L. p25/Cdk5-mediated retinoblastoma phosphorylation is an early event in neuronal cell death. *Journal of cell science*. 2005; 118:1291-1298.
 23. Futatsugi A, Utreras E, Rudrabhatla P, Jaffe H, Pant HC and Kulkarni AB. Cyclin-dependent kinase 5 regulates E2F transcription factor through phosphorylation of Rb protein in neurons. *Cell cycle (Georgetown, Tex)*. 2012; 11:1603-1610.
 24. Pfragner R, Hofler H, Behmel A, Ingolic E and Walser V. Establishment and characterization of continuous cell line MTC-SK derived from a human medullary thyroid carcinoma. *Cancer research*. 1990; 50:4160-4166.
 25. Nguyen C, Nishi A, Kansy JW, Fernandez J, Hayashi K, Gillardon F, Hemmings HC, Jr., Nairn AC and Bibb JA. Regulation of protein phosphatase inhibitor-1 by cyclin-dependent kinase 5. *The Journal of biological chemistry*. 2007; 282:16511-16520.
 26. Hashiguchi M, Saito T, Hisanaga S and Hashiguchi T. Truncation of CDK5 activator p35 induces intensive phosphorylation of Ser202/Thr205 of human tau. *The Journal of biological chemistry*. 2002; 277:44525-44530.
 27. Fu AK, Fu WY, Ng AK, Chien WW, Ng YP, Wang JH and Ip NY. Cyclin-dependent kinase 5 phosphorylates signal transducer and activator of transcription 3 and regulates its transcriptional activity. *Proceedings of the National Academy of Sciences of the United States of America*. 2004; 101:6728-6733.

28. Lin H, Chen MC, Chiu CY, Song YM and Lin SY. Cdk5 regulates STAT3 activation and cell proliferation in medullary thyroid carcinoma cells. *The Journal of biological chemistry*. 2007; 282:2776-2784.
29. Sherr CJ and Roberts JM. CDK inhibitors: positive and negative regulators of G1-phase progression. *Genes & development*. 1999; 13:1501-1512.
30. Thullberg M, Bartkova J, Khan S, Hansen K, Ronnstrand L, Lukas J, Strauss M and Bartek J. Distinct versus redundant properties among members of the INK4 family of cyclin-dependent kinase inhibitors. *FEBS letters*. 2000; 470:161-166.
31. Goretzki PE, Gorelov V, Dotzenrath C, Witte J and Roehrer HD. A frequent mutation/polymorphism in tumor suppressor gene INK4B (MTS-2) in papillary and medullary thyroid cancer. *Surgery*. 1996; 120:1081-1088.
32. van Veelen W, Klompmaker R, Gloerich M, van Gasteren CJ, Kalkhoven E, Berger R, Lips CJ, Medema RH, Hoppener JW and Acton DS. P18 is a tumor suppressor gene involved in human medullary thyroid carcinoma and pheochromocytoma development. *International journal of cancer Journal international du cancer*. 2009; 124:339-345.
33. Flicker K, Ulz P, Hoger H, Zeitlhofer P, Haas OA, Behmel A, Buchinger W, Scheuba C, Niederle B, Pfragner R and Speicher MR. High-resolution analysis of alterations in medullary thyroid carcinoma genomes. *International journal of cancer Journal international du cancer*. 2012; 131:E66-73.
34. Franklin DS, Godfrey VL, O'Brien DA, Deng C and Xiong Y. Functional collaboration between different cyclin-dependent kinase inhibitors suppresses tumor growth with distinct tissue specificity. *Molecular and cellular biology*. 2000; 20:6147-6158.
35. Joshi PP, Kulkarni MV, Yu BK, Smith KR, Norton DL, van Veelen W, Hoppener JW and Franklin DS. Simultaneous downregulation of CDK inhibitors p18(Ink4c) and p27(Kip1) is required for MEN2A-RET-mediated mitogenesis. *Oncogene*. 2007; 26:554-570.
36. van Veelen W, van Gasteren CJ, Acton DS, Franklin DS, Berger R, Lips CJ and Hoppener JW. Synergistic effect of oncogenic RET and loss of p18 on medullary thyroid carcinoma development. *Cancer research*. 2008; 68:1329-1337.
37. Gartel AL, Najmabadi F, Goufman E and Tyner AL. A role for E2F1 in Ras activation of p21(WAF1/CIP1) transcription. *Oncogene*. 2000; 19:961-964.
38. Bracken AP, Ciro M, Cocito A and Helin K. E2F target genes: unraveling the biology. *Trends in biochemical sciences*. 2004; 29:409-417.
39. Kurzrock R, Sherman SI, Ball DW, Forastiere AA, Cohen RB, Mehra R, Pfister DG, Cohen EE, Janisch L, Nauling F, Hong DS, Ng CS, Ye L, Gagel RF, Frye J, Muller T, et al. Activity of XL184 (Cabozantinib), an oral tyrosine kinase inhibitor, in patients with medullary thyroid cancer. *Journal of clinical oncology : official journal of the American Society of Clinical Oncology*. 2011; 29:2660-2666.
40. Plattner F, Angelo M and Giese KP. The roles of cyclin-dependent kinase 5 and glycogen synthase kinase 3 in tau hyperphosphorylation. *The Journal of biological chemistry*. 2006; 281:25457-25465.
41. Livak KJ and Schmittgen TD. Analysis of relative gene expression data using real-time quantitative PCR and the 2(-Delta Delta C(T)) Method. *Methods*. 2001; 25:402-408.
42. Pozo K, Cingolani LA, Bassani S, Laurent F, Passafaro M and Goda Y. beta3 integrin interacts directly with GluA2 AMPA receptor subunit and regulates AMPA receptor expression in hippocampal neurons. *Proceedings of the National Academy of Sciences of the United States of America*. 2012; 109:1323-1328.
43. Bibb JA, Snyder GL, Nishi A, Yan Z, Meijer L, Fienberg AA, Tsai LH, Kwon YT, Girault JA, Czernik AJ, Haganir RL, Hemmings HC, Jr., Nairn AC and Greengard P. Phosphorylation of DARPP-32 by Cdk5 modulates dopamine signalling in neurons. *Nature*. 1999; 402:669-671.

Differential expression of cell cycle regulators in CDK5-dependent medullary thyroid carcinoma tumorigenesis

Supplementary Material

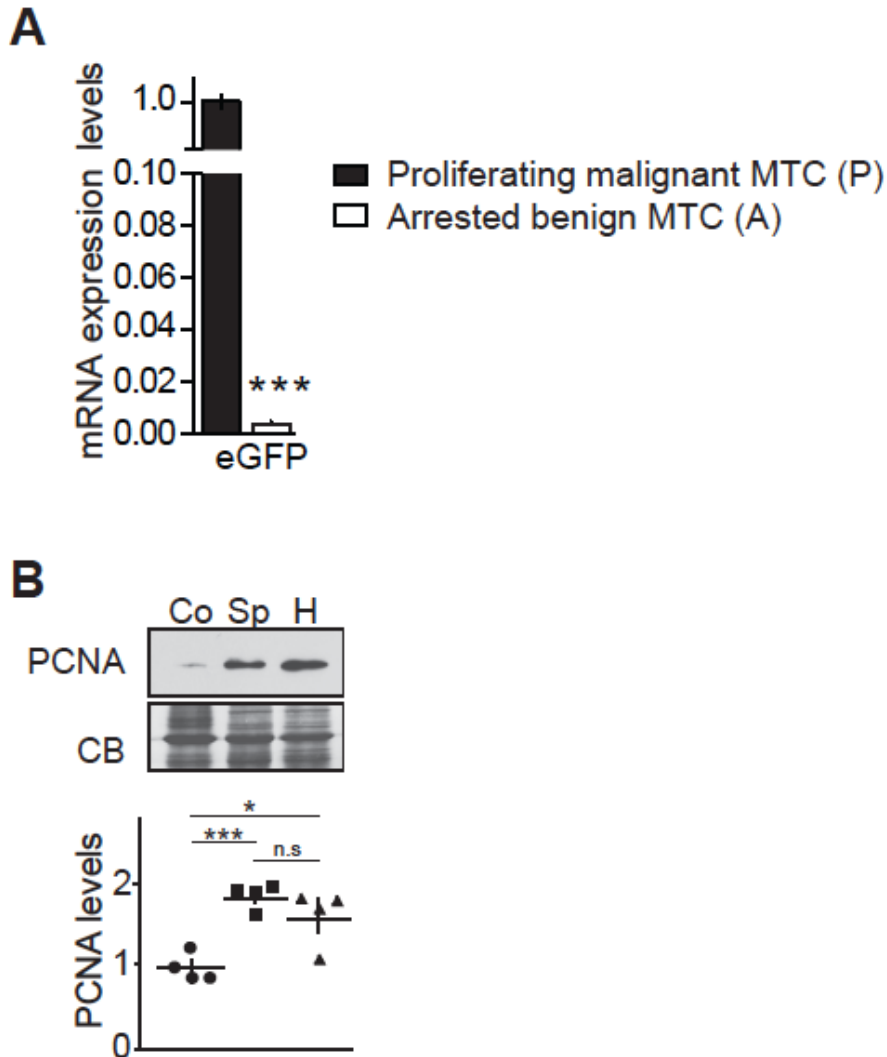


Figure S1. (A) RT-qPCR analysis of eGFP mRNA expression in proliferating malignant mouse MTC compared to arrested benign mouse MTCs; p-value < 0.0001 (N = 6 for each conditions). (B) Immunoblot of lysates from control, sporadic and hereditary human MTC probed with anti-PCNA antibodies. P-values were p = 0.2419 for Sp vs H, p = 0.0003 for Sp vs Co and p = 0.0223 for H vs Co. Data are represented as mean +/- SEM, N = 4 for each condition.

Table S1: A Table showing genes that are upregulated in proliferating malignant compared to arrested benign mouse MTCs. Genes that are mentioned in the main text are bolded.

GENE SYMBOL	LOG2-FOLD UPREGULATION	P-VALUE	GENE DESCRIPTION
eGFP	6.88	0.00006	
Troap	5.2	0.00000	trophinin associated protein
Pbk	5.1	0.00005	PDZ binding kinase
Spc25	4.95	0.00003	SPC25, NDC80 kinetochore complex component, homolog (<i>S. cerevisiae</i>)
LOC640739	4.91	0.00000	hypothetical protein LOC640739
2810417H13Rik	4.9	0.00034	predicted gene 15428; RIKEN cDNA 2810417H13 gene; predicted gene 9171
Kif18b	4.68	0.00070	kinesin family member 18B
Birc5	4.63	0.00000	budding uninhibited by benzimidazoles 1 homolog, beta (<i>S. cerevisiae</i>)
Clspn	4.62	0.00002	claspin homolog (<i>Xenopus laevis</i>)
Gtse1	4.44	0.00000	G two S phase expressed protein 1
Ckap2	4.43	0.00037	cytoskeleton associated protein 2
Crabp1	4.38	0.00024	cellular retinoic acid binding protein I
LOC100042970	4.31	0.00006	
Brrn1	4.29	0.00001	barren homolog (<i>Drosophila</i>)
Arhgef39	4.26	0.00056	Rho guanine nucleotide exchange factor (GEF) 39
Cdc2a	4.22	0.00013	cyclin-dependent kinase 1
Plk1	4.18	0.00108	polo-like kinase 1 (<i>Drosophila</i>)
Rad51	4.18	0.00010	RAD51 homolog (<i>S. cerevisiae</i>)
Cdca3	4.14	0.00028	cell division cycle associated 3
Ccnb1	4.13	0.00008	cyclin B1
Ncaph	4.12	0.00084	non-SMC condensin I complex, subunit H
Knstrn	4.06	0.00039	kinetochore-localized astrin/SPAG5 binding
Aurkb	4.06	0.00114	aurora kinase B
Rrm2	4.05	0.00007	ribonucleotide reductase M2
Cenpa	4.03	0.00076	centromere protein A
Cdkn3	4.01	0.00043	cyclin-dependent kinase inhibitor 3
LOC667005	4.01	0.00068	
Clhc1	4	0.00098	clathrin heavy chain linker domain containing 1
Kif4	3.91	0.00006	kinesin family member 4
Nusap1	3.85	0.00024	nucleolar and spindle associated protein 1
Spag5	3.85	0.00066	sperm associated antigen 5
Sgol1	3.83	0.00053	shugoshin-like 1 (<i>S. pombe</i>)

Uhrf1	3.83	0.00008	ubiquitin-like, containing PHD and RING finger domains, 1; predicted gene 5648; similar to nuclear zinc finger protein Np95
Top2a	3.78	0.00010	topoisomerase (DNA) II alpha
Cit	3.77	0.00055	citron
Prc1	3.77	0.00022	protein regulator of cytokinesis 1
Esco2	3.76	0.00048	establishment of cohesion 1 homolog 2 (<i>S. cerevisiae</i>)
Mcm10	3.76	0.00000	minichromosome maintenance deficient 10 (<i>S. cerevisiae</i>)
Cenpi	3.74	0.00003	centromere protein I
Kif15	3.66	0.00009	kinesin family member 15
Mki67	3.62	0.00013	antigen identified by monoclonal antibody Ki 67
Cdca8	3.56	0.00003	cell division cycle associated 8
C79407	3.56	0.00022	expressed sequence C79407
Cdc20	3.54	0.00005	cell division cycle 20 homolog (<i>S. cerevisiae</i>)
Hist1h2ag	3.53	0.00001	histone cluster 1, H2ad; histone cluster 1, H2ae; histone cluster 1, H2ag; histone cluster 1, H2ah; histone cluster 1, H2ai; similar to histone 2a; histone cluster 1, H2an; histone cluster 1, H2ao; histone cluster 1, H2ac; histone cluster 1, H2ab
Ccne2	3.52	0.00062	cyclin E2
Ckap2l	3.49	0.00010	cytoskeleton associated protein 2-like
Cdc25c	3.45	0.00040	cell division cycle 25 homolog C (<i>S. pombe</i>)
Kif23	3.42	0.00002	kinesin family member 23
Sapcd2	3.41	0.00005	suppressor APC domain containing 2
Iqgap3	3.39	0.00024	IQ motif containing GTPase activating protein 3
Cenpm	3.34	0.00002	centromere protein M
Kif11	3.32	0.00114	kinesin family member 11
Cd177	3.32	0.00078	CD177 antigen
Chek1	3.27	0.00005	checkpoint kinase 1 homolog (<i>S. pombe</i>)
Hist1h2ah	3.23	0.00006	histone cluster 1, H2ad; histone cluster 1, H2ae; histone cluster 1, H2ag; histone cluster 1, H2ah; histone cluster 1, H2ai; similar to histone 2a; histone cluster 1, H2an; histone cluster 1, H2ao; histone cluster 1, H2ac; histone cluster 1, H2ab
Sgol2	3.23	0.00002	shugoshin-like 2 (<i>S. pombe</i>)
Ncapg2	3.2	0.00009	non-SMC condensin II complex, subunit G2
Dmkn	3.19	0.00032	dermokine
Ska3	3.18	0.00049	spindle and kinetochore associated complex subunit 3
Hist1h2ak	3.17	0.00003	histone cluster 1, H2ak
Hist1h2ad	3.13	0.00024	histone cluster 1, H2ad; histone cluster 1, H2ae; histone cluster 1, H2ag; histone

			cluster 1, H2ah; histone cluster 1, H2ai; similar to histone 2a; histone cluster 1, H2an; histone cluster 1, H2ao; histone cluster 1, H2ac; histone cluster 1, H2ab
Rad54b	3.13	0.00101	RAD54 homolog B (<i>S. cerevisiae</i>)
Cenpn	3.12	0.00011	centromere protein N
Ccna1	3.1	0.00058	cyclin A1
2210011C24Rik	3.05	0.00000	RIKEN cDNA 2210011C24 gene
Depdc1b	3.05	0.00020	DEP domain containing 1B
Hmgb2	3.05	0.00008	predicted gene 13160; predicted gene 8681; predicted gene 13237; predicted gene 4169; predicted gene 8284; similar to High mobility group box 2; predicted gene 13167; high mobility group box 2; predicted gene 13232
Cenph	3.02	0.00033	centromere protein H
Kif18a	2.92	0.00077	kinesin family member 18A
Hist1h2af	2.87	0.00001	histone cluster 1, H2af
Tcf19	2.86	0.00003	transcription factor 19
Nrm	2.85	0.00010	nurim (nuclear envelope membrane protein)
Cep55	2.83	0.00033	centrosomal protein 55
Hist2h2ab	2.82	0.00011	histone cluster 2, H2ab
Hist1h2an	2.81	0.00010	histone cluster 1, H2ad; histone cluster 1, H2ae; histone cluster 1, H2ag; histone cluster 1, H2ah; histone cluster 1, H2ai; similar to histone 2a; histone cluster 1, H2an; histone cluster 1, H2ao; histone cluster 1, H2ac; histone cluster 1, H2ab
Oip5	2.78	0.00058	Opa interacting protein 5
BC004701	2.76	0.00029	baculoviral IAP repeat-containing 5
Tyms	2.74	0.00019	thymidylate synthase
Fbln1	2.7	0.00108	fibulin 1
Rad51ap1	2.69	0.00076	RAD51 associated protein 1
Chaf1b	2.68	0.00045	chromatin assembly factor 1, subunit B (p60)
Pif1	2.67	0.00015	PIF1 5'-to-3' DNA helicase homolog (<i>S. cerevisiae</i>)
Tmem91	2.61	0.00068	transmembrane protein 91
Gins1	2.6	0.00040	GINS complex subunit 1 (Psf1 homolog)
Bub1b	2.54	0.00023	budding uninhibited by benzimidazoles 1 homolog, beta (<i>S. cerevisiae</i>)
Fam132b	2.53	0.00101	family with sequence similarity 132, member B
Rad54l	2.47	0.00064	RAD54 like (<i>S. cerevisiae</i>)
Hist1h2ai	2.44	0.00012	histone cluster 1, H2ad; histone cluster 1, H2ae; histone cluster 1, H2ag; histone cluster 1, H2ah; histone cluster 1, H2ai; similar to histone 2a; histone cluster 1, H2an; histone cluster 1, H2ao; histone

			cluster 1, H2ac; histone cluster 1, H2ab
Tyms-ps	2.44	0.00006	thymidylate synthase, pseudogene
Ifi27	2.43	0.00050	interferon, alpha-inducible protein 27
Melk	2.42	0.00005	maternal embryonic leucine zipper kinase
Psrc1	2.42	0.00063	proline/serine-rich coiled-coil 1
B230323D24Rik	2.39	0.00073	
Phf19	2.36	0.00014	PHD finger protein 19
Cthrc1	2.35	0.00061	collagen triple helix repeat containing 1
Cenpw	2.33	0.00007	centromere protein W
Recql4	2.31	0.00011	RecQ protein-like 4
Pkmyt1	2.28	0.00029	protein kinase, membrane associated tyrosine/threonine 1
scl0002507.1_236	2.26	0.00044	
Kcne2	2.25	0.00009	potassium voltage-gated channel, Isk-related subfamily, gene 2
Gas2l3	2.24	0.00012	similar to growth arrest-specific 2 like 3; growth arrest-specific 2 like 3
Slc4a1	2.22	0.00053	solute carrier family 4 (anion exchanger), member 1
Ccr5	2.21	0.00008	chemokine (C-C motif) receptor 5
Pcna	2.21	0.00071	proliferating cell nuclear antigen; similar to proliferating cell nuclear antigen (DNA polymerase delta auxiliary protein)
Dbf4	2.2	0.00050	DBF4 homolog (<i>S. cerevisiae</i>)
Fam111a	2.19	0.00001	family with sequence similarity 111, member A
Tmpo	2.16	0.00033	thymopoietin
Mad2l1	2.15	0.00014	similar to spindle assembly checkpoint protein; MAD2 mitotic arrest deficient-like 1 (yeast)
Spink4	2.14	0.00033	serine peptidase inhibitor, Kazal type 4
Smc4	2.13	0.00003	structural maintenance of chromosomes 4
Fabp5	2.12	0.00043	fatty acid binding protein 5, epidermal
4930427A07Rik	2.11	0.00048	RIKEN cDNA 4930427A07 gene
LOC245892	2.1	0.00037	
Arpp21	2.06	0.00027	cyclic AMP-regulated phosphoprotein, 21
Ddx11	2.03	0.00109	DEAD/H (Asp-Glu-Ala-Asp/His) box polypeptide 11 (CHL1-like helicase homolog, <i>S. cerevisiae</i>)

Table S2: A Table showing downregulated genes in proliferating malignant compared to arrested benign mouse MTCs

GENE SYMBOL	LOG2-FOLD UPREGULATION	P-VALUE	GENE DESCRIPTION
Epb4.1l5	-2.54	0.001	erythrocyte protein band 4.1-like 5
KIF17	-2.45	0.001	kinesin family member 17
Leprel1	-2.23	0.001	leprecan-like 1
Lgals4	-2.21	0.000	lectin, galactose binding, soluble 4
LOC385274	-2.19	0.001	
Luzp2	-2.36	0.001	leucine zipper protein 2
Mtap2	-3.52	0.000	microtubule-associated protein 2

Supplemental methods: analysis of somatic RET mutation

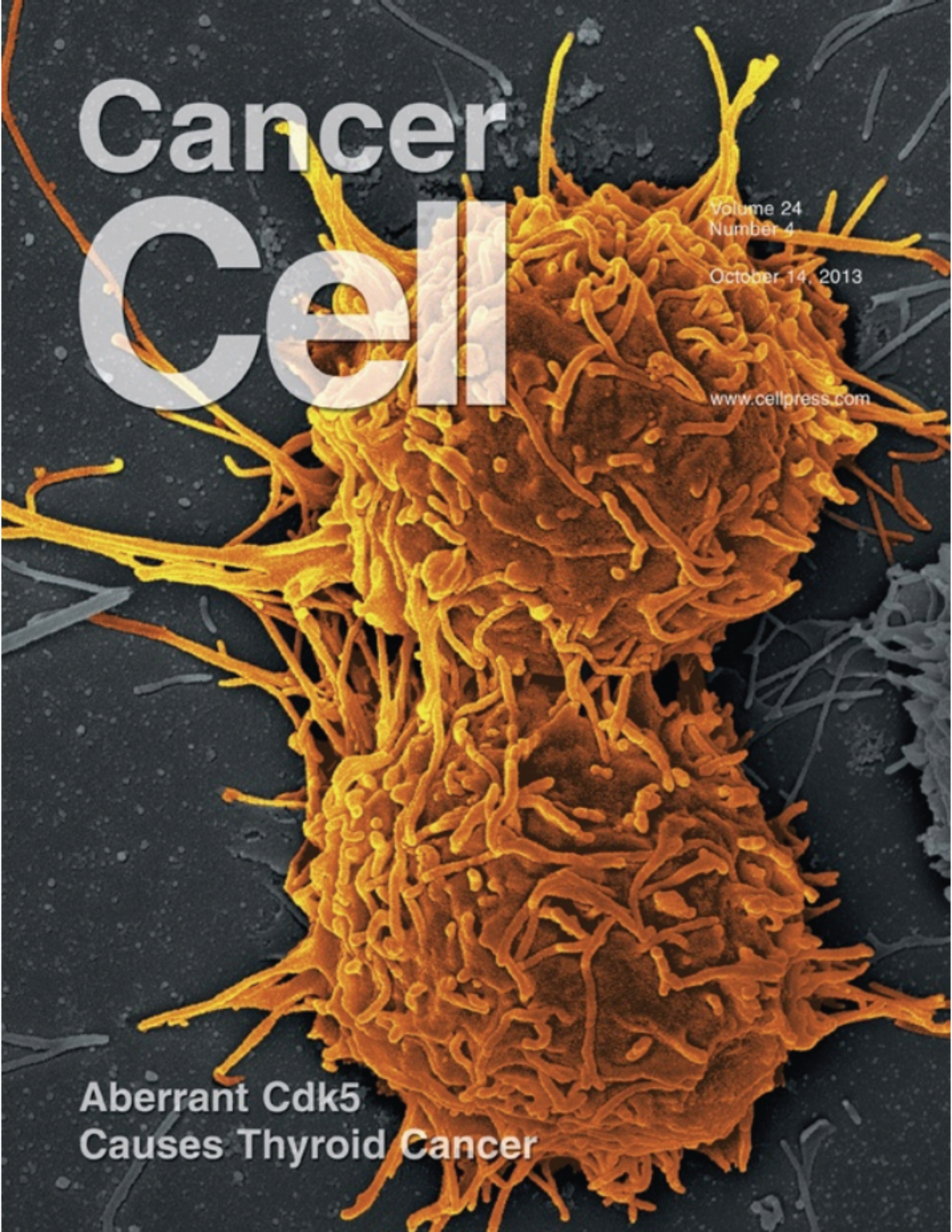
Genomic DNA was isolated from dissected sections containing at least 80% of neoplastic cells using the QIAamp DNA FFPE tissue kit (QIAGEN, Valencia, CA) according to the manufacturer's instructions. DNA was amplified by PCR using primers flanking known mutational hotspots (see Table below). PCR reactions were performed in 25 μ L and consisted of: 1 \times PCR buffer, 250 ng of genomic DNA, 0.4 μ mol/L each primer, 0.1 mmol/L each deoxynucleoside triphosphates, 0.75 unit of TaKaRa LA Taq DNA Polymerase (TaKaRa Bio USA, Madison, WI). After an initial cycle of denaturation at 94°C for 3 minutes, amplifications were performed as follows: 40 cycles of denaturation at 94°C for 45 seconds, annealing at 58°C for 30 seconds, and extension at 72°C for 90 seconds with and final extension at 72°C for 10 minutes. The PCR products were cleaned up with ExoSAP-IT (USB, Cleveland, OH) according to manufacturer instructions and sent to the core facility for sequencing using nested primers.

EXON	FORWARD PRIMER SEQUENCE (5'-3')	REVERSE PRIMER SEQUENCE (5'-3')	SEQUENCING PRIMER (5'-3')
10	GGCTAAGCCAAGCTG CTG	CCATGAAACTTCCCTCCC TC	TATGCTTGCGACACCAGTTG
11	GTTCTCAGGCCTTCCC ACAC	TGCGGGGCAGGGAAGAT CCCC	ACACCTCCATGGCCACTTC
13	CTCTCTGTCTGAACTT GGGC	CTACTGCTCCTGCCCTGT T	AGGTCCATCCTGACCTGGTA
14	TCCACCCCCTTACTCA TTGG	GGAAAGATACCGAAGATT AGTG	GCATGGTGGGCTAGAGTGT G
15	TCCACCCCCTTACTCA TTGG	GGAAAGATACCGAAGATT AGTG	CATGTCACACCCTGACTCCA
16	ACTCCCGCCAGCATCT CAG	GTTCTGTGAGGCAAATGG CT	GCCCCTTCAAAGATGTGTGT

Exons 14 and 15 were amplified as a single PCR product

Table S3: Primers used for the RT-qPCR analyses

GENE NAME	GENE SYMBOL	ACCESSION NO	PRIMER SEQUENCE 5' - 3'	AMPLICON (BP)
	eGFP		F: ATCATGGCCGACAAGCAGAAGAAC R: GTACAGCTCGTCCATGCCGAGAGT	257
	B2m	NM009735	F: TGCTATCCAGAAAACCCCTCAA R: CAATGTGAGGCGGGTGGAA	110
p15INK4b	cdkn2b	NM007670	F: AGCTGGATCTGGTCCTTGAG R: GATCCAAGAATTTCCCTTGC	130
p16INK4a	cdkn2a	NM009877	F: CAAGAGCGGGGACATCAAGA R: TTGAGCTGAAGCTATGCCCG	127
p18INK4c	cdkn2c	NM007671	F: GGCTGTCCGTTTCACTAT CA R: TTTTGAAGGATTTGGCTGCT	85
p19INK4d	cdkn2d	NM009878	F: TTGAAGAAGGGAGTGGGAGGA R: ACCGTTTAGATGGCTGTTGC	153
p21CIP/WAF1	cdkn1a	NM007669	F: GTA CTTCCTCTGCCCTGCTG R: TCTGCGCTTGGAGTGATAGA	173
p27KIP	cdkn1b	NM009875	F: GTCCAGGGATGAGGAAGCGAC R: CAGTGCCAGCGTTCGGG	108
cyclin A1	ccna1	NM007628	F: ATCCTGAACAGGGGGACAGA R: GCATTGGGGAAACTGTGTTGA	135
cyclin B1	ccnb1	NM172301	F: GCTCTCCATGCTGGACTACG R: TAGCCAGGTGCTGCATAACA	170
cyclin D1	ccnd1	NM007631	F: GCGTACCCTGACACCAATCT R: CACAGACCTCCAGCATCCAG	160
cyclin E1	ccne1	NM007633	F: GGCAAATGTGGCCGTGTTTT R: GGATGAAAGAGCAGGGGTCC	131
cyclin E2	ccne2	NM001037134	F: AGAGAAAAACAGCACAGGATGTC R: ATGCAAGGGCTGATTCCTCC	115
p35	cdk5r1	NM009871	F: TGGCTTGGGGTTTGAAGTG R: GGAAACCCTCCGCAGTATCTT	110
Cdk1	cdk1	NM007659	F: GTCCGTCGTAACCTGTTGAGT R: ACCACACCGTAAGTACCTTCTC	78
Cdk2	cdk2	NM016756	F: CTGGGCTGCAAGTACTACTCC R: CCTGCGGGTCAACATTTCA	78
Cdk4	cdk4	NM009870	F: GACCGATCCCCGGTGTATG R: GAAGCAGGGGATCTTACGCT	98
Cdk5	cdk5	NM007668	F: ACCCAGCTACAACATCCTTGG R: CGCTGCACAGGGTTACTT	97
Cdk6	cdk6	NM009873	F: ACCCACAGAAACCATAAAGGATA R: GCGGTTTCAGATCACGATGC	95



Cancer Cell

Volume 24
Number 4

October 14, 2013

www.cellpress.com

**Aberrant Cdk5
Causes Thyroid Cancer**

The Role of Cdk5 in Neuroendocrine Thyroid Cancer

Karine Pozo,¹ Emely Castro-Rivera,¹ Chunfeng Tan,¹ Florian Plattner,¹ Gert Schwach,² Veronika Siegl,² Douglas Meyer,¹ Ailan Guo,³ Justin Gundara,⁴ Gabriel Mettlach,¹ Edmond Richer,⁵ Jonathan A. Guevara,⁶ Li Ning,⁷ Anjali Gupta,⁵ Guiyang Hao,⁵ Li-Huei Tsai,⁸ Xiankai Sun,⁵ Pietro Antich,⁵ Stanley Sidhu,⁴ Bruce G. Robinson,⁴ Herbert Chen,⁷ Fiemu E. Nwariaku,^{9,10} Roswitha Pfragner,² James A. Richardson,^{11,12} and James A. Bibb^{1,10,13,*}

¹Department of Psychiatry, University of Texas Southwestern Medical Center, Dallas, TX 75390, USA

²Institute of Pathophysiology and Immunology, Medical University of Graz, 8010 Graz, Austria

³Cell Signaling Technology, Danvers, MA 01923, USA

⁴Department of Cancer Genetics, Kolling Institute of Medical Research, University of Sydney, Sydney, NSW 2650, Australia

⁵Department of Radiology, University of Texas Southwestern Medical Center, Dallas, TX 75390, USA

⁶Department of Internal Medicine, University of Texas Southwestern Medical Center, Dallas, TX 75390, USA

⁷Endocrine Surgery Research Laboratory, University of Wisconsin Carbone Cancer Center, Madison, WI 53792, USA

⁸Department of Brain and Cognitive Sciences, Massachusetts Institute of Technology, Cambridge, MA 02139, USA

⁹Department of Surgery, University of Texas Southwestern Medical Center, 5323 Harry Hines Boulevard, Dallas, TX 75390, USA

¹⁰Harold B. Simmons Comprehensive Cancer Center, University of Texas Southwestern Medical Center, 5323 Harry Hines Boulevard, Dallas, TX 75390, USA

¹¹Department of Pathology, University of Texas Southwestern Medical Center, 5323 Harry Hines Boulevard, Dallas, TX 75390, USA

¹²Department of Molecular Biology, University of Texas Southwestern Medical Center, 5323 Harry Hines Boulevard, Dallas, TX 75390, USA

¹³Department of Neurology and Neurotherapeutics, University of Texas Southwestern Medical Center, 5323 Harry Hines Boulevard, Dallas, TX 75390, USA

*Correspondence: james.bibb@utsouthwestern.edu

<http://dx.doi.org/10.1016/j.ccr.2013.08.027>

SUMMARY

Medullary thyroid carcinoma (MTC) is a neuroendocrine cancer that originates from calcitonin-secreting parafollicular cells, or C cells. We found that Cdk5 and its cofactors p35 and p25 are highly expressed in human MTC and that Cdk5 activity promotes MTC proliferation. A conditional MTC mouse model was generated and corroborated the role of aberrant Cdk5 activation in MTC. C cell-specific overexpression of p25 caused rapid C cell hyperplasia leading to lethal MTC, which was arrested by repressing p25 overexpression. A comparative phosphoproteomic screen between proliferating and arrested MTC identified the retinoblastoma protein (Rb) as a crucial Cdk5 downstream target. Prevention of Rb phosphorylation at Ser807/Ser811 attenuated MTC proliferation. These findings implicate Cdk5 signaling via Rb as critical to MTC tumorigenesis and progression.

INTRODUCTION

Neuroendocrine tumors are relatively rare neoplasms characterized by abnormal hormone secretion, an indolent course, specific genetic mutations, and a poor response to conventional therapies. Medullary thyroid carcinoma (MTC) arises from C cells and metastasizes frequently to regional lymph nodes, bones, lungs, liver, and brain. Although MTC accounts for only 3–5% of all thyroid cancers, it represents more than 14% of thyroid-cancer-related deaths and affects both men and women, almost equally (Massoll and Mazzaferri, 2004; Sippel et al., 2008).

Approximately 25% of MTC cases are hereditary and occur as familial MTC or as a component of the multiple endocrine neoplasia 2 (MEN2) syndromes. MEN2A and MEN2B are autosomal-dominant syndromes in which MTC is frequently associated with pheochromocytoma (adrenal gland cancer). MEN2B is the more severe form of the syndromes, and affected patients develop additional symptoms such as mucosal neuromas and marfanoid habitus. These genetic forms of MTC originate from activating germline mutations in the rearranged during transfection (*RET*) proto-oncogene (Liska et al., 2005), which encodes a tyrosine kinase receptor for the glial-derived neurotrophic factor

Significance

Neuroendocrine tumors are indolent malignancies arising from hormone-producing cells scattered throughout the body. MTC stems from the thyroid C cells and has a high mortality rate with rising incidence. Complete thyroid removal is the current primary therapy, but recurrence is common and more effective treatments are needed. Here, we show that Cdk5 promotes human MTC proliferation and that transgenic induction of aberrant Cdk5 activity in mouse thyroid C cells causes MTC. Furthermore, we reveal Rb protein as a downstream effector by which Cdk5 drives neuroendocrine cell neoplasia. Therefore, Cdk5 may be a promising drug target against MTC.

family (GDNF; neurturin, artemin, and persephin) (Takahashi, 2001). Mechanisms by which RET mutations lead to MTC have been extensively studied (Asai et al., 2006). However, the majority of MTC cases (>75%) arise spontaneously, and only 40% of these so-called sporadic cases are caused by somatic RET mutations.

The molecular basis of sporadic MTC is poorly understood (Hu and Cote, 2012), although mutations in the RAS family of small GTPase genes have recently been identified in RET-negative MTC cases and RAS has been proposed to act as an alternative driver to RET in MTC tumorigenesis (Agrawal et al., 2013; Boichard et al., 2012; Ciampi et al., 2013). Consequently, therapeutic strategies are limited (Schlumberger et al., 2008). Currently, complete surgical removal of the thyroid remains the primary treatment for early-stage MTC patients (Fialkowski and Moley, 2006). However, recurrence is common and metastases are resistant to chemotherapy. The recent FDA approval of the tyrosine-kinase inhibitor Vandetanib provides a treatment option for MTC (Wells et al., 2012). However, the use of this drug is limited to unresectable, late-stage, and metastatic MTC and may produce unwanted side effects (Sherman, 2013). Thus, additional therapies are needed and identifying novel molecular mechanisms underlying MTC tumorigenesis is crucial for the development of treatments for MTC.

Cyclin-dependent kinase 5 (Cdk5) is a proline-directed serine/threonine kinase essential for the central nervous system development and brain function (Angelo et al., 2006). Binding with its noncyclin cofactors p35 and p39 activates Cdk5. Cellular stress can induce the cleavage of p35 by the Ca²⁺-dependent protease calpain to p25, which aberrantly activates Cdk5, thereby promoting the phosphorylation of substrates implicated in neurodegeneration (Kusakawa et al., 2000). Cdk5's functions beyond the nervous system are still emerging. It modulates insulin secretion in pancreatic β cells (Lilja et al., 2001; Wei et al., 2005) and may contribute to cell cycle regulation and some forms of cancer (Goodyear and Sharma, 2007; Jiang et al., 2005; Kim et al., 2006; Lin et al., 2007; Lopes and Agostinho, 2011; Strock et al., 2006). Indeed, elevated Cdk5 activity has been detected in pancreatic and lung cancers (Demelash et al., 2012; Feldmann et al., 2010). Furthermore, Cdk5 regulates motility and migration of a variety of cancer cell lines, which suggests a role for Cdk5 in tumor progression and metastasis (Huang et al., 2009; Quintavalle et al., 2011; Strock et al., 2006).

Neuroendocrine and neuronal cells both originate from the neural crest and share common physiological features (Pang and Südhof, 2010). Given that Cdk5 plays a crucial role in neuronal physiology, we hypothesized that Cdk5 also regulates neuroendocrine cell function. Here, we investigate the role of Cdk5 in human MTC tumorigenesis.

RESULTS

The Role of Cdk5 and Its Activators p35 and p25 in Human MTC Proliferation

We detected Cdk5 in human thyroid gland and specifically in neuroendocrine C cells as shown by colocalization of Cdk5 with calcitonin (Figures 1A and 1B). Expression of p35/p25 was also evident in both follicular and C cells as detected by immunostaining contiguous thyroid sections with a p35 antibody,

which also detects p25 (Figure 1A; Figures S1A and S1B available online). Because neoplastic C cell hyperplasia is an early step in the development of MTC, we examined Cdk5 and p35/p25 expression in resected malignant specimens from 17 MTC patients who underwent thyroidectomy. Cdk5 and p35/p25 expression was apparent in all MTC samples (Figures 1A, 1C, and 1D; Figure S1A). Notably, Cdk5 and its activators were expressed at higher levels in sporadic MTC samples than in noncancerous thyroid tissues (Figures 1C and 1D; Figure S1A). Interestingly, Cdk5, p35, and p25 levels were not consistently elevated in MEN2A specimens compared to control tissues, suggesting possible mechanistic differences between at least some hereditary and sporadic forms of this cancer (Figure 1D). Furthermore, rising levels of MTC (% neoplastic cellularity) correlated with increasing p35/p25 expression in sporadic MTC patient samples that were graded histopathologically (Figure 1E). Altogether, these findings suggest that Cdk5 activity may be important for human sporadic MTC tumorigenesis.

To investigate further the possible role of Cdk5 in MTC progression, we assessed Cdk5, p35, and p25 expression in a panel of six human cell lines derived from sporadic MTC (Pfragner et al., 2002). All MTC cell lines exhibited Cdk5 and p35 expression as well as p25 generation (Figure 2A). Because cultures of normal human thyroid C cell cultures are difficult to establish because of the low C cell content in a human thyroid biopsy (~1%), cultured normal human diploid fibroblasts (NDF) were used as controls. NDF also exhibited p35 expression. However, very little Cdk5 or p25 was detected in these cells. Treatment of MTC cells with the Cdk5 inhibitor CP681301 (Karran and Palmer, 2007; Sadleir and Vassar, 2012; Wen et al., 2008) stopped their proliferation and significantly reduced their viability (Figures 2B and S2A). However, Cdk5 inhibition had little or no effect on the proliferation and viability of NDF cells (Figure S2A). With these positive results in hand, MTC-SK and SIN-J were selected as representative for further analysis. MTC-SK cells were derived from a solid sporadic MTC tumor, whereas SIN-J cells originated from metastatic sporadic MTC (Pfragner et al., 1990; Pfragner et al., 1993). Both have been characterized for their close similarity to MTC tumor cells and express appreciable levels of Cdk5, p35, and p25.

CP681301 is moderately selective for Cdk5 over Cdk2 in vitro (2.8-fold). To confirm CP681301 specificity for Cdk5 over Cdk2, we immunoprecipitated either Cdk5 or Cdk2 using cell lysates from CP681301-treated MTC-SK and SIN-J cells and assessed the activity of each kinase in vitro using histone H1 as a substrate. Cdk5 but not Cdk2 activity was inhibited by CP681301 at the concentrations used in this study for both cell lines (Figure 2C; Figure S2B). Furthermore, competing with endogenous Cdk5 activity by expressing a kinase-dead (KD) Cdk5 mutant also reduced MTC-SK (Figure 2D) and SIN-J (Figure S2C) cell proliferation. As for pharmacological inhibition, this reduction in cell growth correlated with a reduction in Cdk5 activity in both cell lines (Figure 2E; Figure S2D). Moreover, siRNA-mediated knockdown of the Cdk5 activator p35 also reduced MTC-SK and SIN-J cell growth (Figure 2F; Figure S2E). Again, p35 siRNA significantly reduced Cdk5 activity in MTC-SK and SIN-J cells without affecting Cdk2 activity (Figure 2G; Figure S2F). Together these findings indicate that Cdk5 activity, as dictated by the expression of its activating cofactors p35 and p25, is critical to

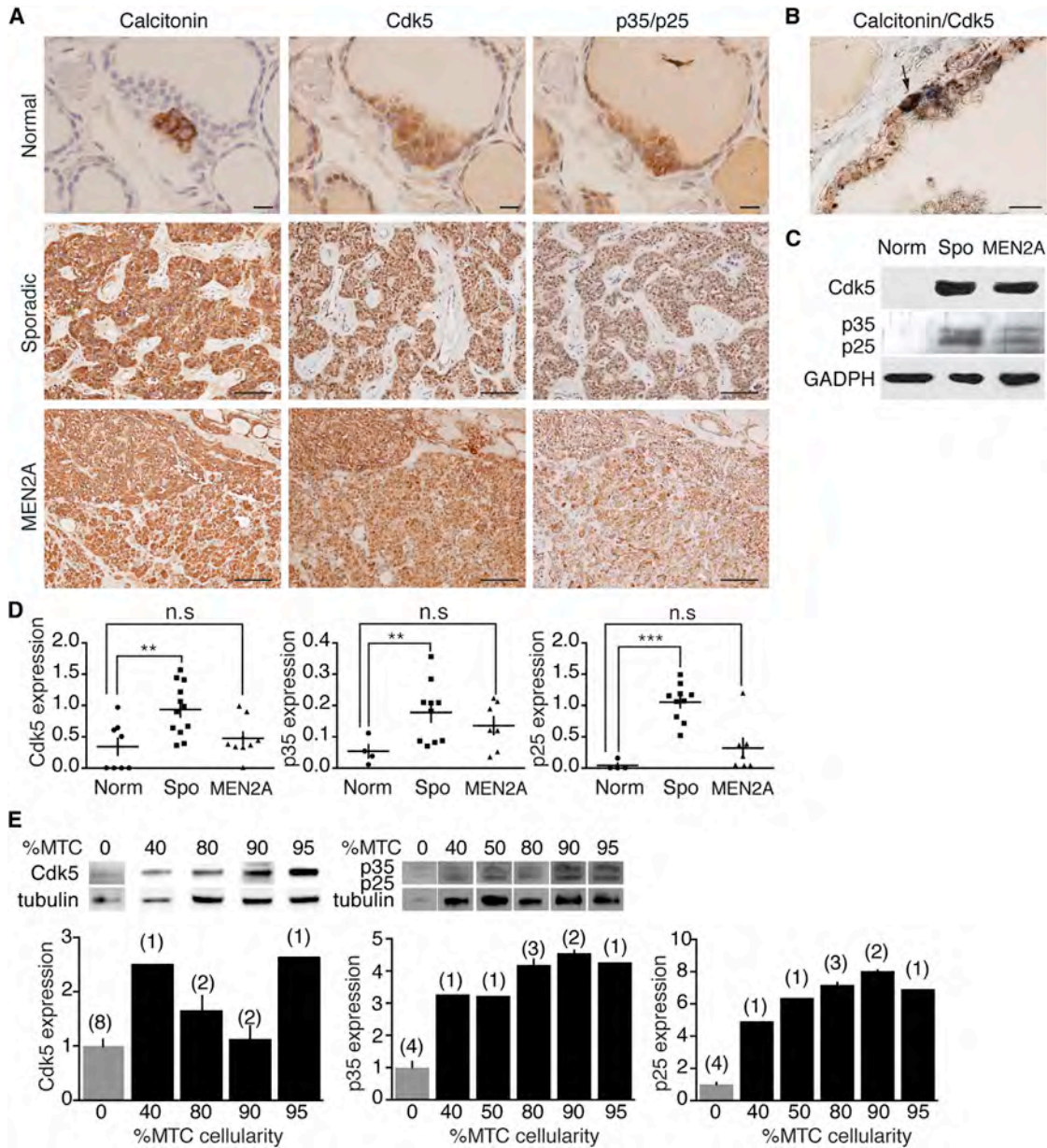


Figure 1. Cdk5 and Its Cofactors Are Expressed in Human Thyroid and in MTC

(A) Contiguous sections of normal human thyroid, sporadic medullary thyroid tumors, and hereditary medullary thyroid tumors (MEN2A syndrome) are immunostained for calcitonin, Cdk5, and p35/p25. Scale bars are 20 μ m for normal tissue stains and 100 μ m for tumor stains (MEN2A, sporadic).

(B) High magnification image of normal thyroid costained for Cdk5 (brown) and calcitonin (dark blue) is shown. The arrow indicates C cell. Scale bar is 20 μ m.

(C) Representative immunoblots of lysates from nonmalignant (Norm), sporadic (Spo), and familial (MEN2A) cancerous human thyroid specimens for Cdk5, p35/p25, and GAPDH are shown.

(D) Quantification of (C) is shown. Each point represents the protein expression level normalized to the loading control for each sample. Horizontal bar lines represent mean values for nonmalignant (n = 4–8), sporadic (n = 10–12), and MEN2A (n = 7). For Cdk5, Spo, p = 0.0048 and MEN2A, p = 0.4411; for p35, Spo, p = 0.0317 and MEN2A, p = 0.0793; for p25, Spo, p < 0.0001 and MEN2A, p = 0.2305 in a two-tailed unpaired Student's t test with Welch's correction. Vertical error bars represent \pm SEM.

(E) Immunoblots show the expression of Cdk5, p35, and p25 in samples of sporadic MTC patients at different stages of the disease and quantification. The percentage of MTC cellularity was determined during the pathological analysis by quantifying microscopically the percentage of a representative slice that was occupied by the MTC (see [Supplemental Experimental Procedures](#)). Values for each MTC sample were normalized to the loading control. Data represents mean values of n = 1–8 samples as indicated. Error bars represent \pm SEM.

See also [Figure S1](#).

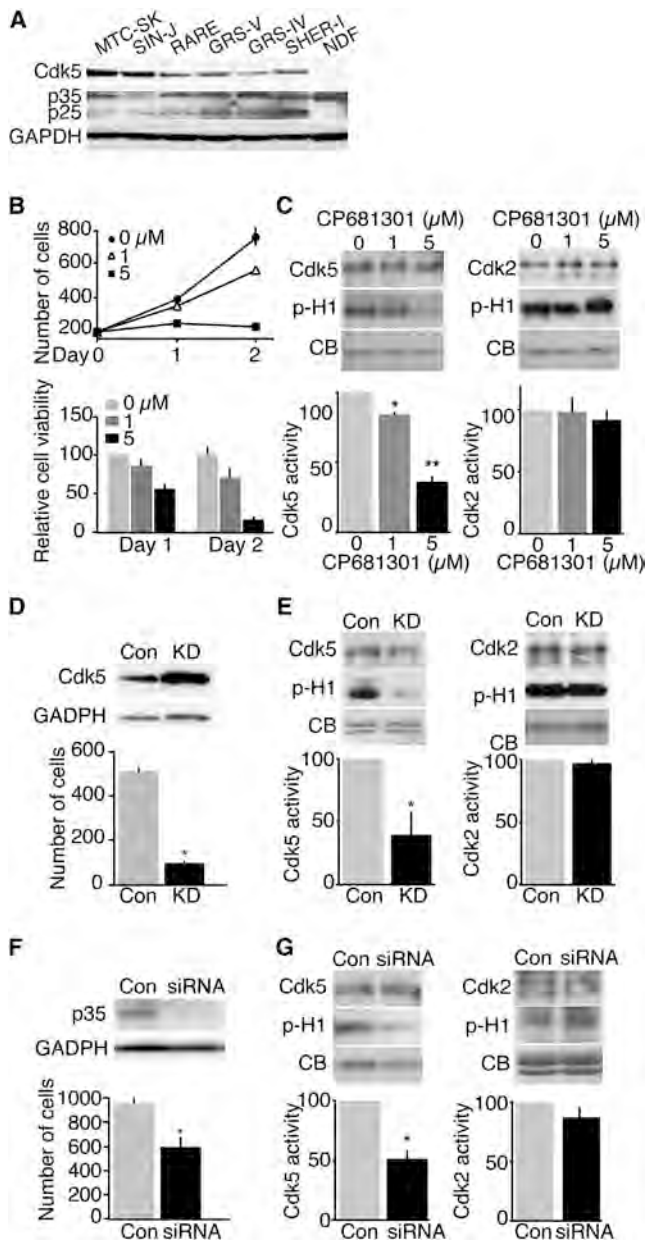


Figure 2. MTC Cell Proliferation Is Dependent upon Cdk5 Activity

(A) Immunoblots of lysates from the indicated human sporadic MTC cell lines and NDF probed with antibodies to Cdk5, p35, p25, and GAPDH are shown. (B) Dose-dependent effect CP681301 on MTC-SK cell proliferation and viability is shown.

(C) Effect of CP681301 on Cdk5 and Cdk2 activity is shown. Cdk5 and Cdk2 were immunoprecipitated from MTC-SK cells treated with 0, 1, or 5 μ M CP681301 for 12 hr and used to phosphorylate histone H1 *in vitro*. Immunoblots show Cdk5 and Cdk2 used in immunoprecipitation-kinase assay reaction mixtures (top). Kinase activity was detected by blotting for phospho-histone H1 (p-H1) (middle). Coomassie-stained (CB) histone H1 controls show the amount of substrate used in reactions (bottom). For quantitation of p-H1, for Cdk5 activity, $p = 0.0037$ for 0 versus 1 μ M; $p = 0.030$ for 0 versus 5 μ M.

(D) Immunoblots of lysates from MTC-SK cells transfected with a control plasmid (Con) or with a KD-Cdk5 expression vector (KD) probed with antibodies to Cdk5 and GAPDH (top) are shown; a histogram summarizing the effect of Con or KD expression on cell proliferation ($p = 0.0057$) is shown below.

the proliferation of human sporadic MTC cells and may contribute to some cases of MTC.

P25 Overexpression and Associated Cdk5 Activity Result in Thyroid Tumor Formation

To delineate the effects of aberrant Cdk5 activation in MTC tumorigenesis, we used the neuron-specific enolase (NSE) promoter to drive GFP-tagged p25 overexpression (p25OE) in C cells. In this bistransgenic mouse model, p25OE is regulated via a tetracycline-controlled transactivator (tTA) system, which is driven by the NSE promoter (Figure 3A) (Meyer et al., 2008). In this model, p25OE can be induced by withdrawal of the tetracycline analog doxycycline from the animal diet (Cruz et al., 2003), while administration of doxycycline readily represses p25OE. The p25OE mice developed large, bilateral thyroid tumors 16–25 weeks after doxycycline removal (Figure 3B). These fast-growing tumors were malignant as shown by FDG uptake during PET imaging (Figures 3C and 3D). No p25OE mice survived past 30 weeks off doxycycline (Figure 3E). In contrast, control littermates that lacked p25-GFP transgene had normal thyroids and survival rates (Figures 3B and 3E). The tumors expressed high levels of p25-GFP (Figures 3F and 3G) and were formed by calcitonin-positive neoplastic C cells that invaded the tracheal muscle and extended into the tracheal lumen, leading to obstruction (Figures 3H and 3I). Clusters of calcitonin-positive C cells invaded and metastasized within the vasculature in the skeletal muscles near the lungs (Figure 3J). Together these histological analyses indicate that these thyroid tumors are MTC.

To monitor MTC tumorigenesis, thyroid samples were examined at different time points following induction of p25OE (Figure 4A). In control animals, thyroid gland was normal, comprised of follicular cells surrounding distinct colloid-filled follicles. C cells were interspersed in-between follicular cells as detected by a calcitonin-specific immunostaining (Figure S3). After 5 weeks of p25OE, mild C cell hyperplasia developed and progressed into small tumors within 11 weeks. By 16 weeks, large bilateral MTC tumors had formed and invaded the space between trachea and esophagus. At this stage, no more follicles were visible. The thyroid tumors were divided by fibrous septa in a nested pattern and consisted of a population of round cells with uniform nuclei and amphophilic cytoplasm, characteristic of MTC. All mice examined died within 30 weeks of p25OE. However, stopping p25OE after 5, 11, or 16 weeks led to 100% survival of mice analyzed for up to 32 weeks (Figure 4B). Indeed,

(E) Immunoblots for p-H1 show Cdk5 and Cdk2 activity in MTC-SK cells transfected with a control plasmid (Con) or with KD-Cdk5 (KD) (for Cdk5 activity, $p = 0.0297$). Immunoprecipitated Cdk5, Cdk2, and Coomassie-stained histone H1 controls are shown.

(F) Immunoblots of lysates from MTC-SK cells transfected with a scrambled siRNA (Con) or a p35 siRNA probed with antibodies to p35 and GAPDH (top); below is a histogram summarizing the effect of Con or p35 siRNA expression on cell proliferation ($p = 0.0365$).

(G) Immunoblots for p-H1 show Cdk5 and Cdk2 activity in MTC-SK cells transfected with scrambled (Con) or p35 siRNA (for Cdk5 activity, $p = 0.0178$). Immunoprecipitated Cdk5, Cdk2, and Coomassie-stained histone H1 controls are shown.

All data represent mean values, error bars are \pm SEM, and p values were determined by a two-tailed paired Student's t test, where $n = 4$ (C–G). For (B), (D), and (G), number of cells is 1,000-fold. See also Figure S2.

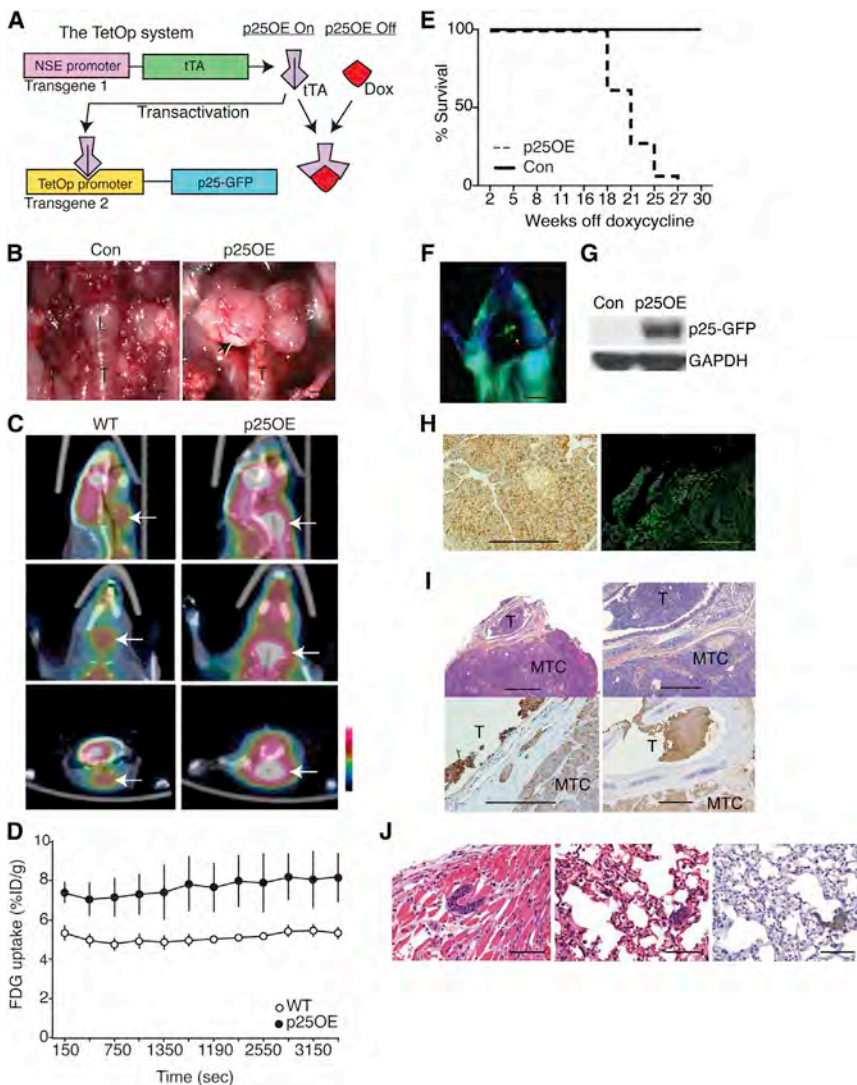


Figure 3. Characterization of an MTC Animal Model

(A) Schematic of the bitransgenic system shows activation of TetOp promoter-controlled p25-GFP expression by doxycycline (Dox)-inhibitable tTa. tTa expression is under NSE promoter control.

(B) Dissection shows the thyroid gland in p25OE and control littermate. The arrow indicates tumors. L, larynx; T, trachea.

(C) In vivo microPET/CT of WT thyroid versus p25OE thyroid tumor (arrows) is shown. Representative sagittal (top), coronal (middle), and transaxial (bottom) images are shown.

(D) Time-dependent [18 F]FDG uptake in thyroid (WT) and thyroid tumors (p25OE) is shown. Mean values are plotted. Error bars represent \pm SEM ($n = 3$).

(E) Survival curve for p25OE and control littermates ($n = 28$) is shown.

(F) Optical fluorescent imaging of thyroid tumors (arrow) in a p25OE mouse is shown.

(G) Immunoblots of thyroid (littermate control, Con) versus p25OE thyroid tumor lysates for p25-GFP (using anti-GFP antibodies) and GAPDH are shown.

(H) Calcitonin staining (left; scale bar is 100 μ m) and GFP immunostaining (right; scale bar is 500 μ m) of a p25OE tumor are shown.

(I) Representative hematoxylin and eosin (HE) stainings (top) and corresponding calcitonin immunostains (bottom) of the thyroid and tracheal region in a p25OE mouse are shown (scale bars are 500 μ m, top left; 200 μ m, top and bottom right; and 100 μ m, bottom left). T, trachea; MTC, medullary thyroid carcinoma.

(J) HE staining of metastatic C cells in skeletal muscle vasculature (left; scale bar is 20 μ m), and HE staining (middle) and calcitonin immunostain (right) of metastatic C cells within alveolar walls of the lung (scale bar is 50 μ m) of contiguous sections are shown.

switching off p25OE at early stages of MTC tumorigenesis (5 weeks) prevented C cell hyperplasia, while repressing p25OE at later stages of the disease (11 or 16 weeks) resulted in the arrest of tumor growth (Figure 4C). As expected, arrested tumors lacked p25-GFP expression. However, repressing p25OE did not affect Cdk5 or p35 protein levels (Figure 4D). Cdk5 activity was significantly reduced in arrested (p25OE Off) tumors compared to proliferating (p25OE On) tumors in which p25 aberrantly activates Cdk5 (Figure 4E).

Together these results demonstrate that NSE promoter-driven p25OE results in the formation of thyroid tumors featuring the characteristics of human MTC (Fialkowski and Moley, 2006) and that aberrant Cdk5 activation by p25-GFP contributes to MTC proliferation in this mouse model.

In Vitro Characterization of p25OE Mice MTC

To further confirm the role of Cdk5 in MTC, we generated a cell line from the MTC of p25OE mice (MTCp25). These cells grew as floating clusters and exhibited anchorage-independent growth and malignant transformation in a soft agar assay (Figure 5A).

Importantly, MTCp25 cells retained the characteristics of the mouse tumors. These cells were calcitonin-positive, expressed p25-GFP and Cdk5 (Figure 5B), and secreted calcitonin in the culture media (approximately 100 pg/ml). As shown in the tumors, p25-GFP expression and Cdk5 activity were controlled by doxycycline (Figures 5C and 5D). Repressing p25-GFP overexpression by culturing the cells in the presence of doxycycline dose-dependently arrested cell proliferation but had no effect on cell viability (Figure 5E). Furthermore, doxycycline had no effect on the proliferation of a heterologous non-small-cell lung carcinoma line, H1299 (Figure S4A). Thus, turning off p25OE with doxycycline stops mouse MTCp25 cell growth without causing cell death.

To substantiate the role of Cdk5 activity on MTC tumorigenesis, the effect of Cdk5 inhibition on MTCp25 cell proliferation and viability was assessed. CP681301 dose-dependently reduced MTCp25 cell proliferation and viability as was observed with human MTC cell lines (Figure 5F). Moreover, two alternate Cdk5 inhibitors, indolinone A and roscovitine, also stopped MTCp25 cell proliferation (Figures S4B and S4C). Finally, siRNA

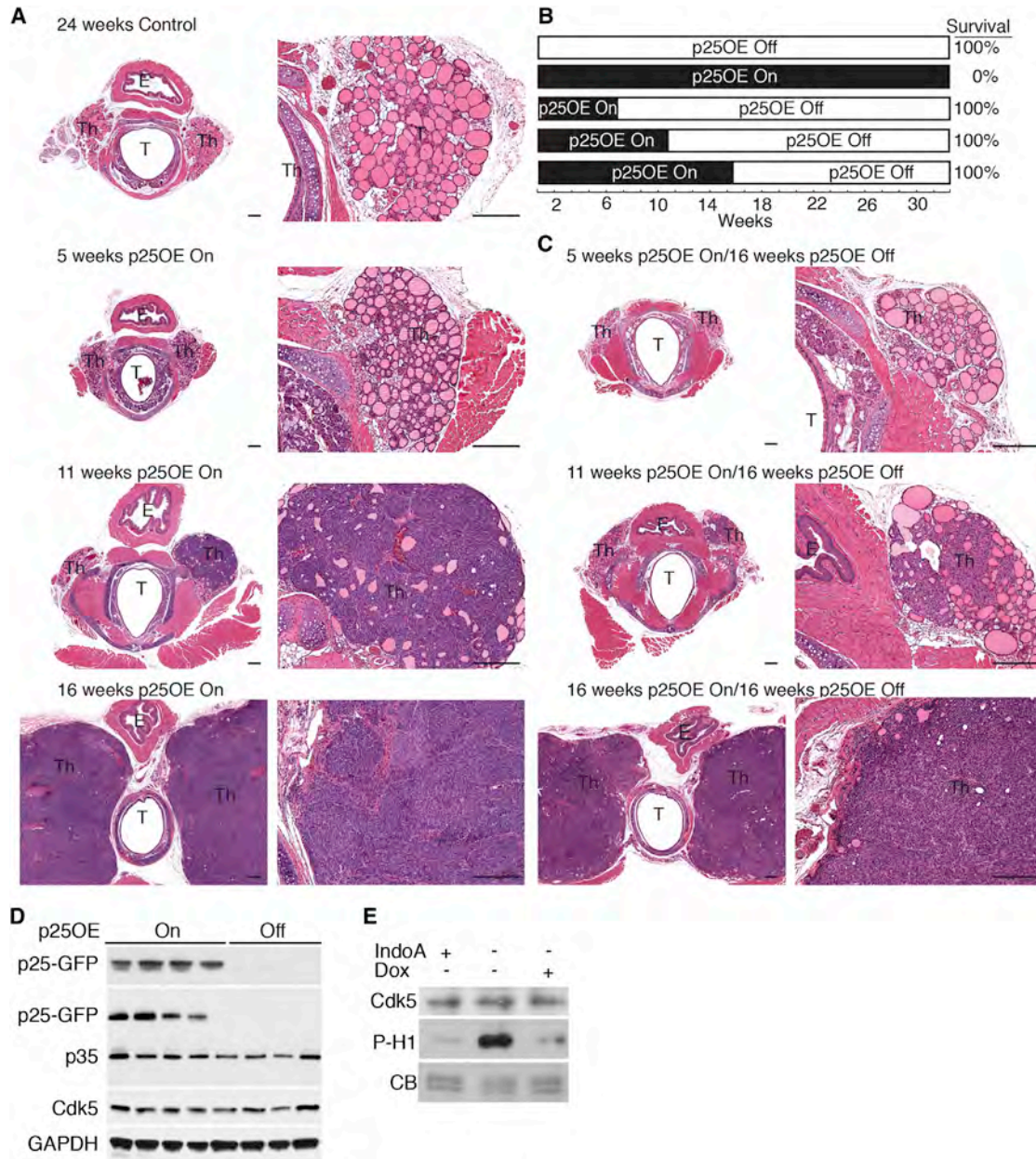


Figure 4. Progression and Arrest of MTC in p25OE Mice Is Controlled by p25 Expression and Associated Aberrant Cdk5 Activity

(A) HE staining of thyroid in control mice and mice with p25OE On for the indicated time period is shown. Scale bars are 100 μ m.

(B) Schematic of p25OE On and Off with survival for each paradigm indicated (n = 4–7) is shown.

(C) Representative HE staining of typical thyroid for each paradigm of p25OE On followed by arrest (p25OE Off) is shown. Scale bars are 100 μ m.

(D) Immunoblots of lysates from proliferating (p25OE On, 16 weeks) and arrested (p25OE On, 16 weeks, followed by p25 Off, 6 weeks) tumors (n = 4) for GFP-tagged p25, p35, Cdk5, and GAPDH are shown. p25-GFP was detected by using either antibodies to GFP or antibodies to p35/p25.

(E) Immunoblot for p-H1 showing Cdk5 activity in proliferating (– Dox) and arrested (+ Dox) tumors as determined by immunoprecipitation/kinase assays using histone H1 as a substrate is shown. Inhibition of Cdk5 by indolinone A, immunoprecipitated Cdk5, and Coomassie-stained (CB) histone H1 controls are shown. See also Figure S3.

knockdown of Cdk5 reduced Cdk5 expression and activity as well as cell growth (Figures 5G and 5H). Taken together, these findings show that MTCp25 cell proliferation is dependent on the Cdk5 activity that is mediated by p25OE, further supporting a role for Cdk5 in MTC progression.

Retinoblastoma Protein Plays a Critical Role Downstream of Cdk5 Activation in MTC Proliferation

To identify Cdk5 downstream effectors, we profiled proteins containing Cdk5 consensus phosphorylation sites in proliferating versus arrested p25OE mouse tumors by phospho-scan

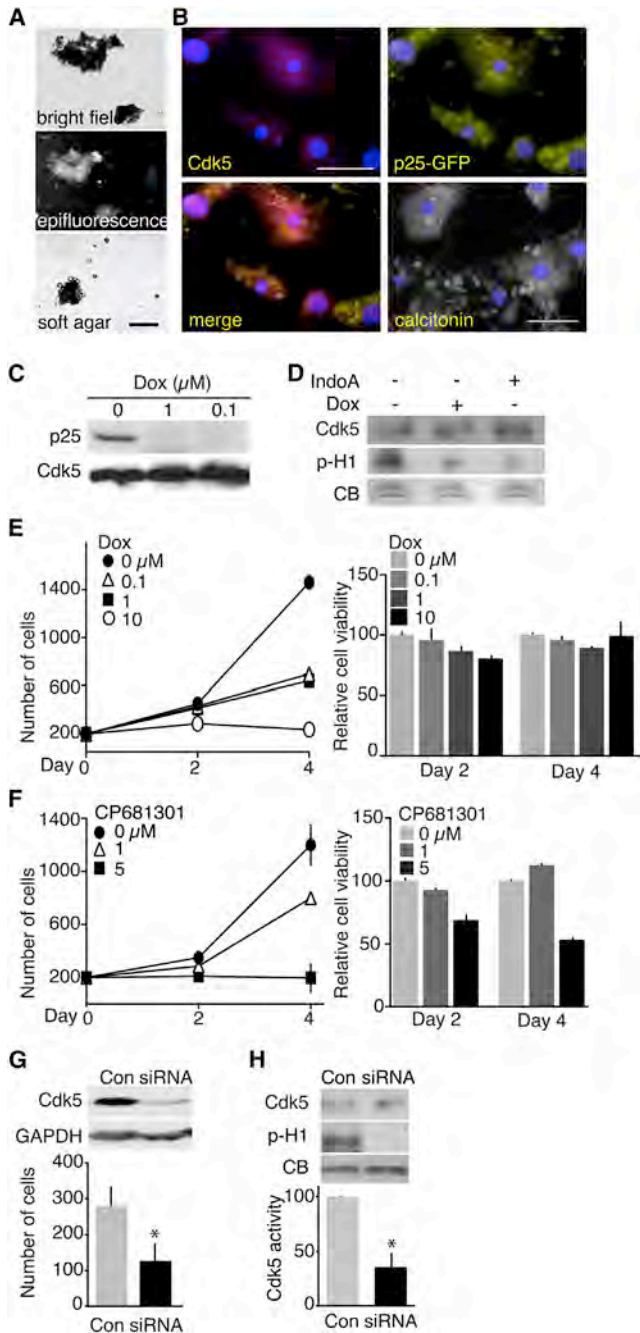


Figure 5. Generation of a Mouse MTC Cell Line—MTCp25—That Retains the Characteristics of p25OE Mice Tumors

(A) Brightfield and epifluorescent images show MTCp25 mouse cells growing in suspension as cell clusters and colony formation in soft agar.

(B) Immunostaining of MTCp25 cells for Cdk5 (magenta), p25-GFP (yellow), calcitonin (gray), and DAPI-stained nucleus (blue) are shown. Scale bar is 20 μ m.

(C) Immunoblots of lysates from doxycycline-treated MTCp25 cells for p25 and Cdk5 show the effect of doxycycline on p25-GFP overexpression and on Cdk5 expression.

(D) Immunoblot for p-H1 shows the effect of doxycycline on Cdk5 activity after immunoprecipitating Cdk5 from MTCp25 cells treated with doxycycline. Cdk5 inhibition by indolinone A, immunoprecipitated Cdk5, and Coomassie-stained (CB) histone H1 controls are shown.

liquid chromatography tandem mass spectrometry (Rush et al., 2005). Peptides phosphorylated at serine 807 of Rb were highly enriched in proliferating mouse tumors compared with arrested tumors (Figure S5A), which was confirmed by immunoblotting (Figure 6A). Likewise, phospho-Ser807/Ser811 Rb levels were increased in doxycycline-deprived cultured MTCp25 cells in which p25OE is induced and Cdk5 activity is elevated (Figure 6B). Furthermore, consistent with Cdk5, p35, and p25 expression, phospho-Ser807/Ser811 Rb was elevated significantly in human sporadic MTC tumors but not MEN2A samples compared to control tissue (Figure 6C). Together, these results suggest a mechanistic link between Cdk5 activity, Rb phosphorylation, and sporadic MTC.

Because Ser807 and Ser811 are known Cdk5 phosphorylation sites (Futatsugi et al., 2012; Hamdane et al., 2005) and Rb deletion has been linked to neuroendocrine tumorigenesis (Takahashi et al., 2006; Williams et al., 1994), we postulated that Rb is a downstream effector of Cdk5 and that Cdk5-Rb signaling promotes MTC. Indeed, inhibiting Cdk5 activity in mouse and human MTC cells by treatment with CP681301 decreased phospho-Ser807/Ser811 Rb in a dose-dependent manner and stopped cell growth (Figures 6D and 6E; Figure S5B; Figure 2B; Figure S2A). Furthermore, disrupting Cdk5 activity in human MTC cells by expressing a kinase-dead Cdk5 or knockdown of p35 diminished phospho-Ser807/Ser811 Rb and reduced MTC cell proliferation (Figures 6F and 6G; Figures 2D and 2F; Figures S5C, S5D, S2C, and S2E). Finally, competing with Cdk5 phosphorylation of Rb by treating mouse or human MTC cell lines with a small inhibiting peptide (SIP) that consisted of a 19-amino-acid Rb sequence encompassing Ser807/Ser811 dose-dependently reduced phospho-Ser807/Ser811 Rb and cell proliferation (Figure 6H; Figure S5E). The SIP had no effect on STAT3 phosphorylation at known Cdk5 sites, indicating specificity for Rb phosphorylation (Figure 6H). Together, these findings identify Rb as a Cdk5 downstream target in MTC tumorigenesis.

Having confirmed Rb as an important Cdk5 target, we investigated the mechanism by which Cdk5-Rb mediates MTC proliferation. Rb acts as a tumor suppressor by binding the E2F transcription factors, thereby blocking their transcriptional activity. Upon Rb phosphorylation by cyclin-dependent kinases, E2Fs are released and activate the expression of their target genes, including Cdk2 and Cyclin A (Chellappan et al., 1991; DeGregori et al., 1997; Knudsen et al., 1999). In agreement with this, arrest of mouse tumor growth by repressing p25OE abolished Cdk2 and Cyclin A expression (Figure 6I). Furthermore, inhibiting Cdk5 activity in human MTC cells with CP681301 attenuated

(E and F) Dose-dependent effect of doxycycline (E) and CP681301 (F) on MTCp25 cell proliferation and viability is shown.

(G) Immunoblots of lysates from MTCp25 cells transfected with a scrambled siRNA (Con) or a Cdk5 siRNA (siRNA) probed with antibodies to Cdk5 and GAPDH (top) are shown; the histogram summarizes the effect of Con or Cdk5 siRNA expression on cell proliferation ($p = 0.023$) (bottom).

(H) Immunoblot for p-H1 shows immunoprecipitated Cdk5 activity in cells transfected with Cdk5 siRNA and quantification ($p = 0.0145$). Immunoprecipitated Cdk5 and Coomassie-stained (CB) histone H1 controls are shown.

All data represent mean values ($n = 4$) and error bars are \pm SEM; p values were determined by a two-tailed paired Student's t test. For (E), (F), and (G), cell numbers are 1,000-fold. See also Figure S4.

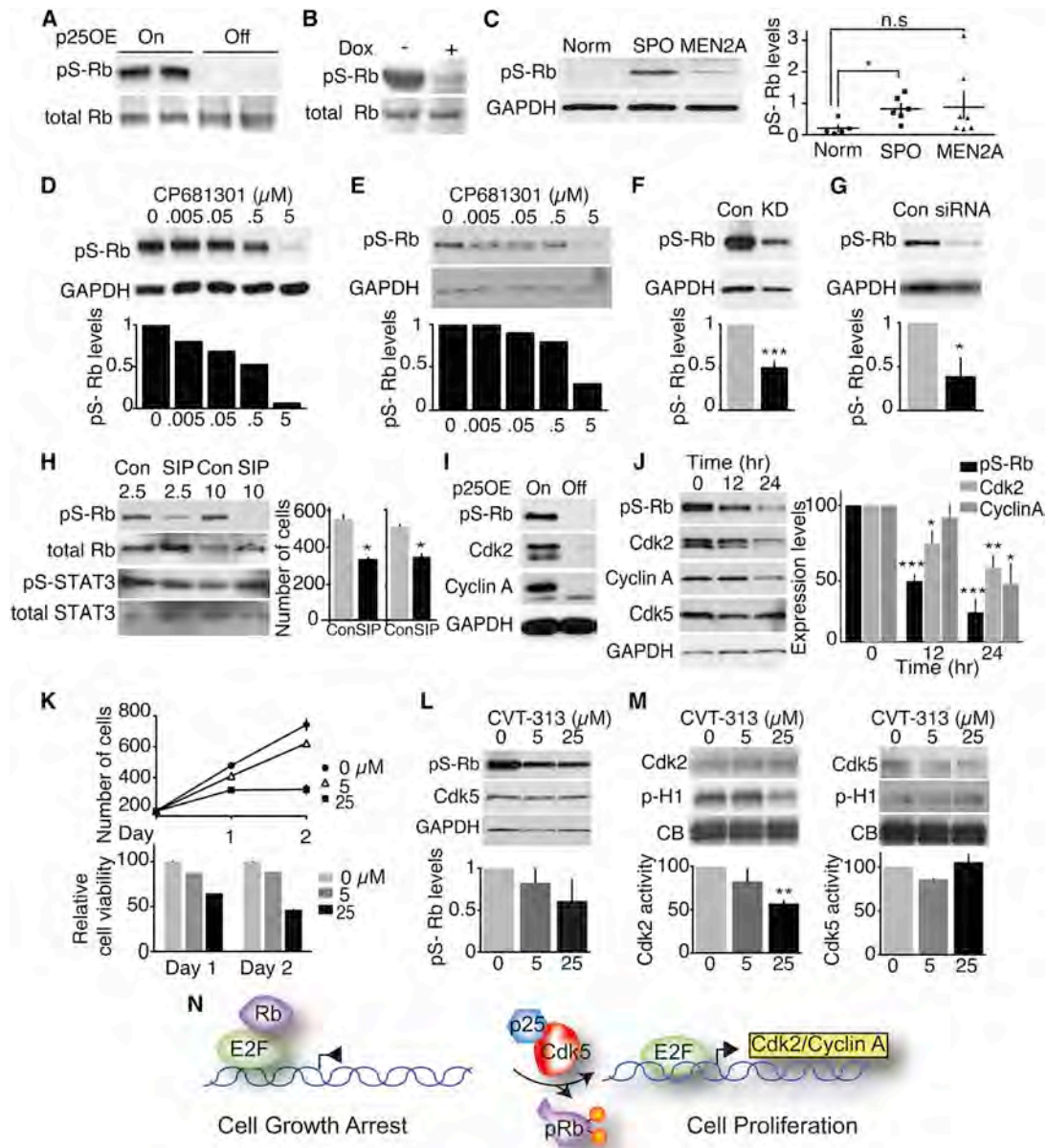


Figure 6. Rb Is a Downstream Target of Cdk5 in MTC

(A) Immunoblots of lysates from proliferating (p25OE On) and arrested (p25OE Off) p25OE tumors probed with antibodies to phospho-Ser807/Ser811 (pS-Rb) and total Rb (n = 4) are shown.

(B) Effect of doxycycline-induced repression on pS-Rb levels in MTCp25 cells is shown.

(C) Immunoblots of lysates from normal thyroid (Norm) (n = 5), sporadic (SPO) (n = 6), and hereditary (MEN2A) (n = 7) MTC patient specimens were probed with antibodies to pS-Rb and GAPDH. For SPO, p = 0.0117; MEN2A, p = 0.1316, two-tailed unpaired Student's t test with Welch's correction.

(D and E) Immunoblots of lysates from MTCp25 cells (D) and MTC-SK cells (E) following a 16 hr CP681301 treatment probed with antibodies to pS-Rb and GAPDH and quantification are shown.

(F and G) Immunoblots from lysates of MTC-SK cells transfected with (F) a control plasmid (Con) or a kinase-dead Cdk5 expression vector (KD) and (G) with a scrambled siRNA (Con) or a p35 siRNA (siRNA) and probed with antibodies to pS-Rb and GAPDH and quantification are shown. In (F), p = 0.0057; in (G) p = 0.0365.

(H) Immunoblots show the effect of SIP on the phosphorylation of endogenous Rb (at Ser807/Ser811) and STAT3 (left panel). Effect of 10 μM Rb SIP on MTCp25 (left) and MTC-SK (right) cell proliferation is shown (right panel). For MTCp25, p = 0.0336; for MTC-SK, p = 0.0157.

(I) Immunoblots of lysates from proliferating (p25OE On) and arrested (p25OE Off) mouse tumors probed with antibodies to pS-Rb, Cdk2, Cyclin A, and GAPDH are shown.

(J) Immunoblots of lysates from MTC-SK cells treated with CP681301 (5 μM) for 0, 12, or 24 hr probed with antibodies to pS-Rb, Cdk2, Cyclin A, Cdk5, and GAPDH and quantification are shown. For pS-Rb, p < 0.0001 for 0 versus 12 hr, and p < 0.0002 for 0 versus 24 hr; for Cdk2, p = 0.0315 for 0 versus 12 hr, and p = 0.0104 for 0 versus 24 hr; for Cyclin A, p = 0.0257 for 0 versus 24 hr.

(legend continued on next page)

Cdk2 and Cyclin A expression in MTC-SK cells by 25% within 12 hr and by 40% after 24 hr of treatment (Figure 6J). In SIN-J cells, CP681301 reduced Cdk2 and Cyclin A levels by more than 50% within 12 hr (Figure S5F). As expected, Rb phosphorylation levels were reduced by more than 50% within 12 hr following CP681301 application to both cell lines. Thus, Cdk2 and Cyclin A appear to be invoked as downstream effectors of the Cdk5-Rb signaling and this cascade may mediate MTC tumorigenesis. In line with these observations, MTC cell growth was reduced by pharmacological blockade of Cdk2 activity with CVT-313 (Figure 6K; Figure S5G). Importantly, inhibition of Cdk2 only partially reduced Rb phosphorylation but had no effect on Cdk5 expression and activity (Figures 6L and 6M; Figure S5H). This effect is consistent with the ability of Cdk2 to contribute to Rb phosphorylation and cell cycle progression (Harbour et al., 1999). Thus, Cdk5 may contribute meaningfully to the progression of some forms of MTC by inactivating Rb and enabling the expression of the E2F target genes, Cdk2 and Cyclin A (Figure 6N).

DISCUSSION

Although tremendous advances have been made in understanding how RET causes MTC, little is known about other mechanisms that contribute to the majority of neuroendocrine thyroid cancers. Here, we demonstrate that Cdk5 is crucial for human MTC cell proliferation and thus it contributes to MTC progression. Previous work implicated Cdk5/p35 in the proliferation of the TT cell line, which was derived from familial human MTC and contains a RET mutation at codon 634 resulting in constitutive RET activation (Berger et al., 1984; Lin et al., 2007). It was suggested that p35, but not p25, drives Cdk5 activity and is necessary to maintain the RET-dependent growth of this cell line, implying that Cdk5 activation may be downstream of RET. However we found that dysregulation of Cdk5 activity by overexpressing p25 caused MTC, thus suggesting that Cdk5 rather than RET may trigger MTC. Nevertheless, a link between Cdk5 activity in human MTC and the RET or RAS signaling pathways cannot be ruled out and should be further explored.

In evaluating pro-proliferative downstream effectors for Cdk5, we found that Cdk5 phosphorylates Rb and that inactivation of Cdk5 prevents Rb phosphorylation and reduces Cdk2 and Cyclin A expression in human MTC cells and arrested mouse tumors. Deregulation of Rb signaling is a well-known cause of cancer (Weinberg, 1995). Rb is a tumor suppressor that prevents cell cycle progression from G1 to S by binding and sequestering E2F transcription factors (Sellers et al., 1995). Upon Rb phosphorylation by cyclin/cyclin-dependent kinase complexes, E2Fs are released and activate the transcription of target genes

whose products are necessary for cell cycle progression (Bracken et al., 2004). Numerous mitogenic and oncogenic pathways invoke Cyclin D expression. The resulting Cyclin D-Cdk4/Cdk6 complexes catalyze the initial Rb phosphorylation while Cyclin A-Cdk2 can contribute to the maintenance of the phospho-Rb-dependent neoplastic state (Nevins, 2001). Our findings raise the possibility that Cdk5 may catalyze the initial Rb phosphorylation and replace Cyclin D-Cdk4/Cdk6 complexes in some neuroendocrine cancers.

In support of this hypothesis, here Rb phosphorylation at Ser807/Ser811 correlated with Cdk5 activity in growing mouse tumors and in human MTC cells and was arrested in MTC cells overexpressing dominant negative, kinase-dead Cdk5 or subjected to p35 knockdown. Previously, Ser807/Ser811 Rb was reported as a substrate of aberrant Cdk5 in injured neurons (Panickar et al., 2008). The present results implicate Rb as a likely Cdk5 substrate in MTC tumorigenesis. Given that Cdk5 plays important roles in the central nervous system, using a Cdk5 inhibitor to treat MTC may have undesirable side effects. Targeting protein-protein interactions such as those of Rb or other proliferative downstream effectors may provide more selectivity for eventual clinical applications.

Previously, loss of Rb and E2F transcription factors alleles has been linked to neuroendocrine cancers including MTC (Salon et al., 2007; Takahashi et al., 2004; Ziebold et al., 2003). For example, mice carrying a single functional copy of the Rb wild-type gene develop MTC and this tendency is increased in the C57BL6 mouse strain (Harrison et al., 1995; Leung et al., 2004; Nikitin et al., 1999; Williams et al., 1994; Yamasaki et al., 1998). In humans, genetic analysis of sporadic and hereditary MTC patients has identified mutations in genes encoding the INK4 and CIP/KIP families of CDK inhibitors, which are negative regulators of the Rb pathway. Specifically, somatic mutations in the *CDKN2C* gene (p18^{INK4} gene) have been found in several studies and correlated to higher MTC proliferation rates (Flicker et al., 2012; van Veelen et al., 2009). Additionally, mutations within chromosome 19p13.2, which contains the *CDKN2D* gene (p19^{INK4D} gene), have also been detected frequently in MTC patients (Flicker et al., 2012; Ye et al., 2008). Finally, the *CDKN2B* gene (p15^{INK4} gene) has been identified as a low-penetrance gene in MTC (Ruiz-Llorente et al., 2007). Thus, these genetic analyses provide ample evidence that, in addition to RET/RAS somatic mutations, targeting of the Rb pathways through inactivation of CDK inhibitor family members contributes to human MTC tumorigenesis.

In our mouse model, NSE promoter-driven p25-GFP expression was predominantly detected in the thyroid. Only low levels of p25-GFP could be detected in lungs and adrenal gland, and no primary tumors were observed in these tissues. The reason for this expression selectivity or possible sensitivity of C cells

(K) Effect of CVT-313 on sporadic MTC-SK cell proliferation and viability is shown.

(L) Immunoblots of lysates from MTC-SK cells treated with CVT-313 for 12–14 hr probed with antibodies to pS-Rb, Cdk5, and GAPDH are shown.

(M) Immunoblot for p-H1 showing Cdk2 and Cdk5 activity in MTC-SK cells treated with CVT-313 for 12–14 hr. For Cdk2, $p = 0.0051$ for 0 versus 25 μM .

(N) A schematic model for the Cdk5-Rb-Cdk2 pathway in MTC is shown. Rb binds to E2F and suppresses its transcriptional activity, thereby preventing cell proliferation. Upon Rb phosphorylation by Cdk5, E2F is released and activates the transcription of target genes including Cdk2 and Cyclin A that mediate cell proliferation.

All data are mean values ($n = 4$) and error bars represent \pm SEM; p values were determined by a two-tailed paired Student's t test. For (H) and (K), cell numbers are 1,000-fold. See also Figure S5.

to Rb inactivation is presently unclear. However, we do not exclude a role for Cdk5 in other neuroendocrine cancers.

Neuroendocrine cancers are silent killers because they are difficult to diagnose due to a lack of symptoms and are often uncovered at advanced stages when the window for effective surgical treatment has passed. Few treatment options are available in part as a result of incomplete understanding of the underlying molecular pathways and the lack of relevant animal models (Knostman et al., 2007). Existing models of MTC include transgenic mice bearing RET mutations (Cranston and Ponder, 2003) and animals deficient for Rb1/p53 (Harvey et al., 1995), prolactin receptor (Kedzia et al., 2005), or Rb1/Nras (Takahashi et al., 2006). However in most of these, constitutive transgene expression or gene knockout may introduce congenital confounds. In the model introduced here, MTC is reversibly and reproducibly induced in an adult with a fully developed and functional thyroid. Importantly, MTC originates from p25-mediated aberrant Cdk5 activation in C cells and not from a RET mutation. Hence, the animal model established here represents a clinically relevant model to study the onset and progression of sporadic MTC carcinogenesis. Furthermore, the ability to arrest the disease at various stages may facilitate the identification of drug-gable targets for therapy development. Finally, this mouse model will be a useful preclinical tool for the development and testing of new adjuvant therapies for MTC (Dar et al., 2012; Wells et al., 2012).

EXPERIMENTAL PROCEDURES

Antibodies, siRNAs, Plasmids, and Peptides

Antibodies for human calcitonin were from DAKO; GFP from Abcam; GADPH from Sigma; and Cdk5, Cdk2, Cyclin A, and p35/p25 from Santa Cruz Biotechnology. The Cdk5 monoclonal Ab was described by Lagace et al. (2008). The p35/p25 polyclonal antibody is directed to an antigen in the C terminus of p35 and does not distinguish between p35 and p25. The specificity of p35/p25 antibody has been verified in brain tissues of p35 knockout animals (Figure S1B). Antibodies to total Rb, pRb-Ser807/Ser811, STAT3, and pSTAT3 were from Cell Signaling Technology, and phospho-histone H1 from Millipore. Cdk5 siRNA was from Santa Cruz Biotechnology and p35 siRNA from Sigma. The kinase-dead CDK5 construct pCMV-KD-Cdk5 was previously described (Saito et al., 2007), and the pCMV-EGFP was from Clontech. The peptide was synthesized by the UT Southwestern Protein Chemistry Technology Center. The sequence of the Rb-Cdk5 small interfering peptide (SIP) was R₇-PGGNIYISPLKSPYKISEGL and the control peptide R₇-SYFHKEDRPPRDK.

Human Tissue Samples

Normal human and medullary thyroid specimens were obtained through a human subject institutional-review-board-approved protocol UT Southwestern IRB 052004-044, "Molecular Analysis of Endocrine Tumors." Written consent of subjects was obtained. Diagnosis of the neoplasm was confirmed by pathological review, and RET-germline mutation analyses were obtained from MTC patient records. All MEN2A samples harbored germline point mutation in RET codon 634 resulting from a cysteine to tyrosine substitution.

Generation of NSE TetOp p25-GFP Mice

Bitransgenic mice were generated as described previously (Meyer et al., 2008). Briefly, the p25-GFP340 mouse strain, which contains a human p25-GFP transgene driven by the TetOp promoter (TetOp-p25-GFP), was crossed with the NSE5021 strain, which has a tetracycline transactivator (tTA) directed by the neural-specific enolase promoter (NSE). This form of p25 is functional (Cruz et al., 2003) and the use of the TetOp system to drive NSE-directed expression has been well characterized (Chen et al., 1998).

All mouse strains were maintained on a C57BL/6 background. Transgenic alleles were identified by a PCR-based genotyping strategy for p25-GFP and

NSE-tTA alleles. Bitransgenic p25OE mice were positive for the NSE-tTA and p25-GFP transgenes. Control littermates were positive for NSE-tTA but not p25-GFP. Both groups were treated identically with regard to doxycycline administration. All subjects used in these studies were group-housed on a 12 hr light/dark cycle with access to food and water ad libitum. All procedures were performed during the light cycle between 0600 and 1800, were approved by the Institutional Animal Care and Use Committee of the University of Texas, and conducted in accordance with the applicable portions of the *National Institutes of Health Guide for the Care and Use of Laboratory Animals*.

Cell Culture, Transfections, Drugs, and SIP Treatment

SHER-I, GRS-V, GRS-IV, RARE, SIN-J, and MTC-SK cell lines were derived from human sporadic MTC tumors and maintained as described (Kaczirek et al., 2004; Pfragner et al., 1990, 2002). The MTCp25 mouse line was established by using MTC from mice that were overexpressing p25-GFP for at least 16 weeks. Normal human diploid fibroblasts were obtained from dissected mammary tissue using routine procedures. Cells were cultured in DMEM containing 10% FBS and were employed at passage 4. For drug treatments and small interfering peptide (SIP) assays, MTCp25 cells and each human cell line were plated at a density of 2×10^5 cells/ml and incubated with different concentrations of doxycycline, CP681301, indolinone A, roscovitine, and SIP for up to 5 days. The SIP contained an N-terminal poly-arginine (R7) tag to penetrate the cell. Standard methods were used for transfections and soft agar assays. Detailed procedures can be found in the [Supplemental Experimental Procedures](#).

Cell Proliferation and Viability Assays

For proliferation analysis, cells were plated at a density of 2×10^5 cells/ml. The number of cells was determined on various days after plating by using a CASY-1 Cell Counter and Analyzer TTC (Schärfe System). In the figures, "number of cells" refers to the total number of cells that are counted in 1 ml cell suspension. Thus, the number of cells includes alive and dead cells. For cell viability assays, WST-1 Cell Proliferation Reagent (4-[3-(4-iodophenyl)-2-(4-nitrophenyl)-2H-5-tetrazolio]-1,3-benzene disulfonate) (Roche Diagnostics) was used as per the manufacturer's instructions. Assays were performed in triplicate and repeated at least two times.

Immunoprecipitation-Kinase Assay

Proliferating mouse tumors were collected from mice deprived of doxycycline for at least 16 weeks. Arrested mouse tumors were obtained from mice that were off doxycycline for 16 weeks and replaced on doxycycline for 4 more weeks. MTCp25 cells were plated at a density of 2×10^5 cells/ml and treated, or not, with 10 μ M doxycycline for 4 days. MTC-SK and SIN-J cells were plated at a density of 3×10^5 cells/ml and treated for 12 hr with CP681301 or transfected with pCMV-KD-Cdk5 or p35 siRNA. Transfected cells were harvested 24 hr (pCMV-KD-Cdk5) or 5 days (p35 siRNA) post transfection. Cdk5 or Cdk2 were immunoprecipitated from cell lysates by using anti-Cdk5 or anti-Cdk2 antibodies, and their activity was assessed *in vitro* in saturating enzyme conditions and using histone H1 as a substrate. Detailed procedures can be found in the [Supplemental Experimental Procedures](#).

Immunoblotting

Immunoblotting was carried out as previously described (Bibb et al., 1999).

Statistical Analysis

Data for individual assays represent the mean \pm SEM. All experiments were designed with matched control conditions within each experiment to enable statistical comparison via two-tailed Student's t test, and all p values <0.05 were considered statistically significant. GraphPad Prism 6.0 was used.

SUPPLEMENTAL INFORMATION

Supplemental Information includes Supplemental Experimental Procedures and five figures and can be found with this article online at <http://dx.doi.org/10.1016/j.ccr.2013.08.027>.

AUTHOR CONTRIBUTIONS

K.P., F.P., J.A.R., and J.A.B. wrote the manuscript; K.P., E.C.R., F.P., R.P., and J.A.B. designed experiments; experiments were performed and analyzed by K.P., C.T., J.G., and L.N. for Figures 1 and S1; by K.P., V.S., and R.P. for Figures 2 and S2; E.C.R., D.M., E.R., J.A.G., P.A., A.G., G.H., X.S., and J.A.R. for Figure 3; K.P., E.C.R., F.P., J.A.G., and J.A.R. for Figures 4 and S3; K.P. and E.C.R. for Figures 5 and S4; K.P., G.S., A.G., and R.P. for Figures 6 and S5; G.M. maintained and genotyped the NSE/p25-GFP mouse line; L.H.T., S.S., B.G.R., H.C., F.E.N., and R.P. provided reagents.

ACKNOWLEDGMENTS

We thank G. Cote for MEN2A and control thyroid lysates; E. Knudsen for NDF cells and helpful advice; E. Nestler for NSE-Tta mice; K. Richter and L. Lau (Pfizer) for CP681301; F. Gillardon (Boehringer Ingelheim) for indolinone A; L. Meijer for roscovitine; and S. Hisanaga for the kinase-dead Cdk5 construct. We thank J. Shelton for histopathology advice; I. Mitchell, T. Singh, T. Crone, and L. O'Connor for technical assistance; and A. Hillmann for reading the manuscript. This research was supported by a North American Neuroendocrine Tumor Society fellowship (to K.P.) and U.S. National Institutes of Health Grants to L.H.T. (NS051874), H.C. (CA121115 and CA109053), F.E.N. (GM067674), and J.A.B. (MH79710, MH083711, DA016672, DA033485, and NS073855); the Howard Hughes Medical Institute (to L.H.T.); and American Cancer Society MEN2 Thyroid Cancer Consortium research grants (RSGM-11-182-01 and RPM-11-080-01 to H.C. and RSGM-11-190-01 to J.A.B.).

Received: September 11, 2012

Revised: June 28, 2013

Accepted: August 26, 2013

Published: October 14, 2013

REFERENCES

- Agrawal, N., Jiao, Y., Sausen, M., Leary, R., Bettgowda, C., Roberts, N.J., Bhan, S., Ho, A.S., Khan, Z., Bishop, J., et al. (2013). Exomic sequencing of medullary thyroid cancer reveals dominant and mutually exclusive oncogenic mutations in RET and RAS. *J. Clin. Endocrinol. Metab.* **98**, E364–E369.
- Angelo, M., Plattner, F., and Giese, K.P. (2006). Cyclin-dependent kinase 5 in synaptic plasticity, learning and memory. *J. Neurochem.* **99**, 353–370.
- Asai, N., Jijiwa, M., Enomoto, A., Kawai, K., Maeda, K., Ichihara, M., Murakumo, Y., and Takahashi, M. (2006). RET receptor signaling: dysfunction in thyroid cancer and Hirschsprung's disease. *Pathol. Int.* **56**, 164–172.
- Berger, C.L., de Bustros, A., Roos, B.A., Leong, S.S., Mendelsohn, G., Gesell, M.S., and Baylin, S.B. (1984). Human medullary thyroid carcinoma in culture provides a model relating growth dynamics, endocrine cell differentiation, and tumor progression. *J. Clin. Endocrinol. Metab.* **59**, 338–343.
- Bibb, J.A., Snyder, G.L., Nishi, A., Yan, Z., Meijer, L., Fienberg, A.A., Tsai, L.H., Kwon, Y.T., Girault, J.A., Czernik, A.J., et al. (1999). Phosphorylation of DARPP-32 by Cdk5 modulates dopamine signalling in neurons. *Nature* **402**, 669–671.
- Boichard, A., Croux, L., Al Ghuzlan, A., Broutin, S., Dupuy, C., Lebouleux, S., Schlumberger, M., Bidart, J.M., and Lacroix, L. (2012). Somatic RAS mutations occur in a large proportion of sporadic RET-negative medullary thyroid carcinomas and extend to a previously unidentified exon. *J. Clin. Endocrinol. Metab.* **97**, E2031–E2035.
- Bracken, A.P., Ciro, M., Cocito, A., and Helin, K. (2004). E2F target genes: unraveling the biology. *Trends Biochem. Sci.* **29**, 409–417.
- Chellappan, S.P., Hiebert, S., Mudryj, M., Horowitz, J.M., and Nevins, J.R. (1991). The E2F transcription factor is a cellular target for the RB protein. *Cell* **65**, 1053–1061.
- Chen, J., Kelz, M.B., Zeng, G., Sakai, N., Steffen, C., Shockett, P.E., Picciotto, M.R., Duman, R.S., and Nestler, E.J. (1998). Transgenic animals with inducible, targeted gene expression in brain. *Mol. Pharmacol.* **54**, 495–503.
- Ciampi, R., Mian, C., Fugazzola, L., Cosci, B., Romei, C., Barollo, S., Cirello, V., Bottici, V., Marconcini, G., Rosa, P.M., et al. (2013). Evidence of a low prevalence of RAS mutations in a large medullary thyroid cancer series. *Thyroid* **23**, 50–57.
- Cranston, A.N., and Ponder, B.A. (2003). Modulation of medullary thyroid carcinoma penetrance suggests the presence of modifier genes in a RET transgenic mouse model. *Cancer Res.* **63**, 4777–4780.
- Cruz, J.C., Tseng, H.C., Goldman, J.A., Shih, H., and Tsai, L.-H. (2003). Aberrant Cdk5 activation by p25 triggers pathological events leading to neurodegeneration and neurofibrillary tangles. *Neuron* **40**, 471–483.
- Dar, A.C., Das, T.K., Shokat, K.M., and Cagan, R.L. (2012). Chemical genetic discovery of targets and anti-targets for cancer polypharmacology. *Nature* **486**, 80–84.
- DeGregori, J., Leone, G., Miron, A., Jakoi, L., and Nevins, J.R. (1997). Distinct roles for E2F proteins in cell growth control and apoptosis. *Proc. Natl. Acad. Sci. USA* **94**, 7245–7250.
- Demelash, A., Rudrabhatla, P., Pant, H.C., Wang, X., Amin, N.D., McWhite, C.D., Naizhen, X., and Linnoila, R.I. (2012). Achaete-scute homologue-1 (ASH1) stimulates migration of lung cancer cells through Cdk5/p35 pathway. *Mol. Biol. Cell* **23**, 2856–2866.
- Feldmann, G., Mishra, A., Hong, S.M., Bisht, S., Strock, C.J., Ball, D.W., Goggins, M., Maitra, A., and Nelkin, B.D. (2010). Inhibiting the cyclin-dependent kinase CDK5 blocks pancreatic cancer formation and progression through the suppression of Ras-Ral signaling. *Cancer Res.* **70**, 4460–4469.
- Fialkowski, E.A., and Moley, J.F. (2006). Current approaches to medullary thyroid carcinoma, sporadic and familial. *J. Surg. Oncol.* **94**, 737–747.
- Flicker, K., Ulz, P., Höger, H., Zeithofer, P., Haas, O.A., Behmel, A., Buchinger, W., Scheuba, C., Niederle, B., Pfragner, R., and Speicher, M.R. (2012). High-resolution analysis of alterations in medullary thyroid carcinoma genomes. *Int. J. Cancer* **131**, E66–E73.
- Futatsugi, A., Utreras, E., Rudrabhatla, P., Jaffe, H., Pant, H.C., and Kulkarni, A.B. (2012). Cyclin-dependent kinase 5 regulates E2F transcription factor through phosphorylation of Rb protein in neurons. *Cell Cycle* **11**, 1603–1610.
- Goodyear, S., and Sharma, M.C. (2007). Roscovitine regulates invasive breast cancer cell (MDA-MB231) proliferation and survival through cell cycle regulatory protein cdk5. *Exp. Mol. Pathol.* **82**, 25–32.
- Hamdane, M., Bretteville, A., Sambo, A.V., Schindowski, K., Bégard, S., Delacourte, A., Bertrand, P., and Buée, L. (2005). p25/Cdk5-mediated retinoblastoma phosphorylation is an early event in neuronal cell death. *J. Cell Sci.* **118**, 1291–1298.
- Harbour, J.W., Luo, R.X., Dei Santi, A., Postigo, A.A., and Dean, D.C. (1999). Cdk phosphorylation triggers sequential intramolecular interactions that progressively block Rb functions as cells move through G1. *Cell* **98**, 859–869.
- Harrison, D.J., Hooper, M.L., Armstrong, J.F., and Clarke, A.R. (1995). Effects of heterozygosity for the Rb-1119neo allele in the mouse. *Oncogene* **10**, 1615–1620.
- Harvey, M., Vogel, H., Lee, E.Y., Bradley, A., and Donehower, L.A. (1995). Mice deficient in both p53 and Rb develop tumors primarily of endocrine origin. *Cancer Res.* **55**, 1146–1151.
- Hu, M.I., and Cote, G.J. (2012). Medullary thyroid carcinoma: who's on first? *Thyroid* **22**, 451–453.
- Huang, C., Rajfur, Z., Yousefi, N., Chen, Z., Jacobson, K., and Ginsberg, M.H. (2009). Talin phosphorylation by Cdk5 regulates Smurf1-mediated talin head ubiquitylation and cell migration. *Nat. Cell Biol.* **11**, 624–630.
- Jiang, H., Luo, S., and Li, H. (2005). Cdk5 activator-binding protein C53 regulates apoptosis induced by genotoxic stress via modulating the G2/M DNA damage checkpoint. *J. Biol. Chem.* **280**, 20651–20659.
- Kaczirek, K., Schindl, M., Weinhäusel, A., Scheuba, C., Passler, C., Prager, G., Raderer, M., Hamilton, G., Mittlböck, M., Siegl, V., et al. (2004). Cytotoxic activity of camptothecin and paclitaxel in newly established continuous human medullary thyroid carcinoma cell lines. *J. Clin. Endocrinol. Metab.* **89**, 2397–2401.
- Karran, E., and Palmer, A.M. (2007). Neurodegenerative disorders and their treatment. *Drug News Perspect.* **20**, 407–412.

- Kedzia, C., Lacroix, L., Ameur, N., Ragot, T., Kelly, P.A., Caillou, B., and Binart, N. (2005). Medullary thyroid carcinoma arises in the absence of prolactin signaling. *Cancer Res.* 65, 8497–8503.
- Kim, E., Chen, F., Wang, C.C., and Harrison, L.E. (2006). CDK5 is a novel regulatory protein in PPARgamma ligand-induced antiproliferation. *Int. J. Oncol.* 28, 191–194.
- Knostman, K.A., Jhiang, S.M., and Capen, C.C. (2007). Genetic alterations in thyroid cancer: the role of mouse models. *Vet. Pathol.* 44, 1–14.
- Knudsen, K.E., Fribourg, A.F., Strobeck, M.W., Blanchard, J.M., and Knudsen, E.S. (1999). Cyclin A is a functional target of retinoblastoma tumor suppressor protein-mediated cell cycle arrest. *J. Biol. Chem.* 274, 27632–27641.
- Kusakawa, G., Saito, T., Onuki, R., Ishiguro, K., Kishimoto, T., and Hisanaga, S. (2000). Calpain-dependent proteolytic cleavage of the p35 cyclin-dependent kinase 5 activator to p25. *J. Biol. Chem.* 275, 17166–17172.
- Lagace, D.C., Benavides, D.R., Kansy, J.W., Mapelli, M., Greengard, P., Bibb, J.A., and Eisch, A.J. (2008). Cdk5 is essential for adult hippocampal neurogenesis. *Proc. Natl. Acad. Sci. USA* 105, 18567–18571.
- Leung, S.W., Wloga, E.H., Castro, A.F., Nguyen, T., Bronson, R.T., and Yamasaki, L. (2004). A dynamic switch in Rb+/- mediated neuroendocrine tumorigenesis. *Oncogene* 23, 3296–3307.
- Lilja, L., Yang, S.N., Webb, D.L., Juntti-Berggren, L., Berggren, P.O., and Bark, C. (2001). Cyclin-dependent kinase 5 promotes insulin exocytosis. *J. Biol. Chem.* 276, 34199–34205.
- Lin, H., Chen, M.C., Chiu, C.Y., Song, Y.M., and Lin, S.Y. (2007). Cdk5 regulates STAT3 activation and cell proliferation in medullary thyroid carcinoma cells. *J. Biol. Chem.* 282, 2776–2784.
- Liska, J., Altanerova, V., Galbavy, S., Stvrtnina, S., and Brtko, J. (2005). Thyroid tumors: histological classification and genetic factors involved in the development of thyroid cancer. *Endocr. Regul.* 39, 73–83.
- Lopes, J.P., and Agostinho, P. (2011). Cdk5: multitasking between physiological and pathological conditions. *Prog. Neurobiol.* 94, 49–63.
- Massoll, N., and Mazzaferri, E.L. (2004). Diagnosis and management of medullary thyroid carcinoma. *Clin. Lab. Med.* 24, 49–83.
- Meyer, D.A., Richer, E., Benkovic, S.A., Hayashi, K., Kansy, J.W., Hale, C.F., Moy, L.Y., Kim, Y., O'Callaghan, J.P., Tsai, L.H., et al. (2008). Striatal dysregulation of Cdk5 alters locomotor responses to cocaine, motor learning, and dendritic morphology. *Proc. Natl. Acad. Sci. USA* 105, 18561–18566.
- Nevins, J.R. (2001). The Rb/E2F pathway and cancer. *Hum. Mol. Genet.* 10, 699–703.
- Nikitin, A.Y., Juárez-Pérez, M.I., Li, S., Huang, L., and Lee, W.H. (1999). RB-mediated suppression of spontaneous multiple neuroendocrine neoplasia and lung metastases in Rb+/- mice. *Proc. Natl. Acad. Sci. USA* 96, 3916–3921.
- Pang, Z.P., and Südhof, T.C. (2010). Cell biology of Ca²⁺-triggered exocytosis. *Curr. Opin. Cell Biol.* 22, 496–505.
- Panicar, K.S., Nonner, D., White, M.G., and Barrett, J.N. (2008). Overexpression of Cdk5 or non-phosphorylatable retinoblastoma protein protects septal neurons from oxygen-glucose deprivation. *Neurochem. Res.* 33, 1852–1858.
- Pfaffner, R., Höfler, H., Behmel, A., Ingolic, E., and Walsler, V. (1990). Establishment and characterization of continuous cell line MTC-SK derived from a human medullary thyroid carcinoma. *Cancer Res.* 50, 4160–4166.
- Pfaffner, R., Wirnsberger, G., Behmel, A., Wolf, G., Passath, A., Ingolic, E., Adamiker, D., and Schauenstein, K. (1993). New continuous cell-line from human medullary-thyroid carcinoma - sinj - phenotypic analysis and in vivo carcinogenesis. *Int. J. Oncol.* 2, 831–836.
- Pfaffner, R., Wirnsberger, G.H., Ingolic, E., and Niederle, B. (2002). Medullary thyroid carcinomas in cell culture—models for future therapies. *Wien. Klin. Wochenschr.* 114, 279–283.
- Quintavalle, M., Elia, L., Price, J.H., Heynen-Genel, S., and Courtneidge, S.A. (2011). A cell-based high-content screening assay reveals activators and inhibitors of cancer cell invasion. *Sci. Signal.* 4, ra49.
- Ruiz-Llorente, S., Montero-Conde, C., Milne, R.L., Moya, C.M., Cebrián, A., Letón, R., Cascón, A., Mercadillo, F., Landa, I., Borrego, S., et al.; Medullary Thyroid Carcinoma Clinical Group. (2007). Association study of 69 genes in the ret pathway identifies low-penetrance loci in sporadic medullary thyroid carcinoma. *Cancer Res.* 67, 9561–9567.
- Rush, J., Moritz, A., Lee, K.A., Guo, A., Goss, V.L., Spek, E.J., Zhang, H., Zha, X.M., Polakiewicz, R.D., and Comb, M.J. (2005). Immunoaffinity profiling of tyrosine phosphorylation in cancer cells. *Nat. Biotechnol.* 23, 94–101.
- Sadleir, K.R., and Vassar, R. (2012). Cdk5 protein inhibition and Aβ42 increase BACE1 protein level in primary neurons by a post-transcriptional mechanism: implications of CDK5 as a therapeutic target for Alzheimer disease. *J. Biol. Chem.* 287, 7224–7235.
- Saito, T., Konno, T., Hosokawa, T., Asada, A., Ishiguro, K., and Hisanaga, S. (2007). p25/cyclin-dependent kinase 5 promotes the progression of cell death in nucleus of endoplasmic reticulum-stressed neurons. *J. Neurochem.* 102, 133–140.
- Salon, C., Merdzhanova, G., Brambilla, C., Brambilla, E., Gazzeri, S., and Eymin, B. (2007). E2F-1, Skp2 and cyclin E oncoproteins are upregulated and directly correlated in high-grade neuroendocrine lung tumors. *Oncogene* 26, 6927–6936.
- Schlumberger, M., Carlomagno, F., Baudin, E., Bidart, J.M., and Santoro, M. (2008). New therapeutic approaches to treat medullary thyroid carcinoma. *Nat. Clin. Pract. Endocrinol. Metab.* 4, 22–32.
- Sellers, W.R., Rodgers, J.W., and Kaelin, W.G., Jr. (1995). A potent transrepression domain in the retinoblastoma protein induces a cell cycle arrest when bound to E2F sites. *Proc Natl Acad Sci U S A* 92, 11544–11548.
- Sherman, S.I. (2013). Lessons learned and questions unanswered from use of multitargeted kinase inhibitors in medullary thyroid cancer. *Oral Oncol.* 49, 707–710.
- Sippel, R.S., Kunnimalaiyaan, M., and Chen, H. (2008). Current management of medullary thyroid cancer. *Oncologist* 13, 539–547.
- Strock, C.J., Park, J.I., Nakakura, E.K., Bova, G.S., Isaacs, J.T., Ball, D.W., and Nelkin, B.D. (2006). Cyclin-dependent kinase 5 activity controls cell motility and metastatic potential of prostate cancer cells. *Cancer Res.* 66, 7509–7515.
- Takahashi, M. (2001). The GDNF/RET signaling pathway and human diseases. *Cytokine Growth Factor Rev.* 12, 361–373.
- Takahashi, C., Contreras, B., Bronson, R.T., Loda, M., and Ewen, M.E. (2004). Genetic interaction between Rb and K-ras in the control of differentiation and tumor suppression. *Mol. Cell. Biol.* 24, 10406–10415.
- Takahashi, C., Contreras, B., Iwanaga, T., Takegami, Y., Bakker, A., Bronson, R.T., Noda, M., Loda, M., Hunt, J.L., and Ewen, M.E. (2006). Nras loss induces metastatic conversion of Rb1-deficient neuroendocrine thyroid tumor. *Nat. Genet.* 38, 118–123.
- van Veelen, W., Klompaker, R., Glicerich, M., van Gasteren, C.J., Kalkhoven, E., Berger, R., Lips, C.J., Medema, R.H., Höppener, J.W., and Acton, D.S. (2009). P18 is a tumor suppressor gene involved in human medullary thyroid carcinoma and pheochromocytoma development. *Int. J. Cancer* 124, 339–345.
- Wei, F.Y., Nagashima, K., Ohshima, T., Saheki, Y., Lu, Y.F., Matsushita, M., Yamada, Y., Mikoshiba, K., Seino, Y., Matsui, H., and Tomizawa, K. (2005). Cdk5-dependent regulation of glucose-stimulated insulin secretion. *Nat. Med.* 11, 1104–1108.
- Weinberg, R.A. (1995). The retinoblastoma protein and cell cycle control. *Cell* 81, 323–330.
- Wells, S.A., Jr., Robinson, B.G., Gagel, R.F., Dralle, H., Fagin, J.A., Santoro, M., Baudin, E., Elisei, R., Jarzab, B., Vasselli, J.R., et al. (2012). Vandetanib in patients with locally advanced or metastatic medullary thyroid cancer: a randomized, double-blind phase III trial. *J. Clin. Oncol.* 30, 134–141.
- Wen, Y., Panell, E., Herman, M., Figueroa, H.Y., Wang, L., Liu, L., Lau, L.F., Yu, W.H., and Duff, K.E. (2008). Interplay between cyclin-dependent kinase 5 and glycogen synthase kinase 3 beta mediated by neuregulin signaling leads to

differential effects on tau phosphorylation and amyloid precursor protein processing. *J. Neurosci.* 28, 2624–2632.

Williams, B.O., Remington, L., Albert, D.M., Mukai, S., Bronson, R.T., and Jacks, T. (1994). Cooperative tumorigenic effects of germline mutations in Rb and p53. *Nat. Genet.* 7, 480–484.

Yamasaki, L., Bronson, R., Williams, B.O., Dyson, N.J., Harlow, E., and Jacks, T. (1998). Loss of E2F-1 reduces tumorigenesis and extends the lifespan of Rb1(+/-)mice. *Nat. Genet.* 18, 360–364.

Ye, L., Santarpia, L., Cote, G.J., El-Naggar, A.K., and Gagel, R.F. (2008). High resolution array-comparative genomic hybridization profiling reveals deoxyribonucleic acid copy number alterations associated with medullary thyroid carcinoma. *J. Clin. Endocrinol. Metab.* 93, 4367–4372.

Ziebold, U., Lee, E.Y., Bronson, R.T., and Lees, J.A. (2003). E2F3 loss has opposing effects on different pRB-deficient tumors, resulting in suppression of pituitary tumors but metastasis of medullary thyroid carcinomas. *Mol. Cell. Biol.* 23, 6542–6552.